جمهورية العراق

وزارة التعليم العالي و البحث العلمي

نمذجة التوزيع الحراري خلال ريشة توربين مبردة بالهواء

رسالة
مقدمة إلى كلية الهندسة في جامعة بابل
كجزء من متطلبات نيل درجة ماجستير علوم
في الهندسة الميكانيكية

أعدت من قبل
نجلاء علي حسين
٢٠٠٤

الخلاصة

أن حساب توزيع درجة الحرارة خلال ريشة التوربين مهم لتجنب الزيادة الفائقة في درجات الحرارة والتدرج الحراري للمعدن .أن تنبؤ توزيع درجة الحرارة تحقق من خلال استخدام طريقة الفرو قات الحدية والتي تم تطبيقها في حل المشكلة مع أسلوب توليد الخلايا وأسلوب نقل الإحداثيات.

تم تطبيق معادلة انتقال الحرارة بالتوصيل ثنائية البعد،للحالة المستقرة للعقد الداخلية في شبكة الفرو قات الحديه للحصول على توزيع درجات الحرارة في تلك العقد،في حين تم تطبيق معادلة انتقال الحرارة بالحمل القسري في العقد السطحية (السطح الخارجي و السطح الداخلي).

في أسلوب توليد الخلايا (grid generation technique) تم فيه تحويل شكل الريشة من الإحداثيات الفيزيائية إلى الإحداثيات الحسابية و الخلايا المتولدة من هذا النقل تم مطابقتها مع حدود الريشة وذلك لضمان تطبيق الشروط الحدودية في المعادلات بصورة صحيحة للحصول على الحل. هذا النوع من توليد الخلايا يسمى بنظام مطابقة إحداثيات الجسم(body-fitted coordinate system) والذي يتعامل مع عدة أنواع من المعادلات التفاضلية.

تم حل المشكلة بمساعدة برنامج حاسبة والذي قام بإيجاد توزيع درجات الحرارة باستخدام طريقة (Gauss-Siedel).

في هذا البحث، ستة حالات دراسية تم استخدامها للتحليل الحراري للريشة والذي يتطلب وصف الشروط الحدودية الخارجية و الداخلية. وأيضا وجدنا من النتائج التي حصلنا عليها بأن أفضل طريقة تبريد لريشة التوربين هي التي حصلنا عليها من الحالة السادسة عندما تم تبريد الريشة باستخدام طريقة (impingement and film cooling).ولقد وجدنا بأنه في الريشة المبردة باستخدام هذه الطريقة أن درجة حرارة الريشة تقل بحوالي (١٧٠ K) عن الريشة المبردة بدون استخدام طريقة التبريد بالغشاء (film cooling method).

إن النتائج التي تم الحصول عليها من التحليل الحراري قورنت مع تلك المستخرجة من المصدر رقم (١٠) باستخدام طريقة العناصر المحددة. وقد أظهرت المقارنة تقارب كبير بين نتائج الفرو قات الحدية والعناصر المحددة مع فرق قليل ممكن حسابه ليصل إلى (٣.٥٪) كأكبر قيمة ويقل هذا الفرق ليصل إلى (٠٪) في معظم المناطق.

Ministry of Higher Education and Scientific Research
Babylon University
College of Engineering
Department of Mechanical Engineering

MODELING OF TEMPERATURE DISTRIBUTION DURING TURBINE BLADE COOLED BY AIR

A THESIS SUBMITTED TO THE COLLEGE OF
ENGINEERING OF THE UNIVERSITY OF
BABYLON IN PARTIAL FULFILLMENT
OF THE REQUIREMENTS FOR
THE DEGREE OF MASTER OF
SCIENCE IN MECHANICAL
ENGI

BY

NAJLAA ALI HUSSIEN

B.SC., 2001
NEERING

AUGUST 2004

بسم الله الرحمن الرحيم

اقرأ وربك الأكرم الذي علم بالقلم علم الإنسان ما لم يعلم

صدق الله العظيم

سورة العلق
الآية (٣-٥)

DEDICATION

To My Family

And

To My Suitor

Najlaa ٢٠٠٤

EXAMINING COMMITTEES CERTIFICATE

We certify that we have read this thesis entitled **“MODELING OF TEMPERATURE DISTRIBUTION DURING TURBINE BLADE COOLED BY AIR”** and as an examining committee, examined the student,**“NAJLAA ALI HUSSIAN”**, in its contents and that in our opinion it meets standard of a thesis for the degree of Master of Science in Mechanical Engineering.

Signature:
Name: Asst.Prof.
Dr. Tahseen A.Al-Hattab
(Supervisor)
Date: / /٢٠٠٥

Signature:
Name: Asst.Prof.
Dr. Haroun A. K. Shahad
(Supervisor)
Date: / /٢٠٠٥

Signature:
Name: Asst.Prof.
Dr. Majid H. Majeed
(Member)
Date: / /٢٠٠٥

Signature:
Name: Asst.Prof.
Dr. Ala’a A. Mahdi
(Member)
Date: / /٢٠٠٥

Signature:
Name: Prof.
Dr. Adil A. Al- moosway
(Chairman)
Date: / /٢٠٠٥

Approval of the Mechanical Engineering Department.
Head of the Mechanical Engineering Department.

Signature:
Name: Asst.Prof.
Dr. Alaa M. Hussian
Date: / /٢٠٠٥

Approval of the College of Engineering.
Dean of the College of Engineering.

Signature:
Name: Prof.
Dr. Haroun A. K. Shahad
Date: / /٢٠٠٥

CHAPTER ONE

1

INTRODUCTION

The turbine extracts kinetic energy from the expanding gases, which flow from the combustion chamber. The kinetic energy is converted to shaft horsepower to drive the compressor and the accessories. The axial-flow turbine consists of a set of stationary vanes (stator) and a turbine wheel (rotor). The set of stationary vanes of the turbine is a plane of vanes (concentric with the axis of the turbine) that are set at an angle to form a series of small nozzles which discharge the gases onto the rotor to allow the kinetic energy of the gases to be transformed to mechanical shaft energy, these are described by Jack, [١].

The turbine rotor increases in length from the first to the last stage. The stage consists of a set of stator blades followed by a set of rotor blades. The function of a turbine rotor is to extract energy from the fluid and convert it to mechanical through the rotation of blades and the purpose of a nozzle is to accelerate the flow and guide it smoothly into the rotor.

The high-pressure, high-temperature gas flows from the combustion chamber is expanded through stationary vanes (nozzles). Static pressure and enthalpy drop occurs through these nozzles, which guide the flow smoothly into a turbine rotor. The flow then passes through the rotor where all the stagnation and static properties change. The absolute velocity increases across the nozzle, and decreases across the rotor, these are defined by Budugur, [٢].

The cycle of gas turbine power plant is shown in Fig. (١-١). The axial gas turbine plants consist of compressor, combustion chamber, and gas turbine.

Fig.(١-١) shows that the cooling air to cool the turbine is bled from the compressor, Ref. [٣].

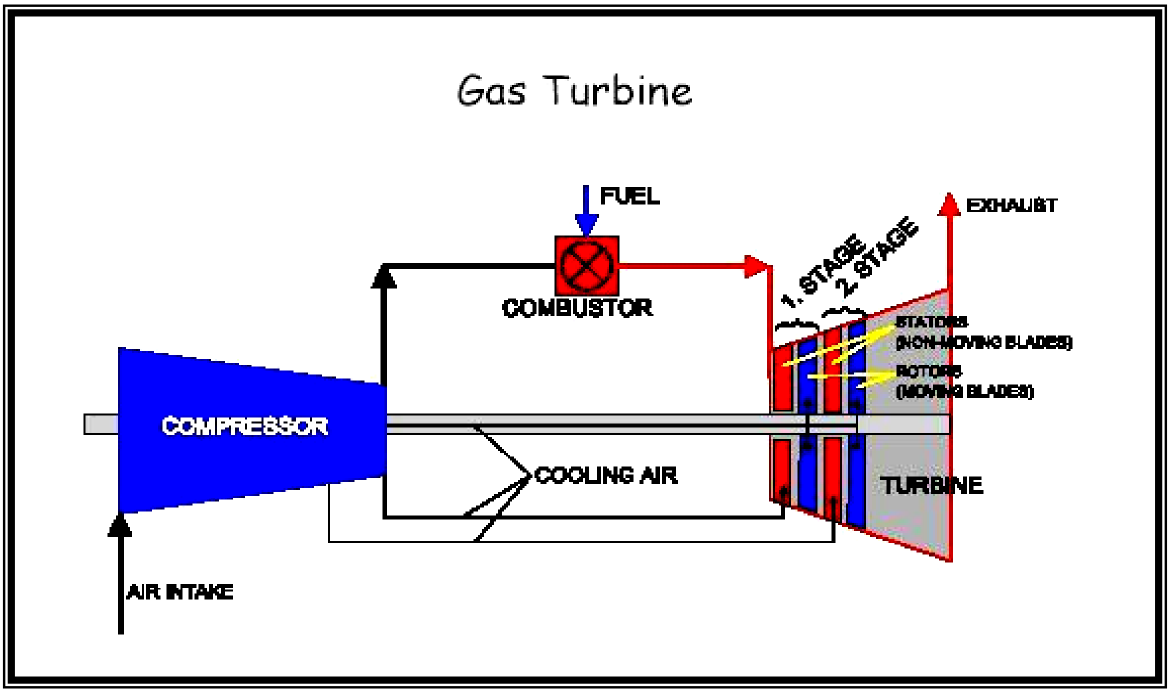

Fig. (١-١) Axial Gas Turbine, Ref. [٣]

١.١ Effect of Turbine Entry Temperature on Engine's Efficiency and Blade Materials: -

In order to increase the thermodynamic efficiency of a gas turbine engine, a high turbine inlet temperature is required. This also means higher-pressure ratios because optimum pressure increases with increasing turbine inlet temperatures for both efficiency and power. High-pressure ratio units have higher capital costs than lower pressure ones, but the decrease in fuel consumption is rapidly payback for this capital cost differential.

The components that suffer most from a combination of high temperatures, high stresses, and chemical attack are those of the turbine first-stage fixed blades (nozzles) and moving blades. They must weldable and castable and must resist corrosion, oxidation and thermal fatigue, [٤].

The gas turbine working at high gas temperature between ٦٥٠°C and ٩٥٠°C, nickel and chromium based alloys are used. Cobalt alloys have high strength and resistance to oxidation up to temperature of ١١٥٠°C, other alloys for gas turbine blades at high temperatures have manganese, molybdenum, copper, columbium, silicon, tungsten vanadium and zirconium, these are described by Turner, [٥].

Therefore, the high temperature passing on the turbine blades causes thermal stress to the turbine blades materials. To reduce the effect of thermal stress upon the materials of blade, cooling of blades is required.

١.٢ Turbine Cooling: -

The turbine components in modern gas turbine engines are subjected to much higher temperatures than the components in turbine bulit ٥٠ years ago. These components can resist high temperature due mainly to improvements in metallurgy and cooling of turbine components.

A schematic diagram of a typical turbine cooling system is shown in figure (١-٢). The stator blades and the outer wall of the turbine flow passage use cooling air that travels from the compressor between the combustor and outer engine case. The turbine rotor blades, disks and inner wall of the turbine flow passage use cooling air that is routed through inner passage ways. The first-stage, stator blades (nozzles) are exposed to the highest turbine temperatures. The first stage, rotor blades are exposed to a some what lower temperature because of circumferential averaging, dilution of turbine gases with first stage stator cooling air and relative velocity effects. The second-stage, stator blades are exposed to an even lower temperature because of additional cooling air dilution and power extraction from the turbine stage. The turbine temperature decreases in a like manner through each blade row, [١].

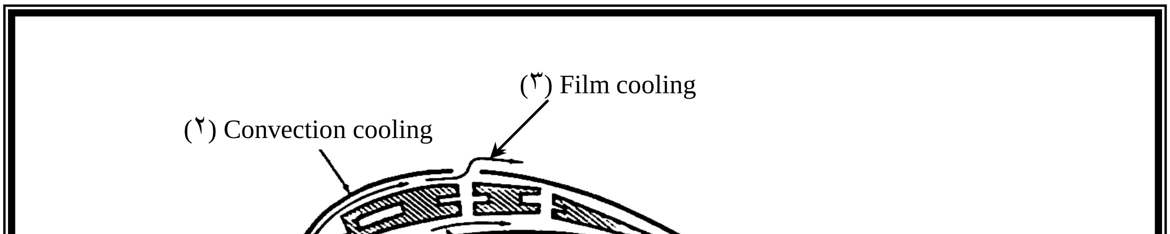

١.٢.١ Methods of Blade Cooling: -

The cooling technology mainly uses air as a coolant fluid and in some cases the water is used to perform this function. Figure (١-٣) illustrates the methods of blade cooling that have received serious attention and research effort, these are reported by Cohen, [٦].

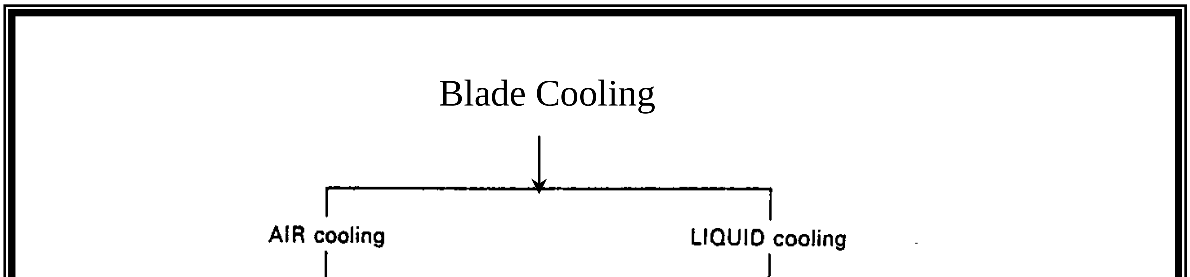

A part from the use of spray cooling for thrust boosting in turbojet engines, the liquid systems have not proved to be practicable. There are difficulties associated with channeling the liquid to and from the blades, whether as primary coolant for forced convection or free convection open thermosyphon systems. It is impossible to eliminate corrosion or the formation of deposits in open systems, and it is very difficult to provide adequate secondary surface cooling area at the base of the blades for closed systems. So, the most common methods used in production of engines are air-cooling, [٦].

The air cooling methods used in the turbine are illustrated in figure (١-٤) and can be divided into the following categories, these are reported by Ref.[١]:

١. Convection cooling.
٢. Impingement cooling.
٣. Film cooling.
٤. Full-coverage film cooling.
٥. Transpiration cooling.

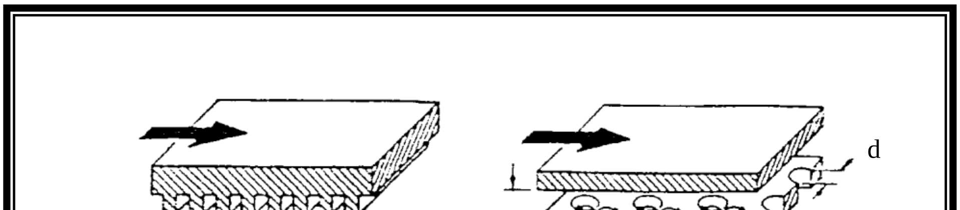

Application of these five methods of cooling to turbine blades are shown in figure (١-٥)

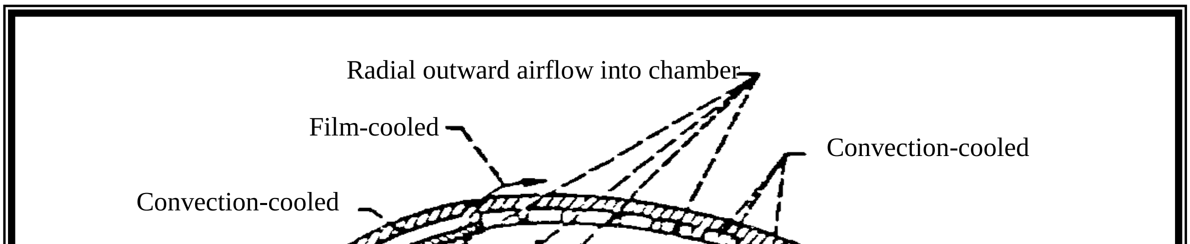

١.٣ The Scope of the Present Work: -

The scope of this research can be summarized in the following stages:

i) To find the temperature distribution in air-cooled turbine blades using transformed finite difference equations by establishing a special technique in the use of the finite difference method with complicated geometries. This technique is known as body-fitted coordinate system. The results of the present work are compared with that using finite element method. This has been dealt within chapter three.

ii) In chapter four deals with the boundary conditions used in this work for six cases and deals with the computer program which is constructed to perform the calculation of temperatures based on the analysis.

iii) The main conclusions drawn from this work and suggestions for further works are given in chapter six.

CHAPTER TWO

2

LITERATURE REVIEW

٢.١ Introduction: -

Temperature distribution in air-cooled gas turbine blades is very important in the design of modern gas turbines. To determine the temperature distribution in the turbine blades there are numbers of experimental work and theoretical researches in this field to get the best means for improving the increase of its operating conditions.

In the following sections, brief reviews of grid generation techniques, analytical, numerical and experimental solutions for turbine blade cooling are discussed.

٢.٢ Numerical Work: -

Several numerical methods are available to solve differential equations of heat transfer conduction. Among these methods are the finite difference, finite element and control volume approaches. In many applications the turbine blades have complex geometries, complex boundary conditions and hence they cannot be solved analytically.

Thompson J.F., [٧], ١٩٨٤, presents a grid generation technique and worked extensively on using elliptic PDE’s to generate grids. The grid generation technique transforms the physical plane into computational plane where the mapping is controlled by a Poisson equation.

Anderson D.A, [٨], ١٩٨٤, classified grid generation techniques into three categories, they are: complex variable methods, algebraic methods and differential equation techniques. Algebraic and differential equation techniques were used on complicated three-dimensional problems in conjunction with finite difference methods. The application of these techniques and a number of examples showing generated grids had been studied.

Gilding B.H., [٩], ١٩٨٨, describes a technique for the generation of boundary-fitted curvilinear coordinate systems for the numerical solution of PDE's in two space dimensions. The technique is algebraic which has a transfinite character, and it is based on the blending of shearing transformations. Applications to numerical grid generation for problems in the field of computational fluid dynamics are presented.

Walker, M.J.B., [١٠], ١٩٨٩, introduced a master thesis that involves the determination of temperature distribution within a turbine blade for three configurations of cooled blades (circular, elliptical cooling holes, and cooling with impingement and trailing edge ejection). The determination was by the use of finite element method and for each type, the analysis was demonstrated with different specific boundary conditions and heat transfer correlations. The results are acceptable in terms of their accuracy. This was determined by applying the procedure to a test case and comparing the results with the reference results.

Dawes W.N., [١١], ١٩٩٤, described the application of a solution-adaptive, three-dimensional Navier-Stokes solver for the flow in turbine internal coolant passages. This solver had been applied to the complex geometry of a serpentine passage in a cooled radial inflow turbine rotor blade. The work has two objectives: first to predict the complex aerodynamics of the coolant passage and second attempting to predict the variation of heat transfer coefficient within the coolant passage.

Tekriwal P., [١٢], ١٩٩٤, used standard and extended K.Є turbulence models to predict three-dimensional heat transfer calculations for radially outward flow in rectangular and square ducts rotating in orthogonal mode. The finite-difference method is used to obtain the results in the present modeling effort. The numerical model predictions for heat transfer have been compared with the limited experimental data. The relative performance of the two K.Є models is also evaluted. Results show that the heat transfer is enhanced at the trailing wall and impaired at the leading wall due to rotational effects, and improvement in heat transfer predictions by the extended K.Є model is observed at high as well as low Reynolds number flows.

Dilzer M. *et al*, [١٣], ١٩٩٩, have optimized a three-layered hybrid ceramic first stage nozzle vane for a stationary gas turbine in order to improve the reliability. The optimization is performed by finite element analyses in combination with failure probability calculations. The concept is based on a three-layered construction (outer ceramic shell, heat insulating layer and metallic core) and an optimization of the thickness of the single layers, in order to obtain a homogenous temperature distribution in the ceramic structure. This method has been applied to increase the reliability of a first stage Sintered Silicon Carbide (SSiC) ceramic nozzle vane of a stationary gas turbine (٧٠ MW/١٤٠٠^{o}c). As a result it was found that the mechanically and thermally induced loads have been reduced considerably and do not exceed (١٠٠ Mpa) thus achieving adequate life based upon failure probability calculations.

Natalini and Sciubba, [١٤], ١٩٩٩, presented the results of a numerical configuration study on a two-dimensional model of an internally cooled gas turbine vane. The vane is internally cooled by a radial flow of air through three separate internal channels. The cooling air assumed to be discharged from the vane tip. The analysis applied to a two-dimensional cascade at medium Reynolds number, subsonic Mach number and steady state. The full Navier-Stokes equations of motion for turbulent viscous flow, together with the appropriate energy equation, are solved by using a standard finite-element code with a K.Є closure, to obtain complete velocity and temperature fields. The procedure in general, can be extended to different configuration and different operational conditions, and provides the designer with a rotational and effective tool to assess the actual losses in the fixed and rotating turbomachinery cascades.

Jaleel J.M., [١٥], ٢٠٠١, illustrated the finite difference method with suitable approximation for curved boundary to determine the temperature distribution within air-cooled turbine blade utilizing circular cooling holes and verified the effectiveness of the irregular finite difference method on curved non-uniform shapes such as turbine blade.

Kuder D.S., [١٦], ٢٠٠٣, submitted a master thesis that involves the prediction of temperature distribution in gas turbine air-cooled blades from hub to tip. It was achieved through the use of control volume technique. The control volume mesh deals with irregular boundary. Unsteady state two dimensional heat transfer was used to get the temperature distribution. The results of thermal analyses obtained in two case studies in which cooling passages were taken as (١٥) circular holes, with different diameters and as (٣) channel passages. Her results show that the surface temperature distribution with channel cooling passages is (٢٠٪) lower than the surface temperature distribution with circular cooling passages.

Marie *et al*, [١٧], ٢٠٠٣, presented a paper to determine the flow and temperature fields around an inlet guide vane numerically by CFD method. The governing equations are solved by ٣D finite-volume Navier-Stockes method. In particular the outer surface temperature, heat transfer coefficient distributions and static pressure distributions are also presented. Three different thermal boundary conditions on the vane blade are analysed:

a) uniform wall temperature on the outer van surface,

b) non-uniform wall temperature distribution on the outer vane surface based on experiments, and

c) conjugate heat transfer wall condition.

He concluded that the results showed the calculated values agree very well when the computed results are compared with experimental data from tests in a hot cascade rig at ABB Alstom Power AB in Sweden.

٢.٣ Analytical Work: -

Debruge and Han, [١٨], ١٩٧٢, analyzed a method of cooling turbine blades internally by continuous injection through an interior baffle. The analytical model consists of a channel formed by a solid wall (blade surface) and a porous plate (injection source). Based on steady flow of an incompressible fluid with constant physical properties and laminar-flow assumptions, the velocity and temperature fields are determined for both the two-dimensional and axisymmetric cases. A turbine blade considered in a high-temperature stream with a constant stagnation temperature T_e and an external heat transfer coefficient h_e which may be variable. The heat flux from the external stream to the blade surface is then

$$q_x = h_e\left[T_e - T_w\right] \qquad \text{...(٢.١)}$$

where, T_w is the blade surface temperature variation given by the following equation,

$$T_w = T_o + \sum_{m=0} C_m \left(x/L\right)^m \qquad \text{...(٢.٢)}$$

Where m: integer index

The Nusselt number for a power-low surface-temperature variation are obtained and expressed in terms of the Prandtl and the Reynolds numbers.

Peter L.M., [١٩], ١٩٧٨, considered the potential benefits of combining full-coverage film cooling with a thermal barrier coating. It was investigated analytically for a turbine vane by calculation the metal and ceramic coating temperatures as functions of coating thickness and coolant flow. Calculations were performed for sections on the suction and pressure sides of a high temperature, high-pressure turbine vane. With a thermal-barrier coating the coolant flows required for the chosen sections were half those of uncoated design, and the metal outer temperatures were simultaneously reduced by over ١٣٣^{o}K (٢٤٠^{o}F). For comparison, transpiration cooling was also investigated. Full-coverage film cooling of a coated vane required more coolant flow than did transpiration cooling.

Eckert E.R.G., [٢٠], ١٩٨٤, presented two calculation methods, “A” for film cooling and “B” for full-coverage film cooling, for the prediction of heat transfer in film cooling. Both are based on the principle of superposition of solutions of the temperature fields for a constant property fluid. The method “A” is based on film cooling effectiveness and heat transfer coefficients has been widely used for the presentation of results obtained in film cooling with injection through slots and a porous section as well as through one or two rows of holes. This method has the advantage that laterally arranged heat transfer coefficients or Stanton numbers defined in this way are independent of the imposed temperature differences for a constant properly situation and are close to values for convection film cooling for the region some distance downstream of injection. For the region close to injection, they increase with decreasing distance to values, which are up to ٢٥ percent higher than those for convection cooling. Method “B” is based on the parameters θ and K. This method has the basic disadvantage that the heat transfer coefficient or the Stanton number vary in an irregular way with the temperature difference $(T_w - T_\infty)$ as defined in equation

$$q_w = h'(T_w - T_\infty) \qquad \ldots(٢.٣)$$

and a dimensionless parameter, θ, is used

$$\theta = \frac{T_2 - T_\infty}{T_w - T_\infty} \qquad \ldots(٢.٤)$$

and

$$\frac{h'}{h'_o} = 1 + K\theta \qquad ...(٢.٥)$$

where,

$$K = \frac{h'_1 - h'_o}{h'_o} \qquad ...(٢.٦)$$

This irregular way can be avoided when the film cooling process for the perforated section is also calculated with method “A”.

٢.٤ Experimental Work: -

Nicholson ***et al***,[٢١], ١٩٧٣,studied optimization for aerodynamic performance in high-pressure turbine blades without any film cooling applied to the surfaces of the blades. This research showed that modern boundary layer prediction techniques are sufficiently accurate to allow the heat transfer to be considered at the profile design stage. Two turbine rotor profiles were designed, each with a heat transfer optimized pressure surface, and a detailed experimental study using transient techniques in the Oxford cascade tunnel. A description of the profile is given, together with transfer rate measurements, pressure distribution and aerodynamic loss measurements and flow visualization photographs. The results of this research show that significant reductions in pressure surface heat transfer can be achieved by boundary layer optimization without compromising the aerodynamic efficiency of the blades.

Frederick ***et al***, [٢٢], ١٩٧٤, investigated the cooling effectiveness of three film-cooled vanes, each with different internal cooling configurations. The cooling effectiveness of two film-cooled vanes was compared to the cooling effectiveness of two-non film - cooled vanes of similar internal cooling geometry. The cooling effectiveness of the third vane was compared to non-film cooled vane which had significantly different internal cooling geometry. The cooling effectiveness values used in the comparisons were obtained from experimental correlations. The comparisons indicated that, for the vane configurations and test conditions examined, film cooling had an adverse effect near the suction-surface trailing edge of the vanes. Film cooling was found to be beneficial to the cooling of the pressure surface of the vanes.

Hay *et al.*, [٢٣], ١٩٨٣, measured the discharge coefficient of single rows of holes in a specially constructed isothermal rig over a wide range of geometric and flow conditions. Mainstream and coolant Mach numbers have been varied independently over the range ٠ to ٠.٤ for pressure ratios in the range ٠ to ٢. Cooling hole length to diameter ratios were varied between ٢ and ٦, and inclinations of ٣٠°, ٦٠° and ٩٠° were used. The results show that the influence of crossflow is strong and complex, particularly with regard to that on the coolant side.

Nealy *et al*, [٢٤], ١٩٨٤, presented the results of an experimental study of aerodynamic and heat transfer distributions over the surfaces of two different, highly loaded, low-solidity contemporary turbine vane designs. The aerodynamic configurations of the two vanes were carefully selected to emphasize fundamental differences in the character of the suction surface pressure distributions and the consequent effect on surface heat transfer distributions. The experimental measurements were made in moderate temperature, three vane cascades under steady state conditions. The principal independent parameters (Mach number, Reynolds number, turbulent intensity, and wall-to-gas temperature ratio) were varied over ranges consistent with actual engine operation, and the test matrix was structured to provide an assessment of the independent influence of each parameter.

York *et al*, [٢٥], ١٩٨٤, introduced a paper to produce a data base of end wall heat transfer in the first-stage stator in advanced turbine engines. A linear, two-dimensional cascade was used to generate the data base. The test plan provided data to examine the effects of exit Mach number, exit Reynolds number, inlet boundary layer thickness, gas-to-wall temperature ratio, inlet pressure gradients, and inlet temperature gradients. The data generated consist of inlet, intrapassage, and exit aerodynamic data plus intrapassage endwall heat flux, adiabatic wall temperature measurements and inlet turbulence data.

Hussain A.K.[٢٦], ١٩٩٠ studied an experimental study of radiation from coated turbine blades. The work consists of both experimental and theoretical prediction of turbine blade temperature distribution. He found that coating type, coating thickness and temperature measurement technique has a big influence on blade metal temperature and hence on turbine life.

Salcudean *et al*, [٢٧], ١٩٩٤, investigated experimentally the film cooling effectiveness by using a flame ionization technique based on the heat and mass transfer analogy. The measurements were made over the surface of the turbine blade model composed of a semi-cylindrical leading edge bonded to a flat after-body. The secondary flow was injected into the boundary layer through four rows of holes located at ±١٥^o and ±٤٤^o about the stagnation line of the leading edge. Discharge coefficients and flow divisions between the ١٥^o and ٤٤^o rows of holes have also been measured. The strong pressure gradient near the leading edge produces a strongly non-uniform flow division between the first (±١٥^o) and the second (±٤٤^o) row of holes at low overall mass flow ratios. This produced a total cutoff of the coolant from the first row of holes at mass flow ratios lower than approximately ٠.٤, leaving the leading edge unprotected near the stagnation line. Stream wise and span wise plots of effectiveness show that the best effectiveness values are obtained in a very narrow range of mass flux ratios near ٠.٤ where there is also considerable sensitivity to changes in Reynolds number.

Mcmillin and Lau, [٢٨], ١٩٩٤, studied the local heat transfer distribution and pressure drop in a pin fin channel that models the cooling passages in modern gas turbine blades. The detailed heat and mass transfer distribution is determine via the naphthalene sublimation technique for flow through a channel with a ١٦-row, staggered ٣×٢ array of short pin fins (with a height-to-diameter ratio of ٠.١, and stream wise and span wise spacing-to-diameter ratios of ٢.٥) and with a flow ejected through holes in one of side walls and at the straight flow exit. The pin fin and the channel wall heat and mass transfer are obtained for the straight-flow only and the ejection flow cases. The results show that the regional pin heat and mass transfer coefficients are generally higher than the corresponding regional wall heat and mass transfer coefficients in both cases.

Ou and Han, [٢٩], ١٩٩٤, investigated experimentally the effect of unsteady wake and film injection on heat transfer coefficients and film effectiveness for a gas turbine blade. Experiments were done with a five airfoil linear cascades in a low-speed wind tunnel at a chord Reynolds number of ٣×١٠^{٥}. A model turbine blade injected air or $CO_{٢}$ through one row of film holes each on the pressure and suction surfaces. The results show that the large-density injecting $CO_{٢}$ causes higher heat transfer coefficients on the suction surface and lower heat transfer coefficients on the pressure surface.

At the same year, **Zhang and Han**, [٣٠], studied the influence of mainstream turbulence on surface heat transfer coefficients of a gas turbine blade. This test was done in the same low-speed wind tunnel. The mainstream Reynolds numbers were ١٠٠,٠٠٠, ٢٠٠,٠٠٠ and ٣٠٠,٠٠٠ based on the cascade inlet velocity and blade chord length. The results show that the mainstream turbulence promotes earlier and broader boundary layer transition causes higher heat transfer coefficients on the suction surface, and significantly enhance the heat transfer coefficient on the pressure surface.

Abuaf and Kercher, [٣١], ١٩٩٤, investigated the aerothermal performance of a typical turbine blade three-pass turbulated cooling circuit geometry in a ١٠X Plexiglas test model. The model closely duplicated the blade’s leading edge, mid chord, and trailing edge cooling passage geometries. Steady-state heat transfer coefficient distributions along the blade pressure side wall of the cooling circuit passages were measured with a thin-foil heater and a liquid crystal temperature sensor assembly. The near-atmospheric experimental data are compared with results of a Computational Fluid Dynamics (CFD) analysis at the operating internal environment for a ١X rotating model of the blade cooling circuit and other turbulator channel geometry heat transfer data investigations.

Moss *et al*, [٣٢], ١٩٩٨, compared the measurements of turbine blade surface heat transfer in a transient rotor facility with predictions and equivalent cascade data. The rotating measurements involved both forward and reverse rotation (wake-free) experiments. The use of this film gases in the Oxford Rotor Facility provides both time-mean heat transfer levels and the unsteady time history. The time-mean level is not significantly affected by turbulence in the wake; this contracts with the cascade response to free-stream turbulence and simulated wake passing. Heat transfer predictions show the extent to which such phenomena are successfully modeled by a time-steady code. The accurate prediction of transition is seen to be crucial if useful predictions are to be obtained.

Drost and Bolcs, [٣٣], ١٩٩٩, studied the aerodynamic performance of a turbine (NGV) airfoil, cooled from several shower head, pressure and suction side stations. Film cooling heat transfer and effectiveness on this airfoil was examined. Tests were conducted in a linear cascade at an exit Reynolds number of ١.٤٥×١٠^{٦} and an exit Mach number ٠.٨. Density ratio effects were studied with air and $CO_{٢}$ injection for the simulation of high-density ratios, the latter has been matched using strongly cooled air and heated $CO_{٢}$. The thermodynamic losses did not match at constant density ratio, but at constant coolant Mach number, when compared at constant coolant mass flow rates.

Ken *et al*, [٣٤], ٢٠٠٠, investigated experimental tests in a low-speed wind tunnel cascade to determine the film-cooling effectiveness of the film-cooling hole geometry on turbine airfoils. This paper presented the results of a parameter study, in which the film-cooling geometry on turbine blades and vanes was varied between shaped film-cooling holes, full coverage film cooling and indicated that shaped film-cooling is one of the most effective cooling methods if it is adopted in the region where the mixing between the mainstream and the film-cooling jet is suppressed. The results of full coverage film-cooling and heat transfer characteristics of rotating serpentine flow passage with and without angled turbulence promoter had been presented in the full paper.

Stefan L.F., [٣٥], ٢٠٠١, have done an experimental evaluation of both standard and prototype blade designs under real base load conditions by using optical pyrometry. Pyrometry is a valuable tool for the quality assurance, since the temperature distribution of each individual blade is determined carefully. This paper describes the application of a newly developed high-resolution pyrometer to the latest prototype, the V٨٤.٣A٢ ٦٠Hz ١٨٠ Mw gas turbine. Thus, using new pyrometer probes in conjunction with a continuous data acquisition mode allows reliable, highly resolved blade surface temperature measurements, where errors and potential risks for the gas turbine are minimized at the same time.

It has been shown from above researches reported here, that their mainly study concentrate on the methods to determine temperature distribution within the blade material. These methods are: analytical, experimental and numerical methods such as control volume, finite element and finite difference method. More progress is needed in present study by using finite difference method with body fitted coordinate system is made to predict the temperature distribution in turbine blade.

CHAPTER THREE

3

MATHEMATICAL MODEL

٣.١ Introduction: -

In order to employ high gas temperatures in gas turbine stages it is necessary to cool the casing, nozzles, rotor blades and disks, [٦]. Heat transfer can be defined as energy in transit due to a temperature difference, [٣٦]. There are three primary modes by which heat transfer process occurs. They are:

١- Conductive heat transfer.

٢- Convective heat transfer.

٣- Radiative heat transfer.

The heat conduction process can be quantified through Fourier's law of conduction, which for one-dimensional system is: -

$$q = -k\,A_c\,\frac{dT}{dy} \qquad \text{......(٣.١)}$$

When cooled turbine blades are employed, heat is transferred through and from blade metal. Heat is carried away by coolants leaving a cooler turbine blade. The second mode of heat transfer that may occur around the turbine blade and in cooling passages is the convective heat transfer, which takes place between the blade surface and the gas flowing around turbine blade and inside the blade cooling passages, it is given by the Newton's law of cooling:

$$q = hA_{conv.}(\Delta T) \qquad \text{......(٣.٢)}$$

Third mode of heat transfer may be emitted from a surface is the radiation. It is given by the following expression:

$$q = \sigma A_r \left(T_s^4 - T_\infty^4 \right) \qquad \text{......(٣.٣)}$$

Where σ is the Stefan-Boltzmann constant $= 5.67 \times 10^{-8} \left(W / m^2 K^4 \right)$

Such a surface is called black body. The heat flux emitted by a real surface is less than that of black body, the equation (٣.٣) becomes:

$$q = \varepsilon \sigma A_r \left(T_s^4 - T_\infty^4 \right) \qquad \text{......(٣.٤)}$$

Where $0 < \varepsilon < 1$ and is called emissivity of the body.

This chapter is concerned mainly with the analysis of the model used to describe the temperature distribution in an air-cooled turbine blade. Thus, the emphasis will be on the assumptions and simplifications which were made in order to set-up the relevant governing equations.

٣.٢ Assumptions: -

The following assumptions were considered in the present analysis:

١- Steady-state conduction, because the transient case is taken during turbine operation only.

٢-Two-dimensional heat flow on the turbine blade, by considering the temperature is the same at any section along the turbine blade.

٣-There is no heat generation in the turbine blade.

٤- The turbine blade material is (CrNi Alloy), ١٩% Cr and ٧% Ni and the thermal conductivity is constant, and equal ١٨.٣W/m.K, These described by Walker[١٠].

٥- Radiative heat transfer is neglected, because the value of radiation is very small.

٣.٣ Cooling Method: -

٣.٣.١ Blade Geometry Cooling Method

Consider a turbine blade cooled by convection –and impingement as shown in Fig. (٣-١)

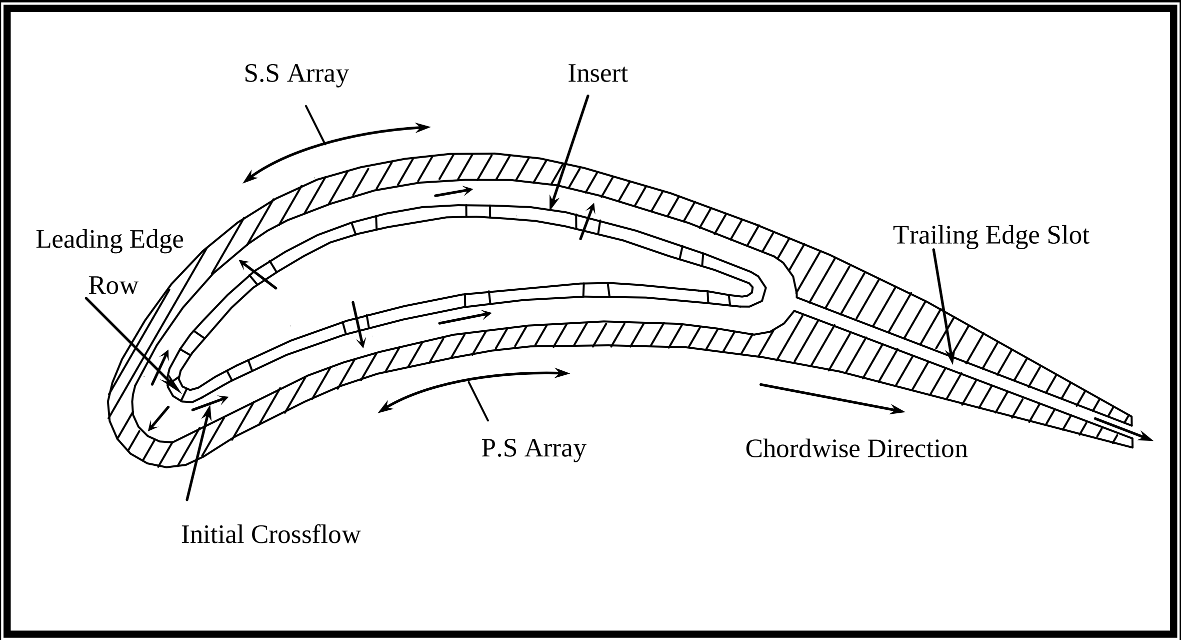

Fig. (٣-١) Convection and Impingement Cooled Blade

To determine the temperature distribution on the turbine blade at various convection boundary conditions, it is necessary to solve the differential equation for a two dimensional steady state heat conduction with the assumptions that no heat generation and constant thermal conductivity. The heat transfer equation for interior nodes is given by,

$$\frac{\partial^2 T}{\partial x^2}+\frac{\partial^2 T}{\partial y^2}=0 \qquad \text{......(٣.٥)}$$

And for the surface nodes is,

$$q_{cnduction} = q_{convection} \qquad \text{......(٣.٦)}$$

٣.٣.٢ The Finite Deference Method

In contrast to an analytical solution, which allows for temperature determination at any point on a plane, a numerical solution such as the finite difference method allows the temperature to be determined at discrete points only.

The initial step is to select the nodal points (or nodes) by subdividing the area of interest into a number of small regions and assigning to each reference point at its centre. In this manner a nodal network, grid or mesh is developed over the region of interest as shown in Fig. (٣-٢ a)

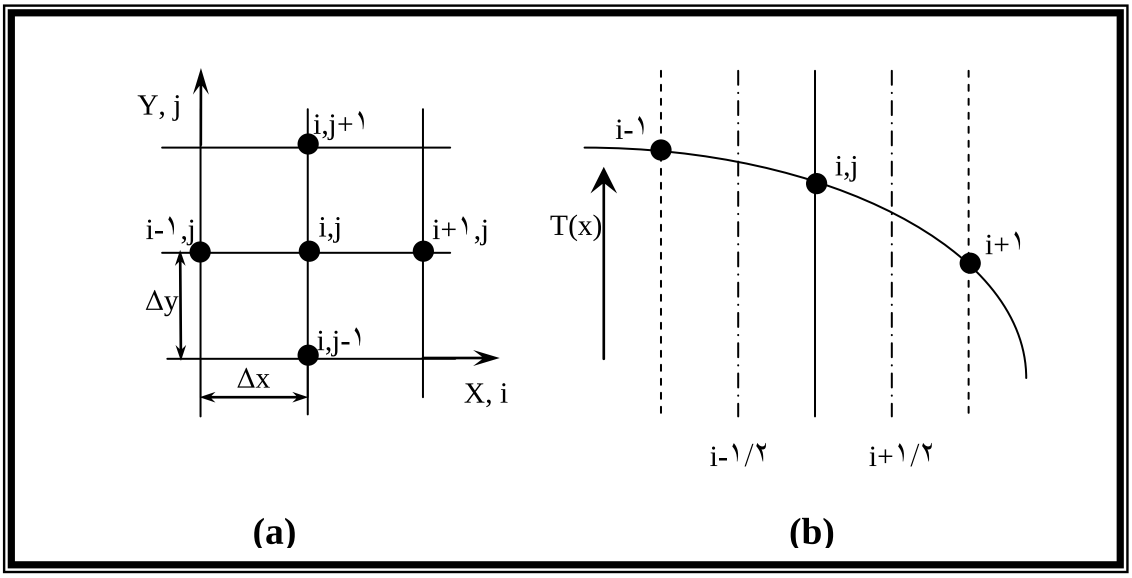

Fig. (٣-٢) (a) The Nodal Network
(b) Assumed temperature Distribution Along Line
(i-١,j) to (i+١,j)

Each nodal point is associated with a surrounding sub-region and the temperature at the nodal point is considered to be representative of the temperature of the sub-region, i.e., the average temperature.

The selection of the nodal point is not arbitrary, but depends upon the geometry of the system to be analyzed and the desired accuracy of the required solution. A fine nodal network with a large number of nodal points will be more accurate, these are reported by Incropera [٣٧].

Equation (٣.٥) gives an “exact” description of energy conservation requirements for any interior point in a two dimensional system. However, when a system is characterized by a nodal network, it is necessary to develop an approximate form of this equation, in this case a finite difference form.

Consider the second derivative $\partial^2 T / \partial x^2$ in relation to Fig. (٣-٢b) describing the temperature distribution.

The value of this derivative for the nodal point (**x,y**) may be approximated by the expression:

$$\left.\frac{\partial^2 T}{\partial x^2}\right)_{i,j} = \frac{\left.\frac{\partial T}{\partial x}\right)_{i+1/2,j} - \left.\frac{\partial T}{\partial x}\right)_{i-1/2,j}}{\Delta x} \qquad \text{......(٣.٧)}$$

The temperature gradient $(\partial T / \partial x)$may similarly be described in terms of the nodal temperatures.

i.e.,

$$\left.\frac{\partial T}{\partial x}\right)_{i+1/2,j} = \frac{T_{i+1,j} - T_{i,j}}{\Delta x} \qquad \text{...... (٣.٨)}$$

$$\left.\frac{\partial T}{\partial x}\right)_{i-1/2,j} = \frac{T_{i,j} - T_{i-1,j}}{\Delta x} \qquad \text{...... (٣.٩)}$$

Substituting equations (٣.٨) and (٣.٩) into equation (٣.٧) we get,

$$\left.\frac{\partial^2 T}{\partial x^2}\right)_{i,j} = \frac{T_{i+1,j} + T_{i-1,j} - 2T_{i,j}}{\Delta x^2} \qquad \text{......(٣.١٠)}$$

Following the same procedure for the derivative $\left.\frac{\partial^2 T}{\partial y^2}\right)_{i,j}$ it results:

$$\left.\frac{\partial^2 T}{\partial y^2}\right)_{i,j} = \frac{T_{i,j+1} + T_{i,j-1} - 2T_{i,j}}{\Delta y^2} \qquad \text{...... (٣.١١)}$$

Both of equations (٣.١٠) and (٣.١١) may be applied to any interior node that it is equidistant from it's four neighboring nodes and simply requires that the sum of the temperature at the surrounding nodal points is four times the temperature of the nodes of interest.

٣.٤ Grid Generation: -

The basic concept behind this grid generation method is the assumption from the outset that the grid to be generated or optimized consists of straight-line segments joining the nodal grid points, these are described by Thompson [٧].

The solution of a system of partial differential equations can be simplified by a well-constructed grid. In some applications, improper choice of grid point locations can lead to an apparent unstability or lack of convergence.

In general, transformations are used which lead to a uniformly spaced grid in the computational plane while points in the physical space may be unequally spaced.

The problem of grid generation is that of determining the mapping which takes the grid points from the physical domain to the computational domain. Several requirements must be placed on such mapping. Therefore a grid system with the following features is desired by Ref.[٨]:

(١) The mapping must be one to one correspondence ensuring grid lines of the same family do not cross each other.

(٢) The grid lines should be smooth to provide continuous transformation derivatives.

(٣) Grid points should be closely spaced in physical domain where large numerical errors are expected.

(٤) Excessive-grid skewness should be avoided.

Grid generation technique can be roughly classified into three categories:

١. Complex variables methods.
٢. Algebraic methods.
٣. Differential equation techniques.

Only the third category is suitable for the present case because of the complex shape. In this technique, elliptic PDE's has been used to generate grids.

This choice can be better understood by considering the solution of a steady heat conduction problem in two dimensions. The solution of this problem produces isotherms, which are smooth and non-intersecting.

The generation of a grid, with uniform spacing, is a simple exercise within a rectangular physical domain. Grid points may be specified as coincident with the boundaries of the physical domain, thus making specification of boundary conditions considerably less complex.

Unfortunately, the majority of the physical domains of interest are nonrectangular. Therefore, imposing a rectangular computational domain on such a physical domain will require some sort of interpolation for the implementation of the boundary conditions. Since the boundary conditions have a dominant influence on the solution of the equation, such an interpolation causes inaccuracies at the place of greatest sensitivity.

To overcome these difficulties, a transformation from physical space to computational space is introduced. This transformation is accomplished by specifying a generalized coordinate system, which will map the nonrectangular grid system, the physical space to a rectangular uniform grid spacing in the computational space, where the mapping is controlled by a Poisson’s equation.

٣.٤.١ Generalized Coordinate Transformation

Generally, the principle of transformation is based on demonstration of how the governing equations can be transformed from a Cartesian coordinate system to any general non-orthogonal (or orthogonal) coordinate system.

The process is done by clustering grid points in regions of large gradients to transform non-rectangular region in the physical plane into a rectangular region in the computational plane.

In other words, if the spacing in any direction in the physical plane is not uniform, it is convenient to apply the transformation in this direction, so that the governing equations can be solved on a uniformly spaced grid in the computational plane as shown in Fig. (٣-٣).

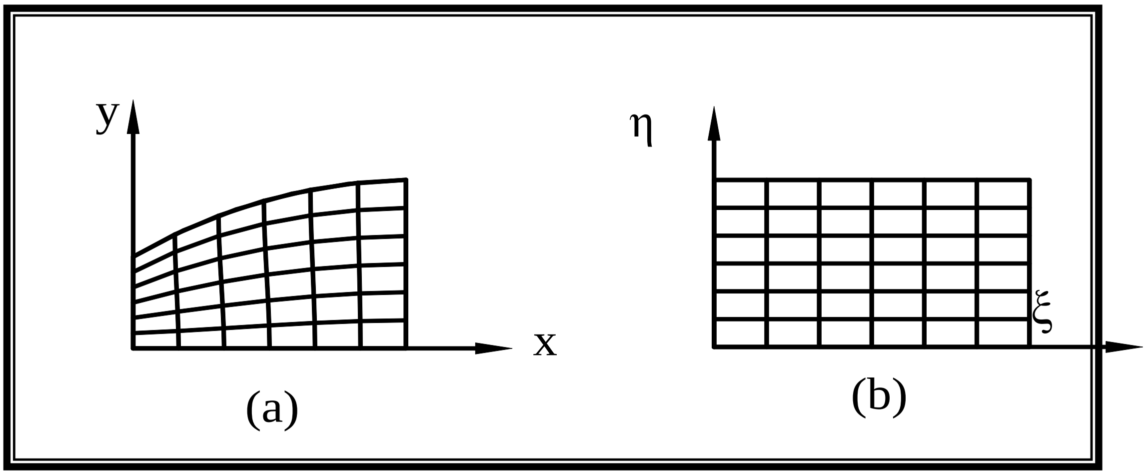

Fig. (٣-٣) Rectangularization of computational grid
physical plane (x,y)
computational plane (ξ,η)

Consider a completely general transformation of the form, these are described by Anderson, [٣٨].

$$\xi = \xi(x, y) \qquad \text{......(٣.١٢)}$$

$$\eta = \eta(x, y) \qquad \text{...... (٣.١٣)}$$

Which can be used to transform the governing equations from the physical domain (x,y) to the computational domain (ξ,η). Using the chain rule of partial differentiation, the partial derivatives become:

$$\frac{\partial}{\partial x} = \frac{\partial}{\partial \xi}\frac{\partial \xi}{\partial x} + \frac{\partial}{\partial \eta}\frac{\partial \eta}{\partial x} \qquad \text{......(٣.١٤)}$$

$$\frac{\partial}{\partial y} = \frac{\partial}{\partial \xi}\frac{\partial \xi}{\partial y} + \frac{\partial}{\partial \eta}\frac{\partial \eta}{\partial y} \qquad \text{......(٣.١٥)}$$

Let,

$$\frac{\partial \xi}{\partial x} = \xi_x \quad , \quad \frac{\partial \xi}{\partial y} = \xi_y \quad , \quad \frac{\partial \eta}{\partial x} = \eta_x \quad , \quad \frac{\partial \eta}{\partial y} = \eta_y$$

Equations (٣.١٤) and (٣.١٥) may be written in matrix forms as:

$$\begin{bmatrix} \frac{\partial}{\partial x} \\ \frac{\partial}{\partial y} \end{bmatrix} = \begin{bmatrix} \xi_x & \eta_x \\ \xi_y & \eta_y \end{bmatrix} \begin{bmatrix} \frac{\partial}{\partial \xi} \\ \frac{\partial}{\partial \eta} \end{bmatrix} \qquad \text{......(٣.١٦)}$$

Now consider the inverse of transformation, given by:

$$x = x(\xi, \eta) \qquad \text{......(٣.١٧)}$$

$$y = y(\xi, \eta) \qquad \text{......(٣.١٨)}$$

Taking the exact differentials, we have

$$dx = x_\xi d\xi + x_\eta d\eta \qquad \text{......(٣.١٩)}$$

$$dy = y_\xi d\xi + y_\eta d\eta \qquad \text{......(٣.٢٠)}$$

Equations (٣.١٩) and (٣.٢٠) are expressed in a matrix form as:

$$\begin{bmatrix} dx \\ dy \end{bmatrix} = \begin{bmatrix} x_\xi & x_\eta \\ y_\xi & y_\eta \end{bmatrix} \begin{bmatrix} d\xi \\ d\eta \end{bmatrix} \qquad \text{......(٣.٢١)}$$

Reversing the role of the independent variables, we may write

$$d\xi = \xi_x dx + \xi_y dy \qquad \text{......(٣.٢٢)}$$

$$d\eta = \eta_x dx + \eta_y dy \qquad \text{......(٣.٢٣)}$$

Or, in matrix form,

$$\begin{bmatrix} d\xi \\ d\eta \end{bmatrix} = \begin{bmatrix} \xi_x & \xi_y \\ \eta_x & \eta_y \end{bmatrix} \begin{bmatrix} dx \\ dy \end{bmatrix} \qquad \text{......(٣.٢٤)}$$

Multiplying both sides of equation (٣.٢١) by $\begin{bmatrix} x_\xi & x_\eta \\ y_\xi & y_\eta \end{bmatrix}^{-1}$ yields

$$\begin{bmatrix} d\xi \\ d\eta \end{bmatrix} = \begin{bmatrix} x_\xi & x_\eta \\ y_\xi & y_\eta \end{bmatrix}^{-1} \begin{bmatrix} dx \\ dy \end{bmatrix} \qquad \text{......(٣.٢٥)}$$

Comparing equation (٣.٢٤) and (٣.٢٥) yields

$$\begin{bmatrix} \xi_x & \xi_y \\ \eta_x & \eta_y \end{bmatrix} = \begin{bmatrix} x_\xi & x_\eta \\ y_\xi & y_\eta \end{bmatrix}^{-1} \qquad \text{......(٣.٢٦)}$$

Let

$$A = \begin{bmatrix} \xi_x & \xi_y \\ \eta_x & \eta_y \end{bmatrix} \qquad \text{......(٣.٢٧)}$$

$$A^{-1} = \begin{bmatrix} x_\xi & x_\eta \\ y_\xi & y_\eta \end{bmatrix} \qquad \text{......(٣.٢٨)}$$

Following the standard rules for creating the inverse of a matrix, Equation (٣.٢٥) is written as:

$$A=\left|A^{-1}\right|^{-1}=\frac{Transpose\ \ of\ \ factor\ \ A^{-1}}{\left|A^{-1}\right|}$$ ……(٣.٢٩)

$$\text{Transpose of factor } A^{-1}=\begin{bmatrix} y_\eta & -x_\eta \\ -y_\xi & x_\xi \end{bmatrix}$$ ……(٣.٣٠)

$$\left|A^{-1}\right|=x_\xi y_\eta - x_\eta y_\xi = J$$ ……(٣.٣١)

Where J is the Jacobian of the transformation which can be defined by:

$$J=\frac{\partial(x,y)}{\partial(\xi,\eta)}=\begin{vmatrix} x_\xi & x_\eta \\ y_\xi & y_\eta \end{vmatrix}$$ …… (٣.٣٢)

$$J^{-1}=\frac{1}{J}=\frac{1}{\dfrac{\partial(x,y)}{\partial(\xi,\eta)}}=\begin{vmatrix} x_\xi & x_\eta \\ y_\xi & y_\eta \end{vmatrix}^{-1}$$

$$J^{-1}=1/\left(x_\xi y_\eta - x_\eta y_\xi\right)$$ ……(٣.٣٣)

Substituting equations (٣.٢٧), (٣.٣٣) and (٣.٣١) in equation (٣.٢٩) yields,

$$A=J^{-1}\begin{bmatrix} y_\eta & -x_\eta \\ -y_\xi & x_\xi \end{bmatrix}$$ ……(٣.٣٤)

The elements of matrix A may be obtained by:

$$\xi_x = J^{-1} y_\eta$$ ……(٣.٣٥ a)

$$\xi_y = -J^{-1} x_\eta$$ ……(٣.٣٥ b)

$$\eta_x = -J^{-1} y_\xi$$ ……(٣.٣٥ c)

$$\eta_y = J^{-1} x_\xi$$ ……(٣.٣٥ d)

Where J^{-1} is defined by equation (٣.٣٣)

To compute the matrices numerically, equations (٣.٣٥) are used, the matrices $\left(x_{\xi}, x_{\eta}, y_{\xi}, y_{\eta}\right)$are computed initially, from which the Jacobian may be evaluated. These expressions are computed numerically using finite difference approximations, in this case a second-order central difference approximation may be used to compute the transformation derivative for the interior grid points, these are reported by Hoffman, [٣٩].

$$x_{\xi} = \frac{x_{i+1,j} - x_{i-1,j}}{2\Delta\xi} \qquad \text{......(٣.٣٦)}$$

$$x_{\eta} = \frac{x_{i,j+1} - x_{i,j-1}}{2\Delta\eta} \qquad \text{......(٣.٣٧)}$$

$$y_{\xi} = \frac{y_{i+1,j} - y_{i-1,j}}{2\Delta\xi} \qquad \text{......(٣.٣٨)}$$

$$y_{\eta} = \frac{y_{i,j+1} - y_{i,j-1}}{2\Delta\eta} \qquad \text{......(٣.٣٩)}$$

٣.٤.٢ Elliptic Grid Generation

Thompson, [٧], worked extensively on using elliptic PDE's to generate grids. This procedure is similar to that used by Hoffman, [٣٩], and transforms the physical plane into the computational plane where the mapping is controlled by a Poisson's equation.

This mapping is constructed by specifying the desired grid points (x,y) on the boundary of the physical domain.

The distribution of points on the interior is then determined by solving,

$$\xi_{xx} + \xi_{yy} = P(x,y) \qquad \text{...... (٣.٤٠)}$$

$$\eta_{xx} + \eta_{yy} = Q(x,y) \qquad \text{......(٣.٤١)}$$

Where (ξ,η)represents the coordinate in the computational domain and $(P,Q)$are terms which control the point spacing on the interior of physical domain.

For numerical evaluation of the grid, equations (٣.٤٠) and (٣.٤١) is found inconvenient to use ξ and η as independent variables, and x and y as dependent variables.

To transform the elliptic (PDEs), the dependent and independent variables are interchanged.

Consider a function (f), where it is required to determine its first- and second-order derivatives in the computational domain. The first-order derivatives are evaluated by using Equations (٣.١٤) and (٣.١٥),

Therefore,

$$\frac{\partial f}{\partial x} = f_x = \xi_x f_\xi + \eta_x f_\eta$$ ……(٣.٤٢)

$$\frac{\partial f}{\partial y} = f_y = \xi_y f_\xi + \eta_y f_\eta$$ ……(٣.٤٣)

These equations may be rearranged by utilizing Equations (٣.٣٥ a) through (٣.٣٥d) hence,

$$f_x = J^{-1}\left(y_\eta f_\xi - y_\xi f_\eta\right)$$ ……(٣.٤٤)

$$f_y = J^{-1}\left(x_\xi f_\eta - x_\eta f_\xi\right)$$ ……(٣.٤٥)

To determine the second-order derivatives, f_{xx} and f_{yy}, the following mathematical manipulations are performed:

$$\begin{aligned}
\frac{\partial^2 f}{\partial x^2} &= \frac{\partial}{\partial x}\left(\frac{\partial f}{\partial x}\right) = \frac{\partial}{\partial x}\left(\xi_x f_\xi + \eta_x f_\eta\right) \\
&= \left(\xi_x \frac{\partial}{\partial \xi} + \eta_x \frac{\partial}{\partial \eta}\right)\left(\xi_x f_\xi + \eta_x f_\eta\right) \\
&= \xi_x \frac{\partial}{\partial \xi}\left(\xi_x f_\xi + \eta_x f_\eta\right) + \eta_x \frac{\partial}{\partial \eta}\left(\xi_x f_\xi + \eta_x f_\eta\right) \\
&= \xi_x^2 f_{\xi\xi} + \xi_x f_\xi \frac{\partial}{\partial \xi}\left(\xi_x\right) + \xi_x \eta_x f_{\xi\eta} + \xi_x f_\eta \frac{\partial}{\partial \xi}\left(\eta_x\right) \\
&\quad + \eta_x \xi_x f_{\xi\eta} + \eta_x f_\xi \frac{\partial}{\partial \eta}\left(\xi_x\right) + \eta_x^2 f_{\eta\eta} + \eta_x f_\eta \frac{\partial}{\partial \eta}\left(\eta_x\right)
\end{aligned}$$ ……(٣.٤٦)

This equation is reduced to the following if relations' (٣.٣٥ a) through (٣.٣٥ d) are used,

i.e.,

$$\frac{\partial^2 f}{\partial x^2} = J^{-1}\left(y_\eta^2 f_{\xi\xi} - 2y_\xi y_\eta f_{\xi\eta} + y_\xi^2 f_{\eta\eta}\right) + J^{-1} y_\eta \left[f_\xi \frac{\partial}{\partial\xi}(\xi_x) + f_\eta \frac{\partial}{\partial\xi}(\eta_x)\right]$$
$$+\left(-J^{-1} y_\xi\right)\left[f_\xi \frac{\partial}{\partial\eta}(\xi_x) + f_\eta \frac{\partial}{\partial\eta}(\eta_x)\right] \qquad \text{......(٣.٤٧)}$$

At this point, the derivatives of the metrics are determined as follows:

$$\frac{\partial}{\partial\xi}(\xi_x) = \frac{\partial}{\partial\xi}\left(J^{-1} y_\eta\right) = \frac{\partial}{\partial\xi}\left(\frac{y_\eta}{x_\xi y_\eta - x_\eta y_\xi}\right)$$
$$= J^{-2}\left[y_{\xi\eta}\left(x_\xi y_\eta - x_\eta y_\xi\right) - y_\eta\left(y_\eta x_{\xi\xi} + x_\xi y_{\xi\eta} - x_\eta y_{\xi\xi} - y_\xi x_{\xi\eta}\right)\right]$$
$$= J^{-2}\left(x_\xi y_\eta y_{\xi\eta} - x_\eta y_\xi y_{\xi\eta} - y_\eta^2 x_{\xi\xi} - x_\xi y_\eta y_{\xi\eta} + x_\eta y_\eta y_{\xi\xi} + y_\xi y_\eta x_{\xi\eta}\right)$$
$$\text{......(٣.٤٨)}$$

Similarly,

$$\frac{\partial}{\partial\xi}(\eta_x) = \frac{\partial}{\partial\xi}\left(-J^{-1} y_\xi\right)$$
$$= -J^{-2}\left(x_\xi y_\eta y_{\xi\xi} - x_\eta y_\xi y_{\xi\xi} - y_\xi y_\eta x_{\xi\xi} - x_\xi y_\xi y_{\xi\eta}\right.$$
$$\left. + x_\eta y_\xi y_{\xi\xi} + y_\xi^2 x_{\xi\eta}\right) \qquad \text{......(٣.٤٩)}$$

$$\frac{\partial}{\partial\eta}(\xi_x) = \frac{\partial}{\partial\eta}\left(J^{-1} y_\eta\right)$$
$$= J^{-2}\left(x_\xi y_\eta y_{\eta\eta} - x_\eta y_\xi y_{\eta\eta} - x_\xi y_\eta y_{\eta\eta} - y_\eta^2 x_{\xi\eta}\right.$$
$$\left. + y_\xi y_\eta x_{\eta\eta} + x_\eta y_\eta y_{\xi\eta}\right) \qquad \text{......(٣.٥٠)}$$

$$\frac{\partial}{\partial\eta}(\eta_x) = \frac{\partial}{\partial\eta}\left(-J^{-1} y_\xi\right)$$
$$= -J^{-2}\left(x_\xi y_\eta y_{\xi\eta} - x_\eta y_\xi y_{\xi\eta} - y_\xi x_\xi y_{\eta\eta} - y_\xi y_\eta x_{\xi\eta}\right.$$
$$\left. + y_\xi^2 x_{\eta\eta} + x_\eta y_\xi y_{\xi\eta}\right) \qquad \text{......(٣.٥١)}$$

Substitution of Equations (٣.٤٨) through (٣.٥١) into Equation (٣.٤٧) and rearranging terms yields:

$$\frac{\partial^2 f}{\partial x^2} = -J^{-2}\left(y_\eta^2 f_{\xi\xi} - 2y_\xi y_\eta f_{\xi\eta} + y_\xi^2 f_{\eta\eta}\right) + J^{-3}\left\{\left(y_\eta^2 y_{\xi\xi} - 2y_\xi y_\eta y_{\xi\eta} + y_\xi^2 y_{\eta\eta}\right)\right.$$
$$\left.\left(x_\eta f_\xi - x_\xi f_\eta\right) + \left(y_\eta^2 x_{\xi\xi} - 2y_\xi y_\eta x_{\xi\eta} + y_\xi^2 x_{\eta\eta}\right)\left(y_\xi f_\eta - y_\eta f_\xi\right)\right\}$$

……(٣.٥٢)

Similarly,

$$\frac{\partial^2 f}{\partial y^2} = J^{-2}\left(x_\eta^2 f_{\xi\xi} - 2x_\xi x_\eta f_{\xi\eta} + x_\xi^2 f_{\eta\eta}\right) + J^{-3}\left\{\left(x_\eta^2 y_{\xi\xi} - 2x_\xi x_\eta y_{\xi\eta} + x_\xi^2 y_{\eta\eta}\right)\right.$$
$$\left.\left(x_\eta f_\xi - x_\xi f_\eta\right) + \left(x_\eta^2 x_{\xi\xi} - 2x_\xi x_\eta x_{\xi\eta} + x_\xi^2 x_{\eta\eta}\right)\left(y_\xi f_\eta - y_\eta f_\xi\right)\right\}$$

……(٣.٥٣)

Now consider the laplacian,

$$\nabla^2 f = \frac{\partial^2 f}{\partial x^2} + \frac{\partial^2 f}{\partial y^2}$$ **……(٣.٥٤)**

And substitute Equations (٣.٥٢) and (٣.٥٣). After simplification and collection of terms, we obtain

$$\begin{aligned}\nabla^2 f = {} & J^{-2}\left[\left(x_\eta^2 + y_\eta^2\right)f_{\xi\xi} - 2\left(x_\xi x_\eta + y_\xi y_\eta\right)f_{\xi\eta} + \left(x_\xi^2 + y_\xi^2\right)f_{\eta\eta}\right] \\ & + J^{-3}\left\{\left[\left(x_\eta^2 + y_\eta^2\right)y_{\xi\xi} - 2\left(x_\xi x_\eta + y_\xi y_\eta\right)y_{\xi\eta} + \left(x_\xi^2 + y_\xi^2\right)y_{\eta\eta}\right]\left(x_\eta f_\xi - x_\xi f_\eta\right)\right. \\ & \left. + \left[\left(x_\eta^2 + y_\eta^2\right)x_{\xi\xi} - 2\left(x_\xi x_\eta + y_\xi y_\eta\right)x_{\xi\eta} + \left(x_\xi^2 + y_\xi^2\right)x_{\eta\eta}\right]\left(y_\xi f_\eta - y_\eta f_\xi\right)\right\}\end{aligned}$$

……(٣.٥٥)

Then

$$\begin{aligned}\nabla^2 f = {} & J^{-2}\left(af_{\xi\xi} - 2bf_{\xi\eta} + cf_{\eta\eta}\right) + J^{-3}\left\{\left(ay_{\xi\xi} - 2by_{\xi\eta} + cy_{\eta\eta}\right)\left(x_\eta f_\xi - x_\xi f_\eta\right)\right. \\ & \left. + \left(ax_{\xi\xi} - 2bx_{\xi\eta} + cx_{\eta\eta}\right)\left(y_\xi f_\eta - y_\eta f_\xi\right)\right\}\end{aligned}$$ **……(٣.٥٦)**

Where

$$a = x_{\eta}^{2} + y_{\eta}^{2}$$ ……(٣.٥٧ a)

$$b = x_{\xi} x_{\eta} + y_{\xi} y_{\eta}$$ ……(٣.٥٧ b)

$$c = x_{\xi}^{2} + y_{\xi}^{2}$$ ……(٣.٥٧ c)

Let,

$$a x_{\xi\xi} - 2b x_{\xi\eta} + c x_{\eta\eta} = \alpha$$

$$a y_{\xi\xi} - 2b y_{\xi\eta} + c y_{\eta\eta} = \beta$$

so, the equation (٣.٥٦) becomes

$$\nabla^{2} f = J^{-2}\left(a f_{\xi\xi} - 2b f_{\xi\eta} + c f_{\eta\eta}\right) + J^{-3}\left\{\beta\left(x_{\eta} f_{\xi} - x_{\xi} f_{\eta}\right) + \alpha\left(y_{\xi} f_{\eta} - y_{\eta} f_{\xi}\right)\right\}$$

……(٣.٥٨)

Let

$$d = J^{-1}\left(\alpha y_{\xi} - \beta x_{\xi}\right)$$ ……(٣.٥٩ a)

$$e = J^{-1}\left(\beta x_{\eta} - \alpha y_{\eta}\right)$$ ……(٣.٥٩ b)

so, the equation (٣.٥٨) becomes

$$\nabla^{2} f = J^{-2}\left(a f_{\xi\xi} - 2b f_{\xi\eta} + c f_{\eta\eta} + d f_{\eta} + e f_{\xi}\right)$$ ……(٣.٦٠)

If f=ξ

$$\xi_{\xi} = \frac{\partial \xi}{\partial \xi} = 1 \quad , \quad \xi_{\eta} = \frac{\partial \xi}{\partial \eta} = 0 \quad , \quad \xi_{\xi\xi} = \frac{\partial}{\partial \xi}\left(\frac{\partial \xi}{\partial \xi}\right) = 0$$
$$\xi_{\eta\eta} = \frac{\partial}{\partial \eta}\left(\frac{\partial \xi}{\partial \eta}\right) = 0 \quad , \quad \xi_{\xi\eta} = \frac{\partial}{\partial \eta}\left(\frac{\partial \xi}{\partial \xi}\right) = 0$$ ……(٣.٦١)

By substitution equation (٣.٦١) in equation (٣.٥٢) we get

$$\xi_{xx} = J^{-3}\left\{y_{\eta}^{2}\left(y_{\xi\xi} x_{\eta} - x_{\xi\xi} y_{\eta}\right) - 2 y_{\xi} y_{\eta}\left(y_{\xi\eta} x_{\eta} - x_{\xi\eta} y_{\eta}\right) + y_{\xi}^{2}\left(y_{\eta\eta} x_{\eta} - x_{\eta\eta} y_{\eta}\right)\right\}$$ ……(٣.٦٢)

And by substitution equation (٣.٦١) in equation (٣.٥٣) we get

$$\xi_{yy} = J^{-3}\left\{x_\eta^2\left(y_{\xi\xi}x_\eta - x_{\xi\xi}y_\eta\right) - 2x_\xi x_\eta\left(y_{\xi\eta}x_\eta - x_{\xi\eta}y_\eta\right) + x_\xi^2\left(y_{\eta\eta}x_\eta - x_{\eta\eta}y_\eta\right)\right\} \qquad \text{......(٣.٦٣)}$$

If f=η

$$\eta_\eta = \frac{\partial\eta}{\partial\eta} = 1 \quad , \quad \eta_\xi = \frac{\partial\eta}{\partial\xi} = 0 \quad , \quad \eta_{\xi\xi} = \frac{\partial}{\partial\xi}\left(\frac{\partial\eta}{\partial\xi}\right) = 0$$
$$\eta_{\eta\eta} = \frac{\partial}{\partial\eta}\left(\frac{\partial\eta}{\partial\eta}\right) = 0 \quad , \quad \eta_{\xi\eta} = \frac{\partial}{\partial\xi}\left(\frac{\partial\eta}{\partial\eta}\right) = 0 \qquad \text{......(٣.٦٤)}$$

By substitution equation (٣.٦٤) in equation (٣.٥٢) we get

$$\eta_{xx} = J^{-3}\left\{y_\eta^2\left(x_{\xi\xi}y_\xi - y_{\xi\xi}x_\xi\right) - 2y_\xi y_\eta\left(x_{\xi\eta}y_\xi - y_{\xi\eta}x_\xi\right) + y_\xi^2\left(x_{\eta\eta}y_\xi - y_{\eta\eta}x_\xi\right)\right\} \qquad \text{......(٣.٦٥)}$$

And by substitution equation (٣.٦٤) in equation (٣.٥٣) we get

$$\eta_{yy} = J^{-3}\left\{x_\eta^2\left(x_{\xi\xi}y_\xi - y_{\xi\xi}x_\xi\right) - 2x_\xi x_\eta\left(x_{\xi\eta}y_\xi - y_{\xi\eta}x_\xi\right) + x_\xi^2\left(x_{\eta\eta}y_\xi - y_{\eta\eta}x_\xi\right)\right\} \qquad \text{......(٣.٦٦)}$$

Using equation (٣.٤٠) and (٣.٤١), it can be written that

$$\nabla^2\xi = P \qquad \text{......(٣.٦٧)}$$

$$\nabla^2\eta = Q \qquad \text{......(٣.٦٨)}$$

From equation (٣.٦٠)

If f=ξ

$$\nabla^2\xi = J^{-2}e \qquad \text{......(٣.٦٩)}$$

By equating both of equation (٣.٦٧) and (٣.٦٩)

$$P = J^{-3}\left(\beta x_\eta - \alpha y_\eta\right) \qquad \text{......(٣.٧٠)}$$

Similarly ,if f=η

$\nabla^2 \eta = J^{-2} d$ ......(٣.٧١)

By equating equation (٣.٦٨) to equation (٣.٧١) we get,

$Q = J^{-3}\left(\alpha y_{\xi} - \beta x_{\xi}\right)$ ......(٣.٧٢)

So, the transformed of equations (٣.٤٠) and (٣.٤١) are:

$a x_{\xi\xi} - 2b x_{\xi\eta} + c x_{\eta\eta} = -J^{2}\left(P x_{\xi} + Q x_{\eta}\right)$ ......(٣.٧٣)

$a y_{\xi\xi} - 2b y_{\xi\eta} + c y_{\eta\eta} = -J^{2}\left(P y_{\xi} + Q y_{\eta}\right)$ ......(٣.٧٤)

To discretize the different terms in equations (٣.٧٣) and (٣.٧٤) for P=Q=٠ (Laplace's equation) as follows:

$$a_{i,j} = \left(\frac{x_{i,j+1} - x_{i,j-1}}{2\Delta\eta}\right)^{2} + \left(\frac{y_{i,j+1} - y_{i,j-1}}{2\Delta\eta}\right)^{2}$$

$$b_{i,j} = \left(\frac{x_{i+1,j} - x_{i-1,j}}{2\Delta\xi}\right)\left(\frac{x_{i,j+1} - x_{i,j-1}}{2\Delta\eta}\right) + \left(\frac{y_{i+1,j} - y_{i-1,j}}{2\Delta\xi}\right)\left(\frac{y_{i,j+1} - y_{i,j-1}}{2\Delta\eta}\right)$$

$$c_{i,j} = \left(\frac{x_{i+1,j} - x_{i-1,j}}{2\Delta\xi}\right)^{2} + \left(\frac{y_{i+1,j} - y_{i-1,j}}{2\Delta\xi}\right)^{2}$$

$$x_{\xi\xi} = \frac{x_{i+1,j} - 2x_{i,j} + x_{i-1,j}}{\Delta\xi^{2}}$$

$$x_{\xi\eta} = \frac{x_{i+1,j+1} - x_{i+1,j-1} - x_{i-1,j+1} + x_{i-1,j-1}}{4(\Delta\xi)(\Delta\eta)}$$

$$x_{\eta\eta} = \frac{x_{i,j+1} - 2x_{i,j} + x_{i,j-1}}{\Delta\eta^{2}}$$

$$y_{\xi\xi}=\frac{y_{i+1,j}-2y_{i,j}+y_{i-1,j}}{\Delta\xi^2}$$

$$y_{\xi\eta}=\frac{y_{i+1,j+1}-y_{i+1,j-1}-y_{i-1,j+1}+y_{i-1,j-1}}{4(\Delta\xi)(\Delta\eta)}$$

$$y_{\eta\eta}=\frac{y_{i,j+1}-2y_{i,j}+y_{i,j-1}}{\Delta\eta^2}$$

The subscripts (i) , (j) refer to grid points in ξ and η coordinates, respectively. Further, although in the above formulation, grid sizes $\Delta\xi$ and $\Delta\eta$ in the body-fitted coordinate system are constant, this need not be the case in the Cartesian system. This allows clustering of grid points somewhat near points where it matters.

Substitution of the above discretized terms into equation (٣.٧٣) for P=Q=٠ we get,

$$a_{i,j}\left[\frac{x_{i+1,j}-2x_{i,j}+x_{i-1,j}}{\Delta\xi^2}\right]-2b_{i,j}\left[\frac{x_{i+1,j+1}-x_{i+1,j-1}-x_{i-1,j+1}+x_{i-1,j-1}}{4(\Delta\xi)(\Delta\eta)}\right]$$

$$+c_{i,j}\left[\frac{x_{i,j+1}-2x_{i,j}+x_{i,j-1}}{\Delta\eta^2}\right]=0 \qquad \text{......(٣.٧٥)}$$

And if we substitution of the above discretized terms into equation (٣.٧٤) for P=Q=٠ we get,

$$a_{i,j}\left[\frac{y_{i+1,j}-2y_{i,j}+y_{i-1,j}}{\Delta\xi^2}\right]-2b_{i,j}\left[\frac{y_{i+1,j+1}-y_{i+1,j-1}-y_{i-1,j+1}+y_{i-1,j-1}}{4(\Delta\xi)(\Delta\eta)}\right]$$

$$+c_{i,j}\left[\frac{y_{i,j+1}-2y_{i,j}+y_{i,j-1}}{\Delta\eta^2}\right]=0 \qquad \text{......(٣.٧٦)}$$

Both of equation (٣.٧٥) and (٣.٧٦) can be solved easily by the Gauss-Siedel iterative method,

So, the equation (٣.٧٥) is rearranged as:

$$x_{i,j}=\left\{\frac{a_{i,j}}{(\Delta\xi)^2}\left(x_{i+1,j}+x_{i-1,j}\right)+\frac{c_{i,j}}{(\Delta\eta)^2}\left(x_{i,j+1}+x_{i,j-1}\right)-\frac{b_{i,j}}{2(\Delta\xi)(\Delta\eta)}*\right.$$
$$\left.\left(x_{i+1,j+1}-x_{i-1,j+1}-x_{i+1,j-1}+x_{i-1,j-1}\right)\right\}\Big/2\left(\frac{a_{i,j}}{(\Delta\xi)^2}+\frac{c_{i,j}}{(\Delta\eta)^2}\right)\qquad\text{......(٣.٧٧)}$$

Similarly, equation (٣.٧٦) becomes

$$y_{i,j}=\left\{\frac{a_{i,j}}{(\Delta\xi)^2}\left(y_{i+1,j}+y_{i-1,j}\right)+\frac{c_{i,j}}{(\Delta\eta)^2}\left(y_{i,j+1}+y_{i,j-1}\right)-\frac{b_{i,j}}{2(\Delta\xi)(\Delta\eta)}*\right.$$
$$\left.\left(y_{i+1,j+1}-y_{i-1,j+1}-y_{i+1,j-1}+y_{i-1,j-1}\right)\right\}\Big/2\left(\frac{a_{i,j}}{(\Delta\xi)^2}+\frac{c_{i,j}}{(\Delta\eta)^2}\right)\qquad\text{......(٣.٧٨)}$$

To start the solution, an initial distribution of **x** and **y** coordinates of the grid points within the physical domain must be provided by using an algebraic model, and this coordinates (x, y) are used as initial values to solve both of equation (٣.٧٧) and (٣.٧٨). The coefficients **a**, **b** and **c** are determined from equations (٣.٥٧). The resultant mesh is shown in Fig. (٣-٤ b).

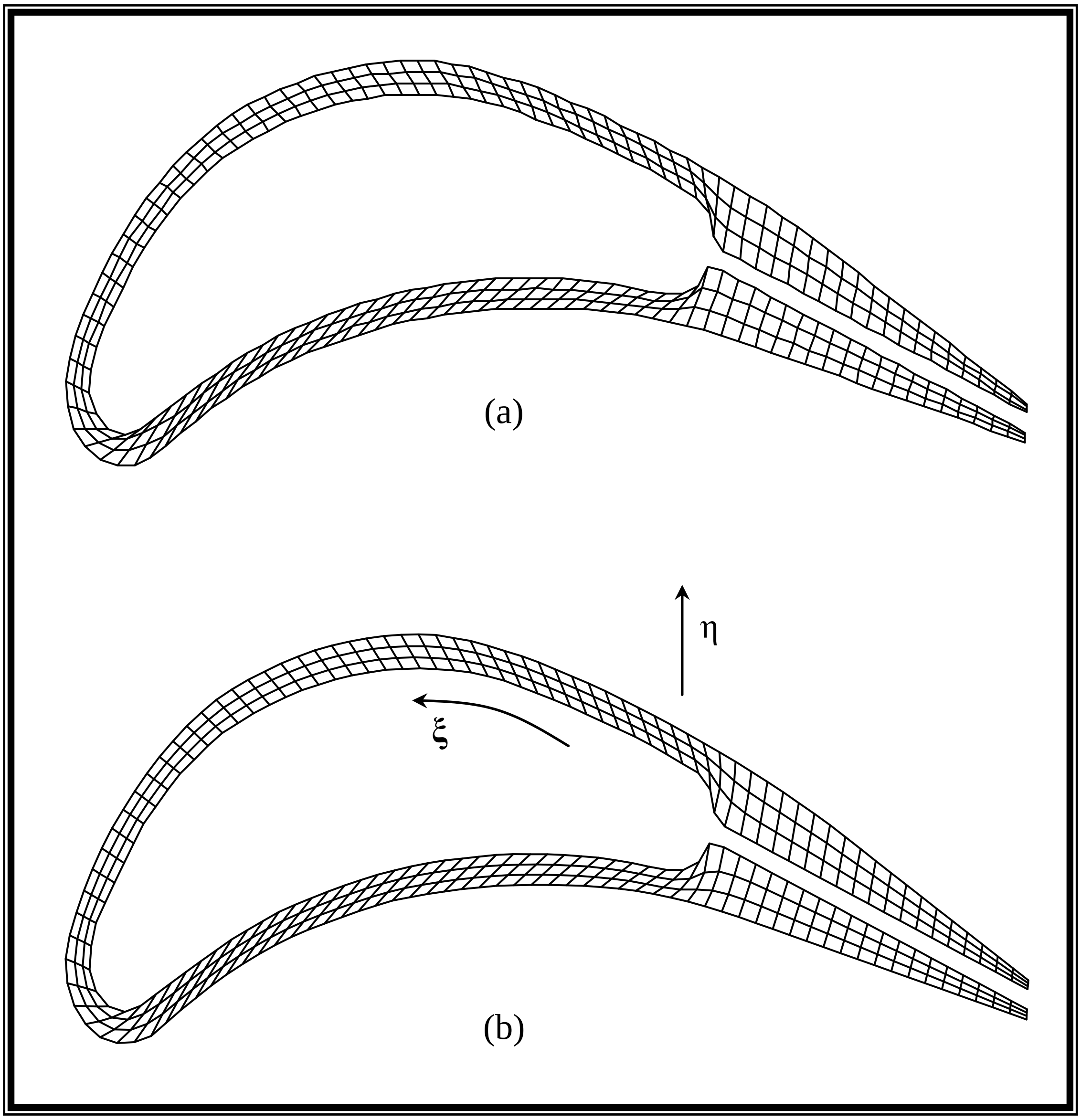

Fig. (٣-٤) (a) Algebraic Grid Generation
(b) Two-Dimensional Grid in Physical Plane

From Fig. (٣-٤ b) there is clearly a high degree of skewness in some regions of the domain. This skewness will cause some difficulty and inaccuracy in the computation of the normal gradients of the temperature at the surface.

So, Poisson's equation was selected to achieve orthogonality of the grid lines at the surface, these are described by Hoffmann, [٣٩].

Therefore, equations (٣.٧٣) and (٣.٧٤) are written again as follows:

$$a x_{\xi\xi} - 2b x_{\xi\eta} + c x_{\eta\eta} = -J^{2}\left(P x_{\xi} + Q x_{\eta}\right) \qquad \text{......(٣.٧٣)}$$

$$a y_{\xi\xi} - 2b y_{\xi\eta} + c y_{\eta\eta} = -J^{2}\left(P y_{\xi} + Q y_{\eta}\right) \qquad \text{......(٣.٧٤)}$$

Where P and Q are source or forcing terms to be prescribed. The $P(\xi,\eta)$ function is used to attract ξ - coordinate line or to a specific point .

Similarly $Q(\xi,\eta)$ is used for attracting η-coordinate lines to a constant η line or to a specific point.

The source terms can be evaluated in a manner based on normal intersection between the boundary and grid lines.

They have the form, showed by ref. [٨]

$$P = \phi(\xi,\eta)\left(\xi_{x}^{2} + \xi_{y}^{2}\right) \qquad \text{......(٣.٧٩)}$$

$$Q = \psi(\xi,\eta)\left(\eta_{x}^{2} + \eta_{y}^{2}\right) \qquad \text{......(٣.٨٠)}$$

Substituting in equation (٣.٧٣) and (٣.٧٤) both of this equation can be written as:

$$a\left(x_{\xi\xi} + \phi\, x_{\xi}\right) - 2b x_{\xi\eta} + c\left(x_{\eta\eta} + \psi\, x_{\eta}\right) = 0 \qquad \text{......(٣.٨١)}$$

$$a\left(y_{\xi\xi} + \phi\, y_{\xi}\right) - 2b y_{\xi\eta} + c\left(y_{\eta\eta} + \psi y_{\eta}\right) = 0 \qquad \text{......(٣.٨٢)}$$

Where ϕ and ψ are specified through the boundary conditions. On the boundaries, the ϕ and ψ functions are determined by setting the quantities in parentheses equal to zero.

Along $\xi =$ constant boundaries, Middlecoff and Thomas illustrated by Ref.[٨], require,

$$\begin{aligned} x_{\eta\eta} + \psi\, x_{\eta} &= 0 \\ y_{\eta\eta} + \psi\, y_{\eta} &= 0 \end{aligned} \qquad \text{......(٣.٨٣)}$$

And along η = constant boundaries

$$x_{\xi\xi} + \phi x_{\xi} = 0$$
$$y_{\xi\xi} + \phi y_{\xi} = 0 \qquad \text{......(٣.٨٤)}$$

So, from the above equations

$$\phi = \frac{-\left(x_{\xi} x_{\xi\xi} + y_{\xi} y_{\xi\xi}\right)}{\left(x_{\xi}^{2} + y_{\xi}^{2}\right)} \qquad \text{on } \eta = \eta_b \qquad \text{......(٣.٨٥)}$$

$$\psi = \frac{-\left(x_{\eta} x_{\eta\eta} + y_{\eta} y_{\eta\eta}\right)}{\left(x_{\eta}^{2} + y_{\eta}^{2}\right)} \qquad \text{on } \xi = \xi_b \qquad \text{......(٣.٨٦)}$$

The parameters ϕ and ψ are calculated at each mesh point in the boundary, then its value at interior mesh points can be computed by linear interpolation.

Gauss Siedel method is used to solve equations (٣.٨١) and (٣.٨٢). This application will give us a new grid shown in Fig. (٣-٥)

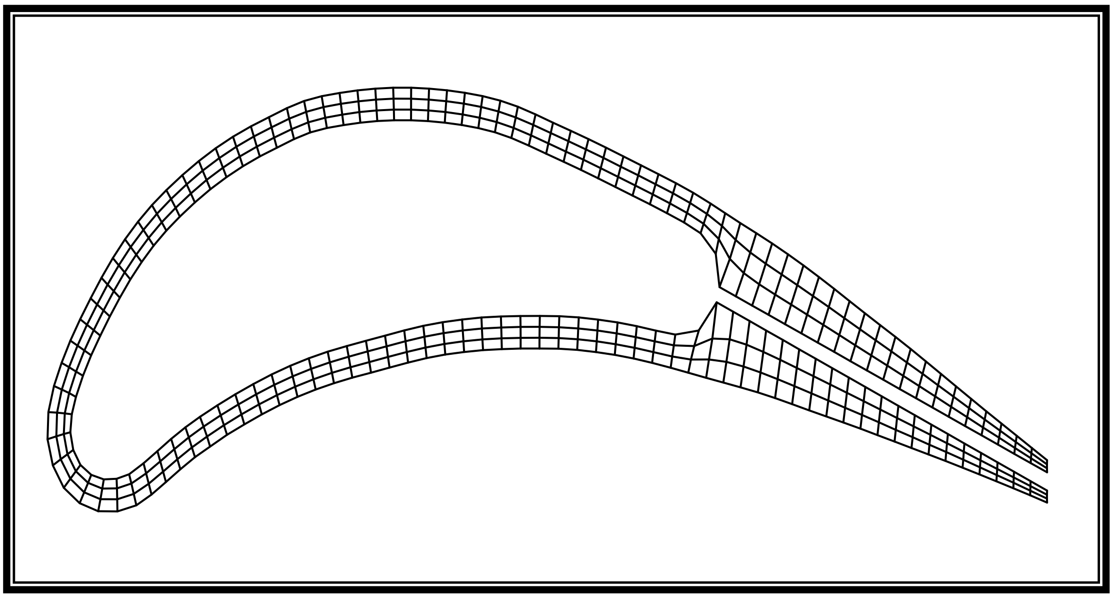

Fig. (٣-٥) Orthogonal Grid Generation

٣.٥ Transformation of Governing Heat Transfer Equations: -

The next step in this work is the transformation of governing heat transfer equations (conduction, convection).

Recalling from section (٣.٤.١), the transformation that includes the demonstration of how the governing equations can be mapped from physical coordinates to computational coordinates.

Firstly, we will transform the equation related to the steady-state heat conduction, which takes place inside the metal of the blade (interior nodes).

For steady-state, two dimensional, the basic equation for temperature field can be written as:

$$\frac{\partial^2 T}{\partial x^2}+\frac{\partial^2 T}{\partial y^2}=0 \qquad \text{......(٣.٨٧)}$$

The two partial derivatives will be transformed to a new computational domain as follows:

$$\frac{\partial T}{\partial x}=\frac{\partial T}{\partial \xi}\frac{\partial \xi}{\partial x}+\frac{\partial T}{\partial \eta}\frac{\partial \eta}{\partial x}$$

$$\frac{\partial T}{\partial x}=T_\xi \xi_x+T_\eta \eta_x \qquad \text{......(٣.٨٨)}$$

Similarly ,

$$\frac{\partial T}{\partial y}=T_\xi \xi_y+T_\eta \eta_y \qquad \text{......(٣.٨٩)}$$

Then,

$$\frac{\partial^2 T}{\partial x^2}=\frac{\partial}{\partial x}\left(\frac{\partial T}{\partial x}\right)=\frac{\partial}{\partial x}\left(T_\xi \xi_x+T_\eta \eta_x\right) \qquad \text{......(٣.٩٠)}$$

Recalling that equation (٣.١٤) for $\partial/\partial \mathbf{x}$, after simplification we get,

$$\frac{\partial^2 T}{\partial x^2} = \xi_x^2 T_{\xi\xi} + 2\xi_x \eta_x T_{\xi\eta} + \eta_x^2 T_{\eta\eta} + \xi_{xx} T_\xi + \eta_{xx} T_\eta \qquad \text{......(٣.٩١)}$$

Similarly,

$$\frac{\partial^2 T}{\partial y^2} = \xi_y^2 T_{\xi\xi} + 2\xi_y \eta_y T_{\xi\eta} + \eta_y^2 T_{\eta\eta} + \xi_{yy} T_\xi + \eta_{yy} T_\eta \qquad \text{......(٣.٩٢)}$$

By substitution both of equations (٣.٩١) and (٣.٩٢) in equation (٣.٨٧) this equation becomes,

$$\begin{aligned} &\left(\xi_x^2 + \xi_y^2\right) T_{\xi\xi} + 2\left(\xi_x \eta_x + \xi_y \eta_y\right) T_{\xi\eta} + \left(\eta_x^2 + \eta_y^2\right) T_{\eta\eta} \\ &+ \left(\xi_{xx} + \xi_{yy}\right) T_\xi + \left(\eta_{xx} + \eta_{yy}\right) T_\eta = 0 \end{aligned} \qquad \text{......(٣.٩٣)}$$

Equation (٣.٩٣) can be applied to the interior nodes to get the temperature distribution in these nodes.

Where ξ_x , ξ_y , η_x , η_y ,and ξ_{xx} , ξ_{yy} , η_{xx} , η_{yy} were defined in the last sections. For central-difference approximation

$$T_{\xi\xi} = \frac{T_{i+1,j} - 2T_{i,j} + T_{i-1,j}}{\Delta\xi^2} \qquad \text{......(٣.٩٤)}$$

$$T_{\xi\eta} = \frac{T_{i+1,j+1} - T_{i+1,j-1} - T_{i-1,j+1} + T_{i-1,j-1}}{4(\Delta\xi)(\Delta\eta)} \qquad \text{......(٣.٩٥)}$$

$$T_{\eta\eta} = \frac{T_{i,j+1} - 2T_{i,j} + T_{i,j-1}}{\Delta\eta^2} \qquad \text{......(٣.٩٦)}$$

$$T_\xi = \frac{T_{i+1,j} - T_{i-1,j}}{2\Delta\xi} \qquad \text{......(٣.٩٧)}$$

$$T_\eta = \frac{T_{i,j+1} - T_{i,j-1}}{2\Delta\eta} \qquad \text{......(٣.٩٨)}$$

Let,

$$\left.\begin{aligned} a_1 &= \xi_x^2 + \xi_y^2 \\ b_1 &= \xi_x\eta_x + \xi_y\eta_y \\ c_1 &= \eta_x^2 + \eta_y^2 \\ d_1 &= \xi_{xx} + \xi_{yy} \\ e_1 &= \eta_{xx} + \eta_{yy} \end{aligned}\right\} \quad \text{......(٣.٩٩)}$$

By substitution the equations (٣.٩٤ to ٣.٩٩) in equation (٣.٩٣) we get,

$$\left(T_{i+1,j} + T_{i-1,j}\right) + \frac{b_1}{2\Delta\xi\Delta\eta}\left(T_{i+1,j+1} - T_{i+1,j-1} - T_{i-1,j+1}\right.$$

$$\left.{}_{j-1}\right) + \frac{c_1}{\Delta\eta^2}\left(T_{i,j+1} + T_{i,j-1}\right) + \frac{d_1}{2\Delta\xi}\left(T_{i+1,j} - T_{i-1,j}\right)$$

$$+\frac{e_1}{2\Delta\eta}\left(T_{i,j+1} - T_{i,j-1}\right)\Big\} \Big/ \left(\frac{2a_1}{\Delta\xi^2} + \frac{2c_1}{\Delta\eta^2}\right) \quad \text{......(٣.١٠٠)}$$

For surface nodes (outer and inner) where convection heat transfer is the interested mode, the transformation applied to the distances between nodes along the blade in order to be acceptable for using in determining the temperature distribution in these nodes.

The distance along the blade as shown in Fig. (٣-٦) is:

$$s = \sqrt{dx^2 + dy^2} \quad \text{...... (٣.١٠١)}$$

Recalling from equations (٣.١٩) and (٣.٢٠) and along constant (η) lines, dη =٠, dξ =١ so that,

$$dx = x_\xi \ , \ dy = y_\xi$$

It gives,

$$s_\xi = \sqrt{x_\xi^2 + y_\xi^2} \quad \text{......(٣.١٠٢)}$$

Along constant (ξ) lines, dξ =٠, dη =١ so that,

$$dx = x_{\eta} \;,\; dy = y_{\eta}$$

it gives,

$$s_{\eta} = \sqrt{x_{\eta}^{2} + y_{\eta}^{2}} \qquad \text{......(٣.١٠٣)}$$

The distance along the blade surface between nodes (i) and (i+١) as shown in Fig. (٣-٦) is,

$$s_{\xi_1} = \sqrt{\left(x_{i+1,j} - x_{i,j}\right)^{2} + \left(y_{i+1,j} - y_{i,j}\right)^{2}} \qquad \text{......(٣.١٠٤)}$$

And between nodes (i) and (i-١) as shown in Fig. (٣-٦) is,

$$s_{\xi_2} = \sqrt{\left(x_{i,j} - x_{i-1,j}\right)^{2} + \left(y_{i,j} - y_{i-1,j}\right)^{2}} \qquad \text{......(٣.١٠٥)}$$

The distance along the line connecting the two surfaces, between node (j) and (j+١) as shown in Fig. (٣-٦) is,

$$s_{\eta_1} = \sqrt{\left(x_{i,j+1} - x_{i,j}\right)^2 + \left(y_{i,j+1} - y_{i,j}\right)^2} \qquad \text{......(٣.١٠٦)}$$

And between nodes (j) and (j-١) as shown in Fig. (٣-٦) is,

$$s_{\eta_2} = \sqrt{\left(x_{i,j} - x_{i,j-1}\right)^2 + \left(y_{i,j} - y_{i,j-1}\right)^2} \qquad \text{......(٣.١٠٧)}$$

The energy equation for the surface nodes can be written as:

$$\mathbf{q_{conduction}} = \mathbf{q_{convection}} \qquad \text{......(٣.١٠٨)}$$

Where,

$$q_{conduction} = -k\, A_c \frac{dT}{dS} \qquad \text{......(٣.١٠٩)}$$

$$q_{convection} = hA_{conv}.\Delta\, T \qquad \text{......(٣.١١٠)}$$

For external surface nodes see Fig. (٣-٦ a) the equation (٣.١٠٨) becomes

$$_1 - k\left(\frac{S_{\eta 1}}{2}\right)T_{\xi 2} - k\left(\frac{S_{\xi 1} + S_{\xi 2}}{2}\right)T_{\eta 1}$$

$$= h_{ex}\left(\frac{S_{\xi 1} + S_{\xi 2}}{2}\right)\left(T_\infty - T_{i,j}\right)$$

Where,

$$T_{\xi 1} = \frac{T_{i+1,j} - T_{i,j}}{S_{\xi 1}} \qquad \text{......(٣.١١٢)}$$

$$T_{\xi 2} = \frac{T_{i-1,j} - T_{i,j}}{S_{\xi 2}} \qquad \text{......(٣.١١٣)}$$

$$T_{\eta 1} = \frac{T_{i,j+1} - T_{i,j}}{S_{\eta 1}} \qquad \text{......(٣.١١٤)}$$

$$T_\infty = T_h \qquad \text{......(٣.١١٥)}$$

Where, T_h is the temperature of a hot gas.

Let,

$$a_2 = \frac{S_{\xi 1} + S_{\xi 2}}{2S_{\eta 1}} \qquad \text{……(٣.١١٦)}$$

$$b_2 = \frac{S_{\eta 1}}{2S_{\xi 1}} \qquad \text{……(٣.١١٧)}$$

$$c_2 = \frac{S_{\eta 1}}{2S_{\xi 2}} \qquad \text{……(٣.١١٨)}$$

$$d_2 = \left(\frac{S_{\xi 1} + S_{\xi 2}}{2k}\right) * h_{ex} \qquad \text{……(٣.١١٩)}$$

So the equation (٣.١١١) after rearrangement becomes,

$$T_{i,j} = \frac{1}{a_2 + b_2 + c_2 + d_2}\left\{a_2 T_{i,j+1} + b_2 T_{i+1,j} + c_2 T_{i-1,j} + d_2 T_h\right\} \qquad \text{……(٣.١٢٠)}$$

Similarly, for the internal surface nodes see Fig. (٣-٦ b) the equation (٣.١٠٨) becomes,

$${}_{1} - k\left(\frac{S_{\eta 2}}{2}\right)T_{\xi 2} - k\left(\frac{S_{\xi 1} + S_{\xi 2}}{2}\right)T_{\eta 2}$$

$$= h_{in}\left(\frac{S_{\xi 1} + S_{\xi 2}}{2}\right)\left(T_{i,j} - T_{\infty}\right)$$

Where,

$T_{\xi ١}$ and $T_{\xi ٢}$ are prescribed in equations (٣.١١٢) and (٣.١١٣)

$$T_{\eta 2} = \frac{T_{i,j-1} - T_{i,j}}{S_{\eta 2}} \qquad \text{……(٣.١٢٢)}$$

$$T_{\infty} = T_c \qquad \text{……(٣.١٢٣)}$$

Where, T_c is the temperature of cooled air.

Let,

$$a_3 = \frac{S_{\xi 1} + S_{\xi 2}}{2S_{\eta 2}} \qquad \text{......(٣.١٢٤)}$$

$$b_3 = \frac{S_{\eta 2}}{2S_{\xi 1}} \qquad \text{......(٣.١٢٥)}$$

$$c_3 = \frac{S_{\eta 2}}{2S_{\xi 2}} \qquad \text{......(٣.١٢٦)}$$

$$d_3 = \left(\frac{S_{\xi 1} + S_{\xi 2}}{2k}\right) * h_{in} \qquad \text{......(٣.١٢٧)}$$

So the equation (٣.١٢١) after rearrangement becomes,

$$T_{i,j} = \frac{1}{a_3 + b_3 + c_3 - d_3}\left\{a_3 T_{i,j-1} + b_3 T_{i+1,j} + c_3 T_{i-1,j} - d_3 T_c\right\} \qquad \text{......(٣.١٢٨)}$$

Equation (٣.١٠٠) is for interior nodes and equations (٣.١٢٠), (٣.١٢٨) are for surface nodes. They are solved by Gauss-Siedel iterative method with central differences for all derivatives except at the surface nodes.

The solution of the equations using Gauss-Siedel method requires a design of a computer program, which serves to complete the iterations for all nodes and to give the final solution. This program uses equations (٣.١٠٠), (٣.١٢٠) and (٣.١٢٨) with a boundary conditions specified in the next chapter and also the coordinates of the outer, inner and interior points are taken from Fig. (٣-٥).

٣.٦ Convergence Criteria

The Gauss-Seidel iterative solution continues until specified convergence criterion is met. For this purpose the total changes in the dependent variables are evaluated as, these are described by Hoffmann, [٣٩].

$$Error\ W = \sum_{\substack{i=2\\ j=2}}^{\substack{j=j\,max-1\\ i=i\,max-1}} ABS\left[W_{i,j}^{n+1} - W_{i,j}^{n}\right] \qquad \text{......(٣.١٢٩)}$$

Where W represents quantity of interest (T, x and y) and n represents the iterative level. The convergence criteria is set as error < error-max where error-max is a specified input.

In the present study, the error-max is taken as ٠.٠٠١

The number of nodes that the temperature distribution will be predicted on it is (٤٩٦) with (I=١٢٤ and J=٤), and hence, ٤٩٦ equations must be solved to get the temperature distribution on the blade. To solve these equations, Gauss-Siedel iterative method can be used to get the solution for this system of equations with the help of computer program which serves to give the temperature distribution with ٥٠٠ iteration.

CHAPTER FOUR

4

THERMAL ANALYSES OF CASE STUDIES

٤.١ Introduction: -

The blade geometry was introduced in the computational plane $(\xi,\eta)$with the application of transformation and grid generation theories in addition to the transformation of heat transfer equations to make them ready for thermal analyses.

Equations (٣.٩٩), (٣.١١٩), and (٣.١٢٧) will be used to determine the temperature distribution within the blade for all nodes resulted from grid generation technique. Equation (٣.٩٩) is concerned with internal nodes where conduction mode takes place, while equations (٣.١١٩) and (٣.١٢٧) are concerned with (external and internal) surface nodes respectively where convection mode takes place.

Thermal analyses of the blade require the specification of external and internal boundary conditions so that equations (٣.٩٩), (٣.١١٩), and (٣.١٢٧) are used to get the solution.

This specification is concerned mainly with the introduction of heat transfer coefficients and temperatures for internal and external boundary conditions.

٤.٢ Analysis (١):

Turbine Blade Cooling with Impingement-and Trailing Edge Ejection

٤.٢.١ Geometry: -

Fig. (٤-١ a) illustrates the blade geometry to be considered in this analysis.

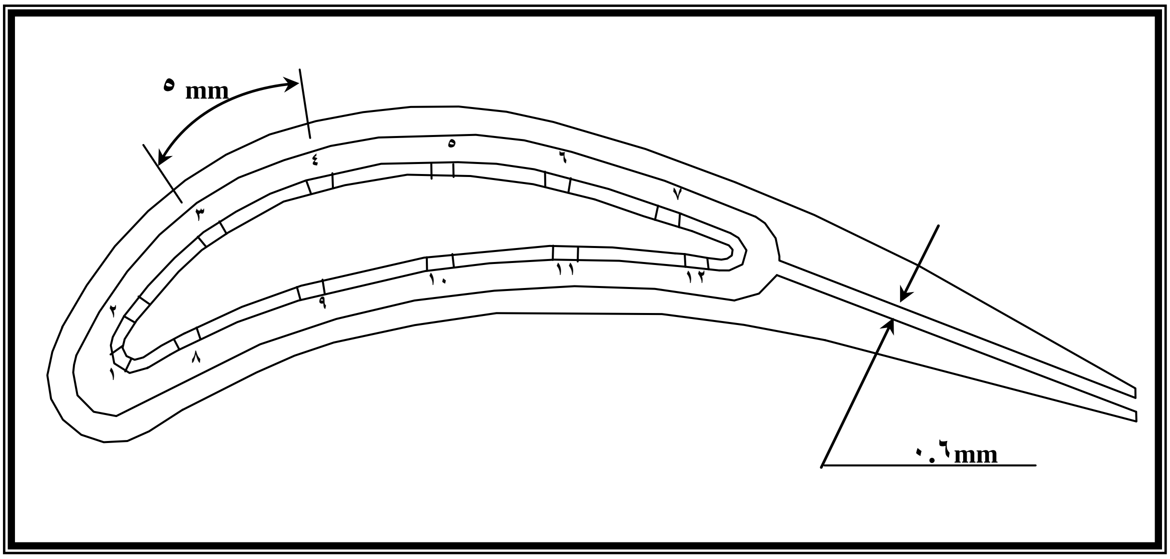

Fig. (٤-١ a) Blade Geometry, Ref. [١٠]

The blade incorporates an insert which serves as the jet plenum, figure (٤-١a) which is perforated by an array of jet orifices, Fig. (٤-١ b), is giving rise to mid-chord impingement arrays which cool the pressure and suction surfaces and an initial jet orifice row at the blade leading edge.

The jet orifices have a diameter (d), a chord-wise spacing of (x_n) a spanwise spacing of (y_n) and the insert is separated from the blade wall by a distance (z_n).

The cooling air, after passing through the orifices and impinging on the blade surface is constrained to flow in the chord wise direction and is discharged at the trailing edge flow from the upstream jets in the array therefore, impose a cross flow on those located down stream.

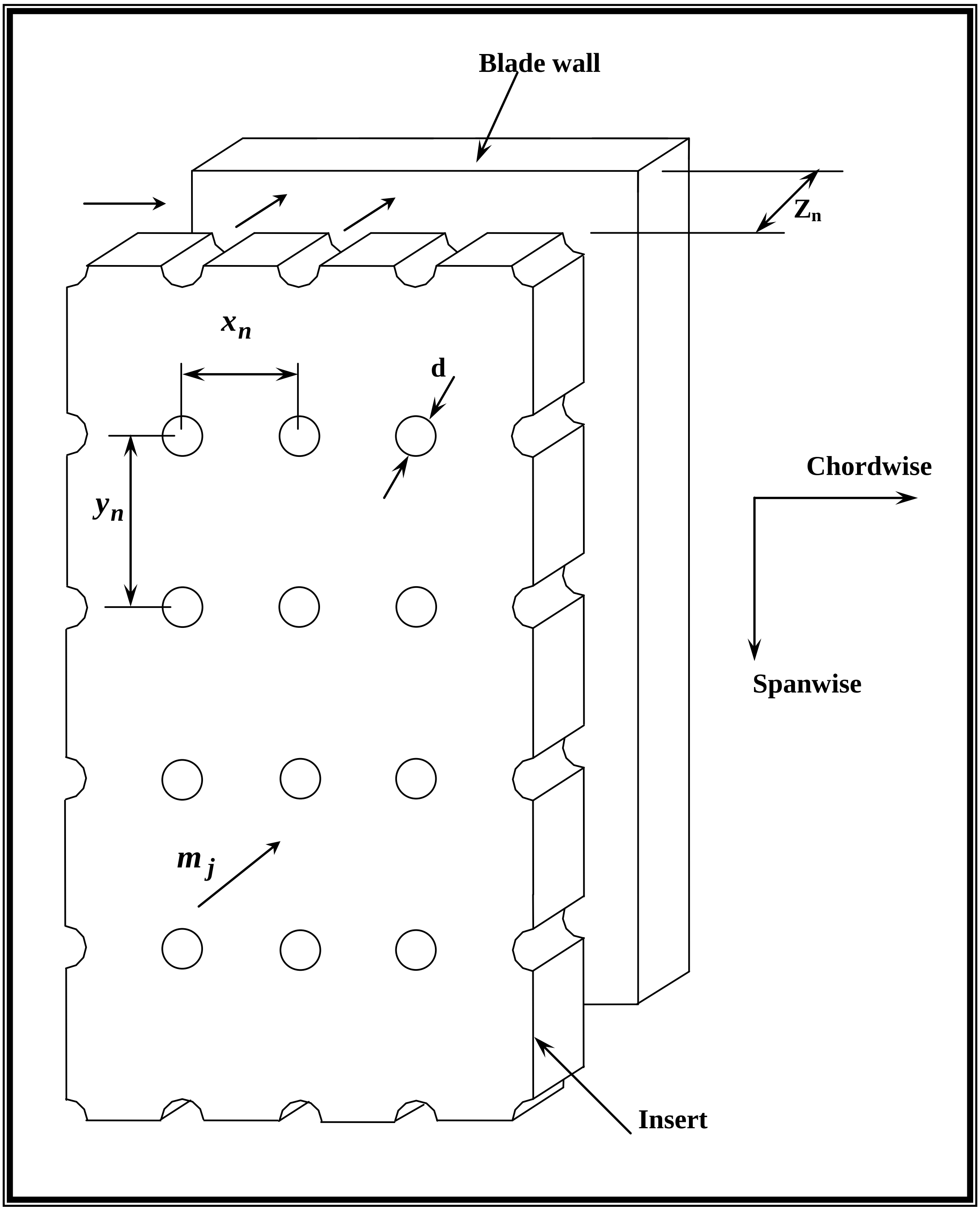

Fig. (٤-١ b) Detail of S.S. and P.S. Arrays

The insert is perforated by (١٢٠) jet orifices and it is separated from the hot blade surface by a distance of (١mm). Each of the (١٢٠) jet orifices are of (١mm) and arranged into (١٢) rows of (١٠) orifices each, i.e., each row consists of (١٠) orifices in the span wise direction.

The rows are arranged so that (٦) rows cool the blade suction surface and (٥) rows cool the pressure surface as shown in Fig. (٤-١ a). For this (١١) rows the chord wise spacing (x_n) is equal to (٥) jet orifice diameters (٥mm), while the spanwise jet spacing (y_n) is equal to (٨) orifice diameters (٨mm).

This jet impingement array will be identified as F (٥,٨) where (٥) refers to the chord wise spacing, and (٨) to the span wise spacing and the letter (F) to the source of the heat transfer correlation used to describe the array by Florschuetz et al [٤٢]. The remaining row is located at the leading edge.

The trailing edge region consists of an (٠.٦mm) wide slot which is (٨٠mm) high, (in the spanwise direction).

The cooling air mass flow rate is taken as ٢٨.٧×١٠^{-٣} Kg/s, all of which passes through the insert and through the jet orifices to form the cooling jets but only half of it, ١٤.٣٥×١٠^{-٣} Kg/s, passes through the trailing edge slot.

The necessity of specifying the three dimensions of this blade results from the heat transfer correlations that will be used. These require various parameters pertaining to the spanwise direction to be quantified. The correlations however provide results that are averaged in the spanwise directions and hence are suitable for a two dimensional analysis.

٤.٢.٢ Specification of Boundary Conditions

The boundary conditions for this analysis will be specified in terms of a heat transfer coefficient and a fluid temperature. Along the external profile (hot gas side), the heat transfer coefficient varies in the manner shown in Fig. (٤-٢) with the hot gas temperature taken to be uniform and it is equal to (٩٦٣K) around the blade external profile, these are described by Walker, [١٠].

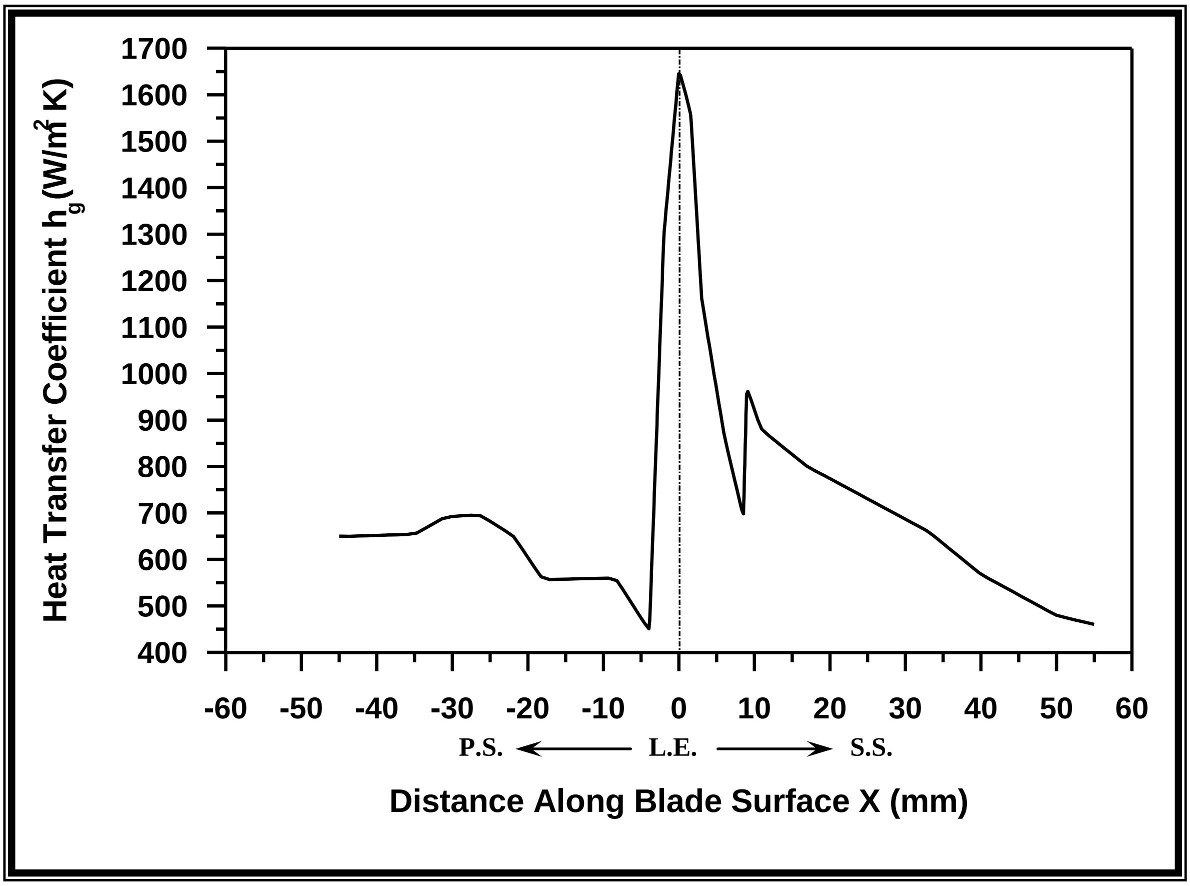

Fig. (٤-٢) The Variation of the External Heat Transfer Coefficient, Ref. [١٠]

For the internal surfaces three distinct regions can be considered;

(A) The Leading Edge Region

The leading edge region is considered to form a distinct area due to the local geometry prevailing there. The highly curved geometry onto which the jets impinge negates the use of correlations based on impingement against flat surfaces and hence requires more appropriate correlations.

Chupp et al, [٤٠], investigated the heat transfer at a simulated internal leading edge region of a turbine blade cooled by a single row of impinging air jets. The results of this experimental work consist of two heat transfer correlations. One for the jet stagnation region and one for the area around the jet stagnation region. These two correlations will be used here to characterize the heat transfer coefficients in this region.

Firstly, a coefficient of discharge, C_D , of the jet orifices will be calculated from the equation; showed by Ref. [٤٠]

$$\frac{\dot{m}_c}{A_j} = C_D \sqrt{2 \Delta P \rho_c} \qquad \text{......(٤.١)}$$

Where, A_j is the total jet orifice area -of all ١٢٠ orifices,

$\dot{m}_c$ is the total coolant mass flow rate, (٢٨.٧×١٠$^{-٣}$ Kg/s)

ΔP is the pressure drop across the insert- taken as ١١٦ kpa and

ρ_c is the coolant density taken at the cooling air jet temperature of ٣٧٨K.

The properties of air at ٣٧٨ K is taken from table (A٥), these are described by Ref. [٤١]

$$\rho = 0.9334 \; Kg/m^3$$
$$\mu = 2.19316 \times 10^{-5} \; Kg/m.s$$
$$K = 0.03178 \; W/m.K$$

Hence from equation (٤.١),

$$C_D = 0.65$$

The mass flow rate through the leading edge row, $\dot{m}_i$, is taken as ٢.٣٩٢×١٠$^{-٣}$ Kg/s, which is one twelfth of the total coolant mass flow rate, $\dot{m}_c$.

From Ref. [٤٠] the spanwise averaged Nusselt Number for the jet stagnation region was correlated from the experimental results to be;

$$Nu_{stag} = 0.44 \, Re_j^{0.7} \left(\frac{d}{y_n}\right)^{0.8} exp\left[-0.85\left(\frac{d_s}{d}\right)\left(\frac{d}{y_n}\right)\left(\frac{d}{d_{le}}\right)^{0.4}\right] \qquad \text{......(٤.٢)}$$

Where Re_j is the jet Reynolds number,

d_{le} is the leading edge diameter and

d_s is the distance between the insert and the leading edge blade wall.

Fig. (٤-٣) illustrated the leading edge region and identifies the geometric parameters which for the blade under consideration are;

$Re_j = 13739$

$d = 1mm$

$d_{Le} = 3.6mm$

$d_s = 2mm$

$y_n = 8mm$

Hence from equation (٤.٢);

$Nu_{stag} = 58$

$h_{stag} = 1825 W/m^2 K$

Around the stagnation region, Chupp et al, [٤٠] established another correlation to found the averaged Nusselt Number from experimental results to be;

$$Nu_{asg} = 0.63\, Re_j^{0.7} \left(\frac{d}{y_n}\right)^{0.5} \left(\frac{d}{d_{le}}\right)^{0.6} exp\left[-1.27\left(\frac{d_s}{d}\right)\left(\frac{d}{y_n}\right)^{0.5}\left(\frac{d}{d_{le}}\right)^{1.2}\right] \quad ...(٤.٣)$$

From which it can be calculated;

$Nu_{asg} = 67$

$h_{asg} = 2121 W/m^2 K$

With the heat transfer coefficient determined for the leading edge region it only remains to specify the fluid temperatures in these areas (T_{stag}) and (T_{asg}) and these were both taken as (٣٧٨K).

B) The Pressure and Suction Surface Jet Arrays

The interior surface of the blade along the pressure and suction surfaces are cooled by (٥) and (٦) rows of jets respectively.

The boundary conditions for these areas will be based on the results of impingement against a flat plate taking into account the effect of an initial cross flow, (from the leading edge coolant) as well as the effect of cross flow from upstream rows in the array.

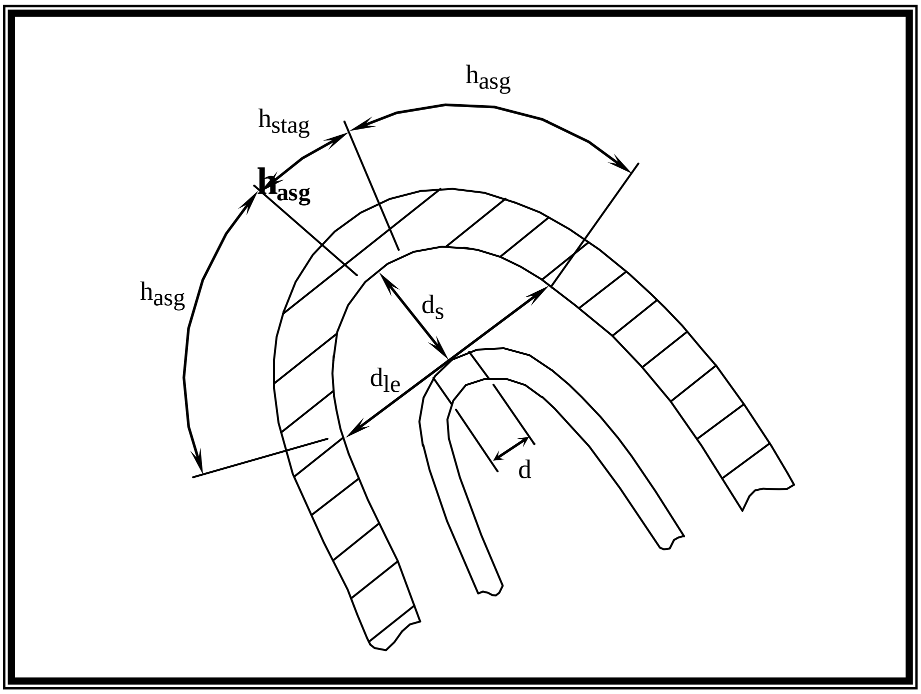

Fig. (٤-٣) Leading Edge Region

(١) Suction Surface- Flow Distribution

The one dimensional incompressible flow distribution model for predicting the flow distribution among the rows in the array is showed by Ref. [٤٢]

$$\frac{G_c}{G_j}=\frac{1}{\sqrt{2}\,C_D}\,\frac{(1+M)\sinh Bx'+M\sinh B(1+x')}{(1+M)\cosh B\tilde{x}-M\cosh B(1+\tilde{x})} \qquad ...(٤.٤)$$

Where G_c is the cross flow mass velocity based on the channel cross-sectional area, i.e.,

$$G_c=\frac{\dot{m}_i}{Z_n S_a} \quad \text{at } x=٠$$

$$G_c=\frac{\dot{m}_i+\dot{m}_{jt}}{Z_n S_a} \quad \text{at } x=L$$

S_a is the spanwise length of the array,

$G_j=\dfrac{\dot{m}_j}{A_o}=\rho V_j$ =the jet mass velocity for one row,

$M = \dfrac{\dot{m}_i}{\dot{m}_{jt}}$ =The initial cross flow rate to the total jet array flow rate,

B is a dimensionless quantity defined as;

$$B = \frac{\sqrt{2} A_{xy} C_D L}{Z_n} \qquad \text{...(٤.٥)}$$

$$A_{xy} = \frac{\frac{\pi}{4} d^2}{x_n y_n}$$

$\tilde{x} = x/L$,

(x) is the chordwise distance along the array,

(L) is the total chordwise length of the array,

$$x' = \tilde{x} - \frac{1}{2}\left(x_n/L\right)$$

For the suction surface array the following parameters are required to calculate the flow distribution according to equation (٤.٣).

$\dot{m}_i = 1.196 \times 10^{-3}\ Kg/s$ - is one half of the leading edge mass flow rate of $2.392 \times 10^{-3}\ Kg/s$.

$\dot{m}_{jt} = 14.35 \times 10^{-3}\ Kg/s$ - This is one half of the total coolant mass flow rate of $28.7 \times 10^{-3}\ Kg/s$ as the suction surface array contains ٦ of the ١٢ rows of holes.

$A_{xy} = 0.019\, m^2$

$L = 30\, mm$ i.e; ٦ rows with a ٥ mm spacing.

$M = 0.083$

$S_a = 80\, mm$ i.e; each row contains ١٠ jets with an ٨ mm spacing.

The flow distributions obtained from equation (٤.٤) are shown in table (٤-١) in terms of the distance of jet spacing (x) along the blade surface.

(٢) Suction Surface-Heat Transfer Coefficients

The heat transfer coefficients for the suction surface can be calculated using the correlation developed by Ref. [٤٣]. The correlation is based on experimental results, the Nusselt Number resolved to one chordwise jet spacing is,

$$Nu_a = A_1\, Re_j^m \left[1 - A_2 \left[\left(\frac{Z_n}{d} \right) \left(\frac{G_c}{G_j} \right) \right]^r \right] Pr^{0.333} \qquad \ldots(٤.٦)$$

Where, $A_1 = 0.67,\ A_2 = 0.237,\ m = 0.719\ and\ r = 0.317$

$$Re_j = \frac{G_j d}{\mu}$$

The calculated values of heat transfer coefficients are shown in table (٤-١) in terms of the distance of jet spacing (x) along the blade surface.

(٣) Suction Surface-Coolant Temperatures

The effect of the initial cross flow possessing a higher temperature than the array jet flow can be taken into account by viewing the cooling arrangement as a three temperature problem, shown in Fig. (٤-٤)

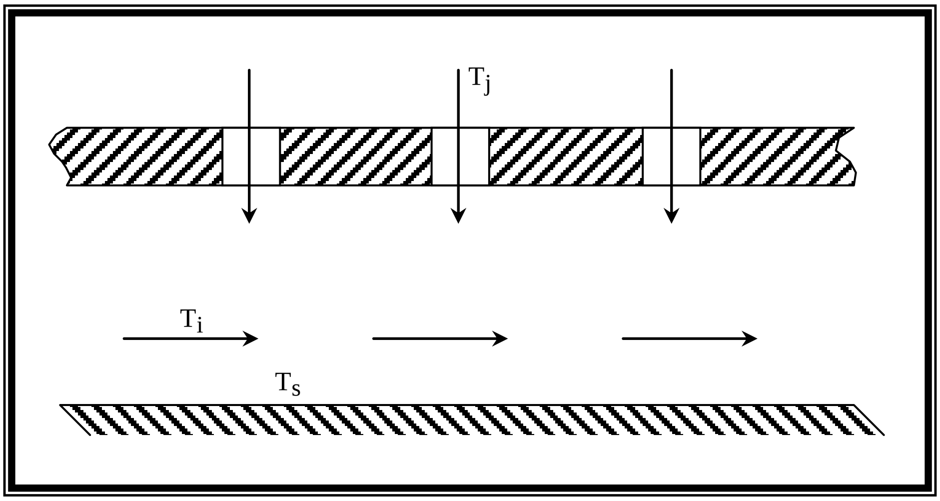

Fig. (٤-٤) Jet Array Impingement with Initial Cross flow, as a Three Temperature Problem.

The driving fluid temperature will be determined with the jet array flow considered as the primary flow and the initial cross flow considered as the influencing secondary flow.

Along the blade wall, (the impingement surface), the heat flux can be defined as:

$$q'' = h_a\left(T_s - T_{aw}\right) \qquad \text{...(٤.٧)}$$

Where(T_{aw}) is the adiabatic wall temperature and can be defined in a non-dimensional effectiveness, (E_T) as:

$$E_T = \frac{T_{aw} - T_j}{T_i - T_j} \qquad \text{...(٤.٨)}$$

Where, T_j : is the jet temperature.

T_i: is the temperature of the initial cross flow, $T_i > T_j$

The driving fluid temperature along the array (T_a) can be taken as (T_{aw}) hence once (E_T) is known (T_a) can be found. Florschuetz [٤٢] estimates the values of (E_T) for an F(٥,٨) array and represented in table (٤.١) together with the calculated values of (T_a), where (T_j) was taken as (٣٧٨K) and (T_i) as (٤٧٧K).

Table (٤-١) Result of Suction-Surface Flow Distribution, Heat Transfer Coefficients and Coolant Temperatures Obtained From Equations ((٤.٤) , (٤.٦) and (٤.٨))

x(mm)	G_c/G_j	h_a (W/m٢K)	E_T	T_a (K)
٠ – ٥	٠.٠٥٢	١٥٨١	٠.٢٥٨	٤٠٣.٥
٥ – ١٠	٠.١٤٨	١٥٣١	٠.٢٢٠	٣٩٩.٨
١٠ – ١٥	٠.٢٤١	١٥١٤	٠.١٩٨	٣٩٧.٦
١٥ – ٢٠	٠.٣٣	١٥١٦	٠.١٦٦	٣٩٤.٥
٢٠ – ٢٥	٠.٣٨٤	١٥٤٠	٠.١٢٠	٣٨٩.٩
٢٥ – ٣٠	٠.٤٩١	١٥٥٩	٠.١٠٠	٣٨٧.٩

(٤) Pressure Surface-Flow Distribution

The determination of the boundary conditions along the impingement cooled pressure surface proceeds exactly the same manner to that used for the suction surface. The difference lies in fact that only ٥ rows of jets are involved rather than ٦ rows.

The initial cross flow from the leading edge, $\dot{m}_i = 1.196 \times 10^{-3}\ Kg/s$.

$$\dot{m}_{jt} = 11.196 \times 10^{-3}\ Kg/s$$

$$M = 0.1$$

$$L = 25\ mm$$

$$A_{xy} = 0.0196\ m^2$$

The flow distribution for the pressure surface can then be calculated according to equation (٤.٤) and the results are shown in table (٤-٢).

(٥) Pressure Surface-Heat Transfer Coefficients

For the pressure surface, the heat transfer coefficients are calculated according to equation (٤.٦) for which only Re_j and G_c/G_j will change and the results are listed in table (٤-٢)

(٦) Pressure Surface Coolant Temperatures

The value of (E_T) reflects the influence of the higher temperature of the initial cross flow from the leading edge and because the ratio of the initial cross flow to the impingement jet array flow, M, has increased from ٠.٠٨٣ to ٠.١, different (E_T) values exist for the pressure surface.

These values, together with the calculated values of (T_a) based on a (T_i) of (٤٧٧K) and (T_j) of (٣٧٨K) as before, are shown in table (٤-٢).

Table (٤-٢) Result of Pressure-Surface Flow Distribution, Heat Transfer Coefficients and Coolant Temperatures Obtained From Equations ((٤.٤) , (٤.٦) and (٤.٨))

x(mm)	G_c/G_j	h_a (W/m^{٢}K)	E_T	T_a (K)
٠ – ٥	٠.٠٥١	١٦٠١	٠.٢٧٨	٤٠٥.٥
٥ – ١٠	٠.١٤٨	١٥٥٠	٠.٢١٩	٣٩٩.٧
١٠ –١٥	٠.٢٤١	١٥٣٣	٠.١٨٢	٣٩٦
١٥ – ٢٠	٠.٣٢٦	١٥٣٦	٠.١٣٥	٣٩١.٤
٢٠ – ٢٥	٠.٤١٣	١٥٥٢	٠.١٠٦	٣٨٨.٥

The boundary conditions for the impingement array along the pressure and suction surfaces are now completed and it just remains to specify the boundary conditions for the third distinct region (the trailing edge slot).

(c) The Trailing Edge Slot

Cooling of the trailing edge is achieved by the technique of trailing edge ejection in which cooling air is passed through a slot at the trailing edge and then ejected from the blade. This slot is (٠.٦mm) wide, (١٥mm) long in the chord wise direction and has a span wise height of (٨٠mm).

The average slot cooling air temperature is calculated according to the equation

$$T_{slot} = \frac{T_{sin} + T_{sout}}{2} \qquad \text{...(٤.٩)}$$

From Ref. [١٠], we found that

$$T_{sin} = 443\,k$$

$$T_{sout} = 471\,k$$

so from equation (٤.٩)

$$T_{slot} = 457\,k$$

By the use of turbulent pipe flow correlation, the heat transfer coefficient for the slot can be calculated to be ;

$$Nu = 0.023\, Re^{0.8}\, Pr^{0.4} \qquad ...(٤.١٠)$$

$$h_{slot} = 1353\, W / m^2 K$$

The slot boundary conditions are therefore now completely specified as constant along the slot with values;

$$h_{slot} = 1353\, W / m^2 K$$

$$T_{slot} = 457\ K$$

٤.٣ Analysis (٢):

Turbine Blade Cooling with Impingement and Trailing Edge Ejection Based on the Turbulent Flow between Two Parallel Plates

The primary purpose of this analysis is to investigate the effect of the use of different heat transfer correlation for the trailing edge slot. In the previous analysis the value of (h_{slot}) was based on a turbulent pipe flow correlation whereas for this analysis the heat transfer correlation will be based on the turbulent flow between two parallel plates.

The blade and insert geometry together with the jet orifices remain unchanged from analysis (١) and the boundary conditions also remain the same as for the analysis (١) except at the trailing edge.

The heat transfer coefficient along the slot is based on the turbulent flow between two parallel plates.

A number of preliminary analyses were performed by Rohsenow,*et al* [٤٤] in order to determine the correct boundary conditions which are presented here as:

$$T_{slot} = 458\ K$$

From Ref. [٤٤], the heat transfer coefficients were determined according to a correlation based on a turbulent flow between parallel plates:

$$Nu_{slot} = Nu_{fs} / (1 - C_T) \quad \text{...(٤.١١)}$$

Where Nu_{fs}: is the nusselt number obtained from the fundamental solutions and

C_T: is an influence coefficient.

From Rohsenow,*et al* [٤٤] the values of Nu_{fs} and C_T are given for the distance along the slot. The result is shown in table (٤-٣) where (x) is the distance along the slot.

Table (٤-٣) Results of Trailing Edge Slot Heat Transfer Coefficients Obtained from Equation (٤.١١).

x(mm)	h_{slot} (W/m٢K)
١	١٦٥١
١.٥	١٣٨٣
٥	١٢٤٩
١٥	١٢٣٣

٤.٤ Analysis (٣)

Impingement Cooling Heat Transfer Correlations Based on Square Jet Array.

This analysis uses the same correlation as used in analysis (٢), the only changes made are to the geometry, where the insert changed from a (٥,٨) array to a (٥,٥) array i.e.; the spanwise and chordwise spacing of the jet orifices were equal. This reduction in jet orifice spacing for all (١٢) rows results in an increase from (١٢٠) to (١٩٢) jet orifices i.e.; each row consists of (١٦) orifices in the span wise direction.

٤.٤.١ Specification of Boundary Conditions

The change in the span wise spacing of the jet orifices results in the boundary conditions along the leading edge and the impingement jet array changing and consequently the boundary conditions along the trailing edge slot. Therefore, the same procedure that was used in analysis (٢), to specify the boundary conditions is applied.

(A) The Leading Edge

The heat transfer coefficient is found to differ from that obtained in the previous analyses due changes in the span wise spacing of the jet orifices from (٨) to (٥), and therefore this value of heat transfer coefficient according to equation (٤.٢) is:

$$h_{stag} = 1773\, W / m^2 K$$

Likewise, the heat transfer coefficient in the area around the stagnation region is calculated according to equation (٤.٣) to be:

$$h_{asg} = 1834\, W / m^2 K$$

The coolant temperature in these regions, $\mathbf{T_{stag}}$ and $\mathbf{T_{asg}}$, are again taken as (٢٧٨K).

(B) The Pressure and Suction Surface Jet Arrays

(١) Suction Surface-Flow Distribution

The flow distribution among the rows is calculated according to equation (٤.٤) using the following changed parameters

$$A_{xy} = 31.4 \times 10^{-3} m^2$$
$$C_D = 0.68$$
$$B = 0.912$$

The results are shown in table (٤-٤)

(٢) Suction Surface Heat Transfer Coefficients

The heat transfer coefficients are calculated according to equation (٤.٦) where due to the change in jet spacing, The parameters A١,A٢,m and r now become;

$$A_1 = 0.0919$$
$$A_2 = 0.2636$$
$$m = 0.7085$$
$$r = 0.2393$$

And the results of this calculation are shown in table (٤.٤).

(٣) Suction Surface Coolant Temperatures

The change in array geometry results in different values of effectiveness (E_T) pertaining along the array. The values of (E_T) from Ref. [٤٢] together with the calculated values of (T_a) are shown in table (٤-٤).

The values of (T_a) are calculated using equation (٤.٢) based on $(T_j = 378K)$ and $(T_i = 474\ K)$

Table (٤-٤) Results of Suction-Surface Heat Transfer Coefficients and Coolant Temperatures Obtained from Equations ((٤.٦) and (٤.٨))

x(mm)	G_c/G_j	h_a (W/m^{٢}K)	E_T	T_a (K)
٠ – ٥	٠.٠٩٢	١٢٠٥	٠.٣٨١	٤١٤.٦
٥ – ١٠	٠.٢٤١	١١٨١	٠.٢٢٧	٣٩٩.٨
١٠ – ١٥	٠.٣٧٥	١١٩٨	٠.١٢٣	٣٨٩.٨
١٥ – ٢٠	٠.٤٩٤	١٢٤١	٠.٠٨٥	٣٨٦.٢
٢٠ – ٢٥	٠.٥٧٧	١٣١٠	٠.٠٥٥	٣٨٣.٣
٢٥ – ٣٠	٠.٧١٣	١٣٨٤	٠.٠٣٦	٣٨١.٥

(٤) Pressure Surface-Flow Distribution

The flow distribution is again calculated from equation (٤.٤) with;

$$M = 0.1$$

$$A_{xy} = 31.4 \times 10^{-3} m^2$$

$$B = 0.760$$

and the results are shown in table (٤-٥).

(٥) Pressure Surface Heat Transfer Coefficients

The heat transfer coefficients along the pressure surface can be determined in the same procedure as for the suction surface. The results of this determination are listed in table (٤-٥).

(٦) Pressure Surface Coolant Temperatures

For this F(٥,٥) the values of E_T from Ref. [٤٢] together with the calculated values of (T_a) based on the same values of (T_j) and (T_i) as per the suction surface are shown in table (٤-٥)

Table (٤-٥) Results of Pressure-Surface Heat Transfer Coefficients and Coolant Temperatures Obtained from Equations ((٤.٦) and (٤.٨))

X(mm)	G_c/G_j	h_a (W/m^{٢}K)	E_T	T_a (K)
٠ – ٥	٠.٠٨٨	١٢٤٩	٠.٤٥٠	٤٢١.٢
٥ – ١٠	٠.٢٣٦	١٢٢٢	٠.٢٢٦	٣٩٩.٧
١٠ – ١٥	٠.٣٦٥	١٢٣٩	٠.١١٩	٣٨٩.٤
١٥ – ٢٠	٠.٤٩١	١٢٨٢	٠.٠٨١	٣٨٥.٨
٢٠ – ٢٥	٠.٥٩٢	١٣٥٠	٠.٠٤٤	٣٨٢.٢

(c) The Trailing Edge Slot

The boundary conditions for the slot will be based on the turbulent flow between parallel plates as used in analysis (٢).

The relevant parameters required to calculate the boundary conditions are shown below and were obtained from a series of prior thermal analyses.

$$T_{sin} = 442\ K$$

$$T_{sout} = 473\ K$$

$$T_{slot} = 457.5\ K$$

Rohsenow, et al [٤٤] investigated the determination of the heat transfer coefficients along the trailing edge slot which is presented in table (٤-٦)

Table (٤-٦) Results of Trailing Edge Slot Heat Transfer Coefficients Obtained from Equation (٤.١١)

x(mm)	h_a (W/m^{٢}K)
١	١٦٤٨
١.٥	١٣٧٩
٥	١٢٤٦
١٥	١٢٢٩

٤.٥ Analysis (٤)

Impingement Cooling Heat Transfer Correlations Based on Square Jet Array By Using Tabakoff Correlation.

The purpose of this analysis is to compare the resulting blade temperature distribution when a different heat transfer correlation is used to describe the jet impingement array areas along the blade suction and pressure surfaces.

This analysis relies upon a correlation provided by Tabakoff and Kercher [٤٥], for square array including the effect of cross flow from upstream rows in the array but not including the effect of an initial cross flow.

٤.٥.١ Specification of Boundary Conditions

In this analysis, the geometry of the blade and insert remain unchanged from analysis (٣) and utilizes an array with a jet spacing of (٥) jet orifice diameters in both the chord wise and span wise directions and hence identified as T(٥,٥) where the letter (T) refers to Ref. [٤٥], the source of the array heat transfer correlation.

The boundary conditions for the leading edge remain the same as for analysis (٣) and hence it was found that the initial cross flow temperature also did not change from analysis (٣) therefore the values of (E_T) for both suction and pressure surfaces also remain the same; see tables (٤-٤) and (٤-٥).

The only boundary conditions that need to be recalculated are the impingement jet array heat transfer coefficients and the trailing edge slot conditions.

(١) Suction Surface Heat Transfer Coefficients

From experimental results of impingement array of jets against a flat plate with the cross flow forced to exit in one direction, Ref. [٤٥] provided the following heat transfer correlation;

$$Nu_a = \phi_1 \phi_2 \, Re_j^m \, Pr^{\frac{1}{3}} \left(\frac{Z_n}{d} \right)^{0.091} \qquad ...(٤.١٢)$$

This correlation applied at the range of

$$1 \le \frac{Z_n}{d} \le 4.8 \quad , \quad 300 \le Re_j \le 3 \times 10^4$$

$$3.1 \le \frac{x_n}{d} \le 12.5 \quad , \quad 0.005 \le A_{xy} \le 0.08$$

where,

$$\phi_1 = f\left(\frac{x_n}{d}, Re_j \right)$$

$$\phi_2 = f\left(\frac{G_c}{G_j}, Re_j, \frac{z_n}{d} \right)$$

$$m = f\left(\frac{x_n}{d}, Re_j \right)$$

The value of $\Phi_{١}$, $\Phi_{٢}$ and m are read from graphs provided in Ref.[٤٥] were found to be;

$$\phi_1 = 0.04$$
$$m = 0.79$$

From equation (٤.١٢) the heat transfer coefficients were calculated to be as shown in table (٤-٧) while the values of (T_a) remain the same as shown in table (٤-٤).

Table (٤-٧) Results of Suction-Surface Heat Transfer Coefficients Obtained from Equation (٤.١٢)

x(mm)	h_a(W/m^{٢}K)
٠ – ٥	١٢٢٠
٥ – ١٠	١١٦٤
١٠ – ١٥	١١٦٣
١٥ – ٢٠	١١٦٤
٢٠ – ٢٥	١٢٢٥
٢٥ – ٣٠	١٢٧٠

(٢) Pressure Surface Heat Transfer Coefficients

Using the Tabakoff correlation, Ref. [٤٥] as given in equation (٤.١٢) the heat transfer coefficients for the pressure surface are given in table (٤-٨) while the values of (T_a) remain the same as shown in table (٤-٥)

Table (٤-٨) Results of Pressure-Surface Heat Transfer Coefficients Obtained from Equation (٤.١٢)

x(mm)	**h_a (W/m^{٢}K)**
٠ _ ٥	١٢٦٧
٥ _ ١٠	١٢٢٠
١٠ _ ١٥	١١٩٧
١٥ _ ٢٠	١٢٠٧
٢٠ _ ٢٥	١٢٧٠

(٣) The Trailing Edge Slot

The specification of the boundary conditions for the trailing edge slot will again be based on the turbulent flow between two parallel plates. The relevant parameters required be shown below and the value of (h_{slot}) presented in table (٤-٩)

$$T_{sin} = 440\ K$$

$$T_{sout} = 472\ K$$

$$T_{slot} = 456\ K$$

Table (٤-٨) Results of Trailing Edge Slot Heat Transfer Coefficients Obtained from Equation (٤.١١)

x(mm)	h_a(W/m^{٢}K)
١	١٦٤٩
١.٥	١٣٨٠
٥	١٢٤٧
١٥	١٢٣٠

٤.٦ Analysis (٥)

Impingement Cooling Heat Transfer Correlations Based on Square Jet Array By Using Chance Correlation.

This is the third analysis whose purpose is to determine the effect of different heat transfer correlations for the impingement jet array areas. The heat transfer correlation is provided by Chance [٤٦] based on a series of experimental results.

The details of the blade geometry, insert geometry, leading edge boundary conditions and flow distribution remain unchanged from analyses (٣) and (٤) and only the changes, which occur to the impingement jet array, and the trailing edge slot will be described here.

٤.٦.١ Suction Surface Heat Transfer Coefficients

The heat transfer correlation given by Chance [٤٦] is based on the experimental results of jet impingement against a flat plate with the spent flow forced to exit in one direction.

This correlation is as follows;

$$Nu_a = P_1 P_2 P_3 \, Re_j^u \, Pr^{\frac{1}{3}} \, A_{xy}^{1.0146} \qquad \ldots(٤.١٣)$$

Where $P_{١}$ is a constant and equal to ١.٨٧٦

$P_{٢}$ is a function of the cross flow;

$$P_2 = 1 - 0.236\left(\frac{G_c}{G_j}\right)\left(\frac{Z_n}{d}\right)$$

$P_{٣}$ is a function of the array geometry;

$$p_3 = 1 - \frac{Z_n}{d}\left(0.023 + 0.182\,A_{xy}^{0.71}\right) = 0.961$$

and (u) is the Re_j exponent and a function of the open area;

$$u = 0.561 / A_{xy}^{0.0835} = 0.75$$

Equation (٤.١٣) correlates data for the following range of parameters;

$$2 \prec Z_n/d \prec 8$$

$$0.012 \prec A_{xy} \prec 0.07$$

$$(G_c/G_j)(Z_n/d) \prec 1.8$$

The result of this correlation is the heat transfer coefficients listed in table (٤-١٠)

٤.٦.٢ Suction Surface Coolant Temperatures

The values of (E_T) remain the same as for analysis (٣) and (٤) but (T_i) was found to change to (٤٧٥ K), which results in the values of (Ta), based on equation (٤.٨) varying slightly from those of the two previous analyses.

Table (٤-١٠) Results of Suction-Surface Heat Transfer Coefficients and Coolant Temperatures Obtained from Equations ((٤.١٣) and (٤.٨))

x(mm)	h_a (W/m^{٢}K)	E_T	T_a (K)
٠ – ٥	١١٦٤	٠.٣٨١	٤١٤.٩
٥ – ١٠	١١٥٣	٠.٢٢٧	٤٠٠.٠
١٠ – ١٥	١١٦٣	٠.١٢٣	٣٩٠.٠
١٥ – ٢٠	١١٩٣	٠.٠٨٥	٣٨٦.٣
٢٠ – ٢٥	١٢٤٩	٠.٠٥٥	٣٨٣.٣
٢٥ – ٣٠	١٣٠٩	٠.٠٣٦	٣٨١.٥

٤.٦.٣ Pressure Surface Heat Transfer Coefficients

In a similar manner to that used for the suction surface the heat transfer coefficients are calculated according to equation (٤.١٣). The results are shown in table (٤-١١).

٤.٦.٤ Pressure Surface Coolant Temperatures

With (T_i) equal to (٤٧٥ K) and (T_j) equal to (٣٧٨ K) and (E_T) as shown below the values of (T_a) are calculated to be:

Table (٤-١١) Results of Pressure-Surface Heat Transfer Coefficients and Coolant Temperatures Obtained from Equations ((٤.١٣) and (٤.٨))

x(mm)	h_a (W/m٢K)	E_T	T_a (K)
٠ – ٥	١٢٠٧	٠.٤٥٠	٤٢١.٦
٥ – ١٠	١١٩٥	٠.٢٢٦	٤٠٠.٠
١٠ – ١٥	١٢٠٦	٠.١١٩	٣٨٩.٥
١٥ – ٢٠	١٢٣٥	٠.٠٨١	٣٨٥.٩
٢٠ – ٢٥	١٢٨٧	٠.٠٤٤	٣٨٢.٣

٤.٦.٥ The Trailing Edge Slot

The specification of the trailing edge boundary conditions is again based on the flow between two parallel plates. For this analysis the required quantities are shown below

$$T_{sin} = 439\ K$$

$$T_{sout} = 470\ K$$

$$T_{slot} = 454.5\ K$$

The variation of the heat transfer coefficients along the slot is given in table (٤-١٢)

Table (٤-١٢) Results of Trailing Edge Slot Heat Transfer Coefficients Obtained from Equations (٤.١١)

X(mm)	h_a (W/m٢K)
١	١٦٤٣
١.٥	١٣٧٥
٥	١٢٤٢
١٥	١٢٢٥

٤.٧ Analysis (٦):

Turbine Blade Cooling with Impingement and Film Cooling

In the previous analyses the impingement jets methods are using to cool the hot blade surfaces. These methods can, however be classified as internal methods of blade cooling, that is the cooling is achieved by the circulation of cooling air within the blade.

The cooling requirements and stresses would be less severe if the heat transfer from the hot gas to the blade could be decreased by the process known as film cooling.

Film cooling blades are not only cooled by convection, impingement methods, but they are also shielded from the outer hot gas with a film of spent cooling air ejected through the blade surface by rows of holes.

The purpose of this analysis to determine the blade temperature distribution for such a film cooled blade. The cooling of the blade will consist of the same internal arrangement as utilized in analysis (٢), that is an F(٥,٨) impingement jet array but in addition film cooling of the outer surface will be achieved through the use of (١٢) rows of (٠.٥٢ mm) diameter ejection holes distributed around the suction and pressure surfaces of the blade.

Internally, the geometry remains unchanged from analysis (٢). There are (١٢٠) jet orifices of (١mm) diameter whose jets impinge on the hot blade surfaces and which are arranged in (١٢) rows of (١٠) jets each, these are showed by Ref. [١٠]

Over the suction and pressure surface jet arrays the jets are ordered with a spacing of (٥) jet orifice diameters in the chord wise direction and (٨) in the span wise direction. One half of the spent cooling air from these jets flows rearwards towards the trailing edge and exits the blade through the trailing slot as in analysis (٢).

The remaining spent cooling air exits the blade through a series of film cooling ejection holes distributed throughout the blade wall. There are in total (٤٦٨) film cooling holes of (٠.٥٢mm) diameter. These are arranged in (١٢)rows each containing (٣٩) holes each.

(٧) of the rows are spaced along the suction surface while (٥) are spaced along the pressure surface as shown in Fig.(٤-٥).Within each row the holes are spaced a distance of (٢mm) apart. The film cooling holes consist of two rows with an ejection angle of ٦٤˚, rows ١ and ٨ and ١٠ rows with an ejection angle of ٤٥˚.

٤.٧.١ Specification of Boundary Conditions

The specification of the boundary conditions can be sub-divided into two main areas:

١-The internal boundary conditions, which will be dealt with in a similar manner to that used in analysis (٢), as the internal cooling arrangement and geometry remains unaltered from this analysis.

٢-The external boundary conditions, which must take into account the presence of the ejected cooler film of air over the outer surface of the blade.

All the previous analyses dealt with the external boundary conditions by defining external heat transfer coefficients, which varied around the blade surface in the manner shown in Fig. (٤-٢) together with specifying a uniform hot gas temperature of (٩٦٣ K). The presence of film cooling radically alters these boundary conditions.

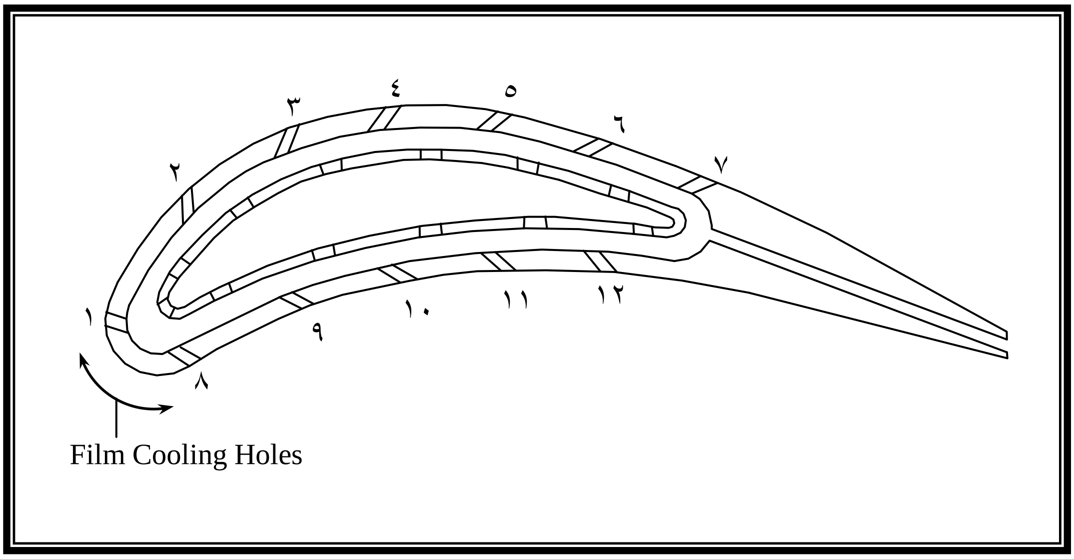

Fig. (٤-٥) Blade Geometry

٤.٧.٢ Internal Boundary Conditions

The boundary conditions at the leading edge are unaltered from analysis (٢) (refer to section ٤.٢.٢ A) for these conditions. Likewise the flow distribution and heat transfer coefficients for the suction and pressure surfaces jet arrays also remain unchanged (refer to section ٤.٢.٢ B (١,٢,٤ and ٥).

However the value of T_a, the array driving temperature does change because the temperature of the initial cross flow, T_i is reduced due to the effect of film cooling in reducing the heat transfer to the blade.

The trailing edge slot conditions also change because the temperature of the cooling air entering the slot, T_{sin} is reduced again because of the decrease in heat transfer to the blade.

٤.٧.٢.١ Suction Surface-Coolant Temperatures

The value of T_i, from a series of preliminary runs was determined to be (٤٦٥K) which is less than the value obtained in analysis (٢) due to the protection obtained from the film cooling which reduces the heat transfer to the blade and consequently to the cooling air.

This value of T_i is then used in equation (٤.٨) to obtain the values of (T_a) as shown in table (٤-١٣) where (E_T) is obtained from analysis (٢), section (٤.٢.٢ B (٢)).

Table (٤-١٣) Results of Suction Surface-Coolant Temperatures Obtained from Equation (٤.٨)

x(mm)	E_T	T_a (K)
٠ – ٥	٠.٢٥٣	٤٠٠.٤
٥ – ١٠	٠.٢٢٠	٣٩٧.١
١٠ – ١٥	٠.١٩٨	٣٩٥.٢
١٥ – ٢٠	٠.١٦٦	٣٩٢.٥
٢٠ – ٢٥	٠.١٢٠	٣٨٨.٤
٢٥ – ٣٠	٠.١٠٠	٣٨٦.٧

٤.٧.٢.٢ Pressure Surface – Coolant Temperatures

Again the initial cross flow temperature, T_i is reduced to (٤٦٥ K) and using the same values of E_T as for analysis (٢), T_a is determined and the results shown in table (٤-١٤).

Table (٤-١٤) Results of Pressure Surface-Coolant Temperatures Obtained from Equation (٤.٨)

x(mm)	E_T	T_a (K)
٠ – ٥	٠.٢٧٨	٤٠٢.٢
٥ – ١٠	٠.٢١٩	٣٩٧.٠
١٠ – ١٥	٠.١٨٢	٣٩٣.٨
١٥ – ٢٠	٠.١٣٥	٣٨٩.٧
٢٠ – ٢٥	٠.١٠٦	٣٨٧.٢

٤.٧.٢.٣ The Trailing Edge Slot

The reduction in the heat addition to the cooling air along the jet arrays at the leading edge due to the film cooling reduces the temperature of the coolant entering the slot and hence alters the slot boundary conditions

The boundary conditions are based on the parallel plate flow with the following required parameters;

$$T_{sin} = 423\ K$$
$$T_{sout} = 428\ K$$
$$T_{slot} = 425.5\ K$$

The calculated values of h_{slot} along the slot are presented in table (٤-١٥)

Table (٤-١٥) Results of Trailing Edge Slot- Heat Transfer Coefficients Obtained from Equation (٤.١١)

x(mm)	h_{slot}(W/m٢K)
١	١٦٧٣
١.٥	١٤٠٤
٥	١٢٨٢
١٥	١٢٦٥

٤.٧.٣ External Boundary Conditions

The ejection of cooling air through the film cooling holes results in a change in the conditions existing along the outer profile of the blade. This section seeks to specify the new boundary conditions that now exist as a result of the film cooling used on this blade.

An analysis of the boundary layer with film cooling results in the specification of the heat flux to the blade surface from the hot gas as;

$$q'' = h_{ext}\left(T_{aw} - T_s\right) \qquad \text{...(٤.١٤)}$$

Where q'' is the heat flux to the blade.

h_{ext} is the heat transfer coefficient without film cooling , i.e.; as given by Fig. (٤.٢).

T_s the blade wall surface temperature.

T_{aw} is the adiabatic wall temperature.

The adiabatic wall temperature can be non-dimensionalized as a film cooling effectiveness, E_f defined by;

$$E_f = \frac{T_g - T_{aw}}{T_g - T_{c2}} \qquad \text{...(٤.١٥)}$$

Where T_g is the gas temperature.

T_{c2} is the temperature of the coolant leaving the film cooling holes, as shown in Fig. (٤-٦).

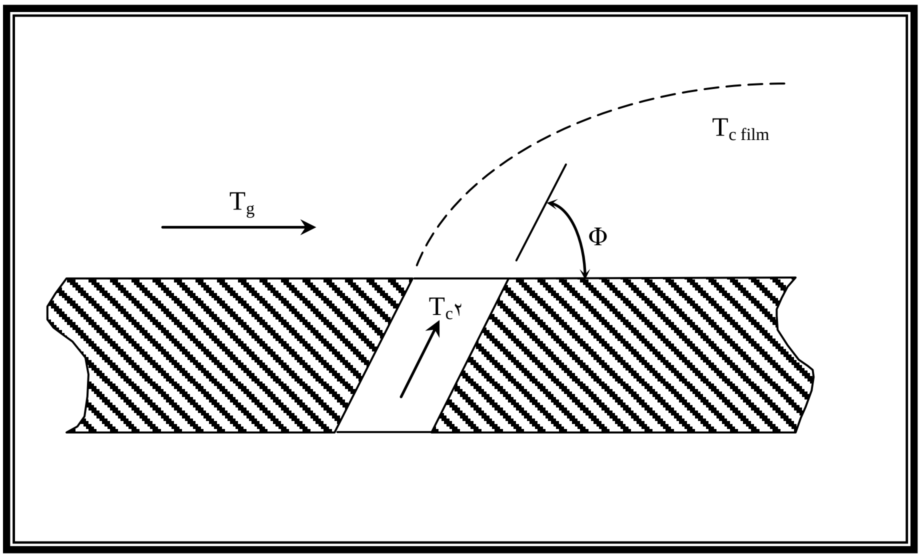

Fig. (٤-٦) Film Cooling Hole

The adiabatic wall temperature is for practical purposes the same as the temperature of the coolant film, T_{cfilm}. The film cooling effectiveness, E_f for a single hole varies from unity at the point of injection, (where $T_{cfilm} = T_{c٢}$) to zero far downstream because of dilution of the injected flow, T_{cfilm} approaches the hot gas temperature, T_g.

Hence, the heat flux q'' with film cooling, as defined by equation (٤.١٤), utilizes the same value of the heat transfer coefficient without film cooling. The specification of the boundary conditions will rely upon defining E_T as a function of distance away from the film cooling holes and from E_f the value of T_{cfilm}. The values of (T_{cfilm}) and (h_{ext}) will then completely define the external boundary conditions with film cooling.

In summary, film cooling results in a change of the external boundary conditions with (T_{cfilm}) replacing (T_g) around the profile while (h_{ext}) remains unchanged.

٤.٧.٤.١ Film Cooling Effectiveness

The specification of E_f will be based on the notational method of replacing each hole by a rectangular slot of a length equal to the hole diameter and a width, Se, such as to give the same area as the hole as shown in Fig. (٤-٩).

The effectiveness from Ref. [١٠] was defined as:

$$E_f = \frac{1.9\left(\frac{d_f}{y_{nf}}\right)Pr_{c2}^{0.666}}{1+0.329\left(\frac{Cp_g}{Cp_{c2}}\right)R^{0.8}Y} \qquad \text{...(٤.١٦)}$$

Where the sub-script ($c_٢$) refers to the coolant leaving the slot and the sub-script (g) to the hot gas,

d_f is the film cooling hole diameter=٠.٥٢ mm

y_{nf} is the spanwise spacing of the film cooling holes=٢ mm

$$R = \left(\frac{x}{1.2\,Se} \right) \left[Re_{c2} \left(\frac{\mu_{c2}}{\mu_g} \right) \right]^{-0.25} \qquad \ldots(٤.١٧)$$

Where (x) is the distance in the downstream direction,

(Se) is the slot width

$$Y = 1 + 1.5 \times 10^{-4}\, Re_{c2} \left(\frac{\mu_{c2}}{\mu_g} \right) \sin\phi \qquad \ldots(٤.١٧)$$

Where Φ is the angle of ejection as shown in Fig. (٤-٨).

E_f can be found with the use of the following parameters,

$Se = 0.4084\ mm$

$T_{c2} = 423\ K$

$T_g = 963\ K$

$Cp_{c2} = 1016\ J/kg.K$

$Cp_g = 1134\ J/kg.K$

$\mu_{c2} = 23.8 \times 10^{-6}\ kg/m.s$

$\mu_g = 40.8 \times 10^{-6}\ kg/m.s$

$\rho_{c2} = 0.83\ kg/m^3$

$\rho_g = 0.36\ kg/m^3$

$Re_{c2} = 3207$

$Pr = 0.7$

so, the effectiveness (E_f) is defined from equation (٤.١٦) for the ٤٥˙ and ٦٤° ejection angles as :

$$E_{f_{45}} = 0.3901 \Big/ \left(1 + 0.44\, R^{0.8} \right) \qquad \ldots(٤.١٩)$$

$$E_{f_{64}} = 0.3901 \Big/ \left(1 + 0.46\, R^{0.8} \right) \qquad \ldots(٤.٢٠)$$

The value of T_g used in equation (٤.١٥) varies from row to row because the films from successive rows reinforce each other, i.e.; the film temperature upstream of a row becomes the gas temperature of the next downstream row.

Rows (١) and (٨), which are the first rows on the suction and pressure surfaces inject the coolant into the external flow which has a temperature of ٩٦٣K the second rows, i.e.; (٢) and (٩), inject their coolant into the film provided by rows (١) and (٨) which is now at a lower temperature. This reduction in the effective T_g continues for the other downstream rows also.

The effective T_g used for each row is shown in table (٤-١٦). This temperature is equal to the value of $T_{c\ film}$ existing just upstream of the row. For example row (٢) is ٧.٧ mm downstream of row (١). For x=٧.٧ mm, $E_{f١٤}$ can be calculated to be ٠.٢٠٢٨ from which T_{cfilm} is ٨٥٣.٥ K, based on a T_g of ٩٦٣ K.

This value of $T_{c\ film}$ is now used as the effective gas temperature, T_g for the calculations for the second row.

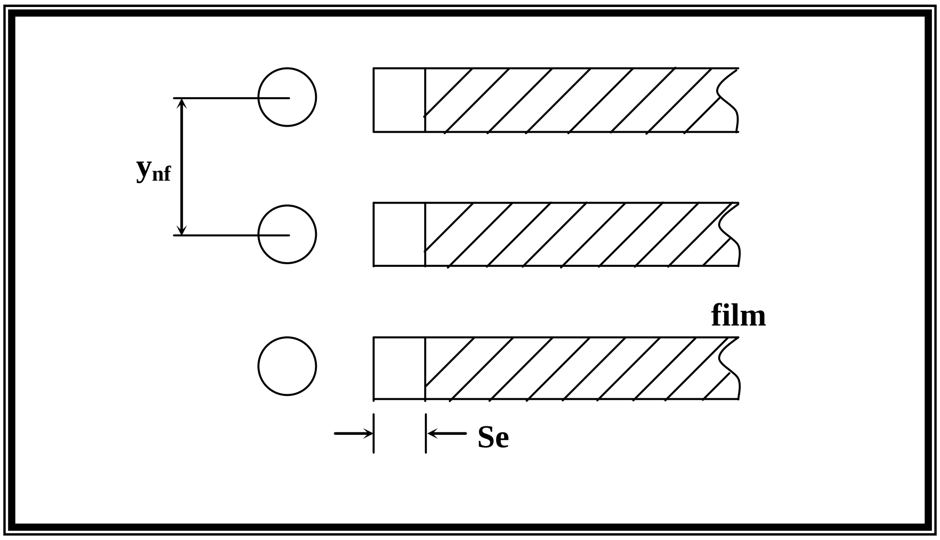

Fig. (٤-٩) Discrete Hole Injection

Summary: -

The boundary conditions along the outer profile of the blade are now completely specified, i.e.; for each node, its distance downstream from a film cooling row is known from which the appropriate value of E_f can be found.

Then, $T_{c\ film}$ is determined by using the correct value of T_g and combining with the correct value of h_{ext} given in Fig. (٤-٢) results in the complete specification of the boundary conditions.

Together with the internal boundary conditions the thermal analysis can now be performed.

Table (٤-١٦) Results of Effective Gas Temperature Obtained from Equation (٤.١٥)

Film Cooling Row	**Effective T_g (K)**
١	٩٦٣
٢	٨٥٣.٥
٣	٧٥٢
٤	٦٦٩
٥	٦٠٩
٦	٥٦٤
٧	٥٢٩
٨	٩٦٣
٩	٨٤٧
١٠	٧٤٢
١١	٦٦٣
١٢	٦٠٣

٤.٨ The Computer Programs

٤.٨.١ Introduction

A Quick Basic language was written for solving the two-dimensional steady state problem to find the blade temperature distribution.

٤.٨.٢ Input Data

The input data required to run the program is as follows:

١- The number of grid points in x-direction and y-direction.
٢- The thermal conductivity of the material.
٣- The convection heat transfer coefficient for hot gas (h_g).
٤- The convection heat transfer coefficient for cooled air (h_c).
٥- The hot gas temperature (T_g).
٦- The cooled air temperature (T_c).

The steps of the main program are outlined in the flowchart, shown in Fig.(٤-٨). The procedure of the subroutine for grid generation is shown in the flowchart in Fig. (٤-٩).

٤.٨.٣ Program Output

١- The grid generation of the blade geometry.
٢- The nodal temperature value.

A grapher program was used for plotting mesh generation and blade surface temperature. While a surfer program was used for plotting contours of blade temperature distribution for all analyses.

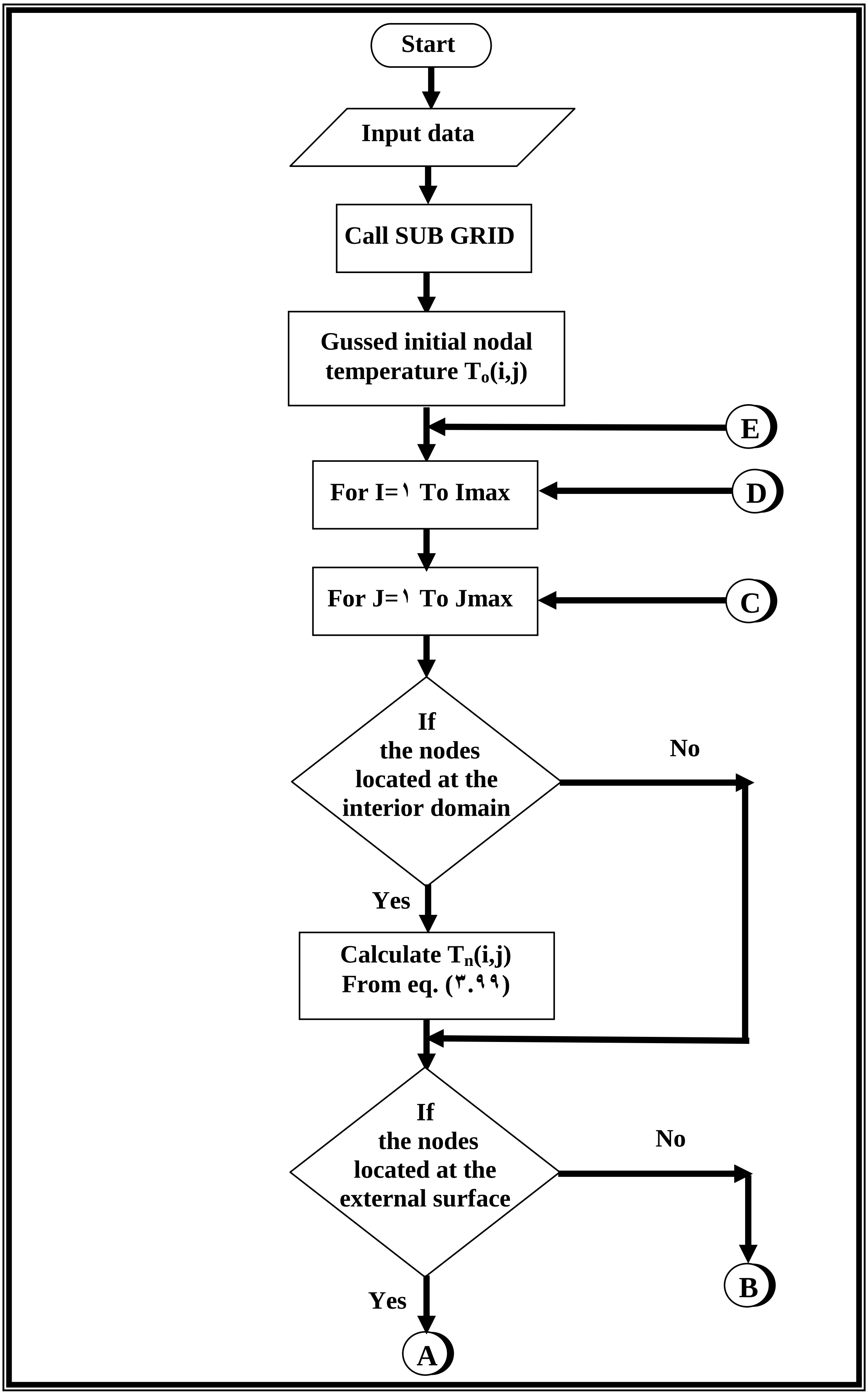

Fig. (٤-٨) Flowchart for Main Program

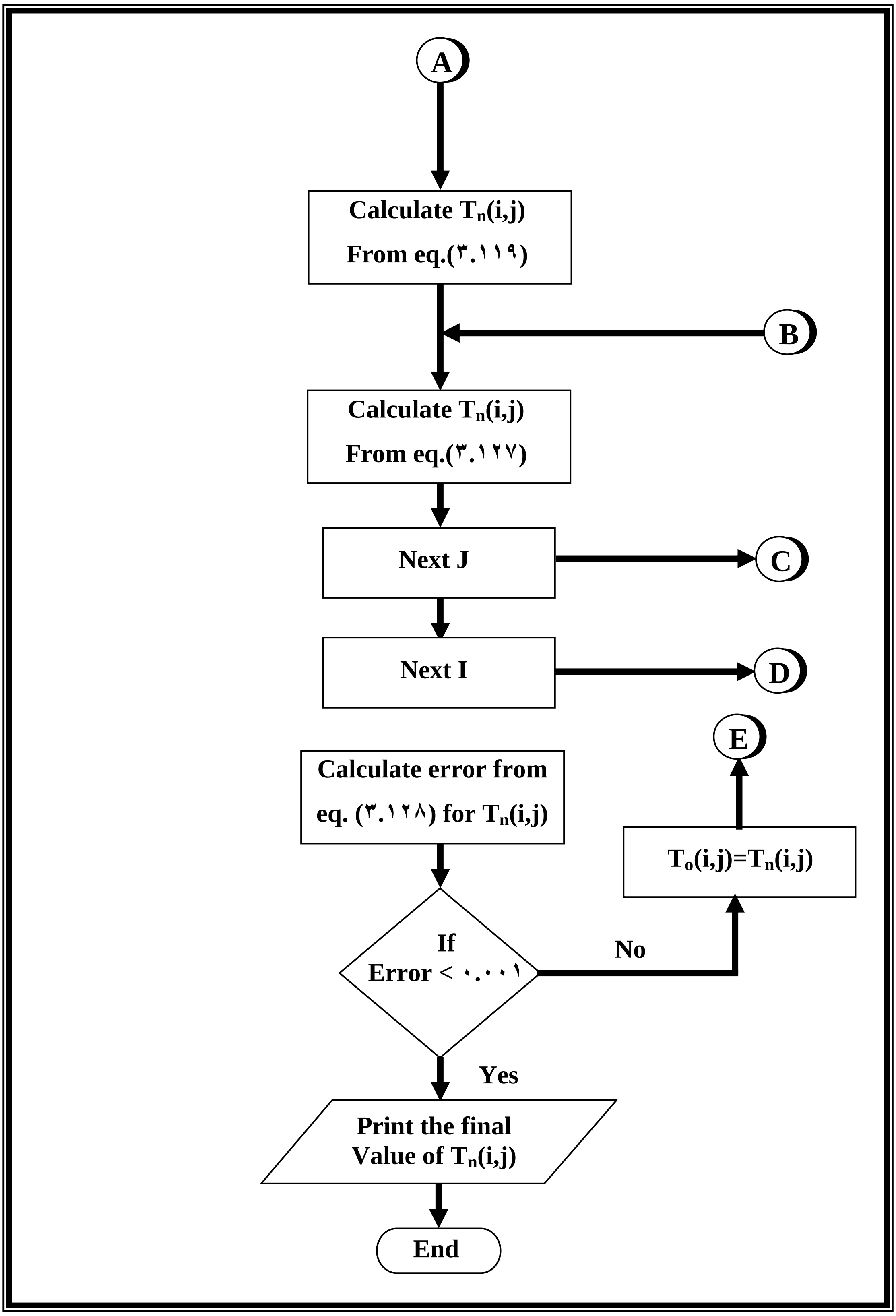

Fig. (٤-٨) Continued

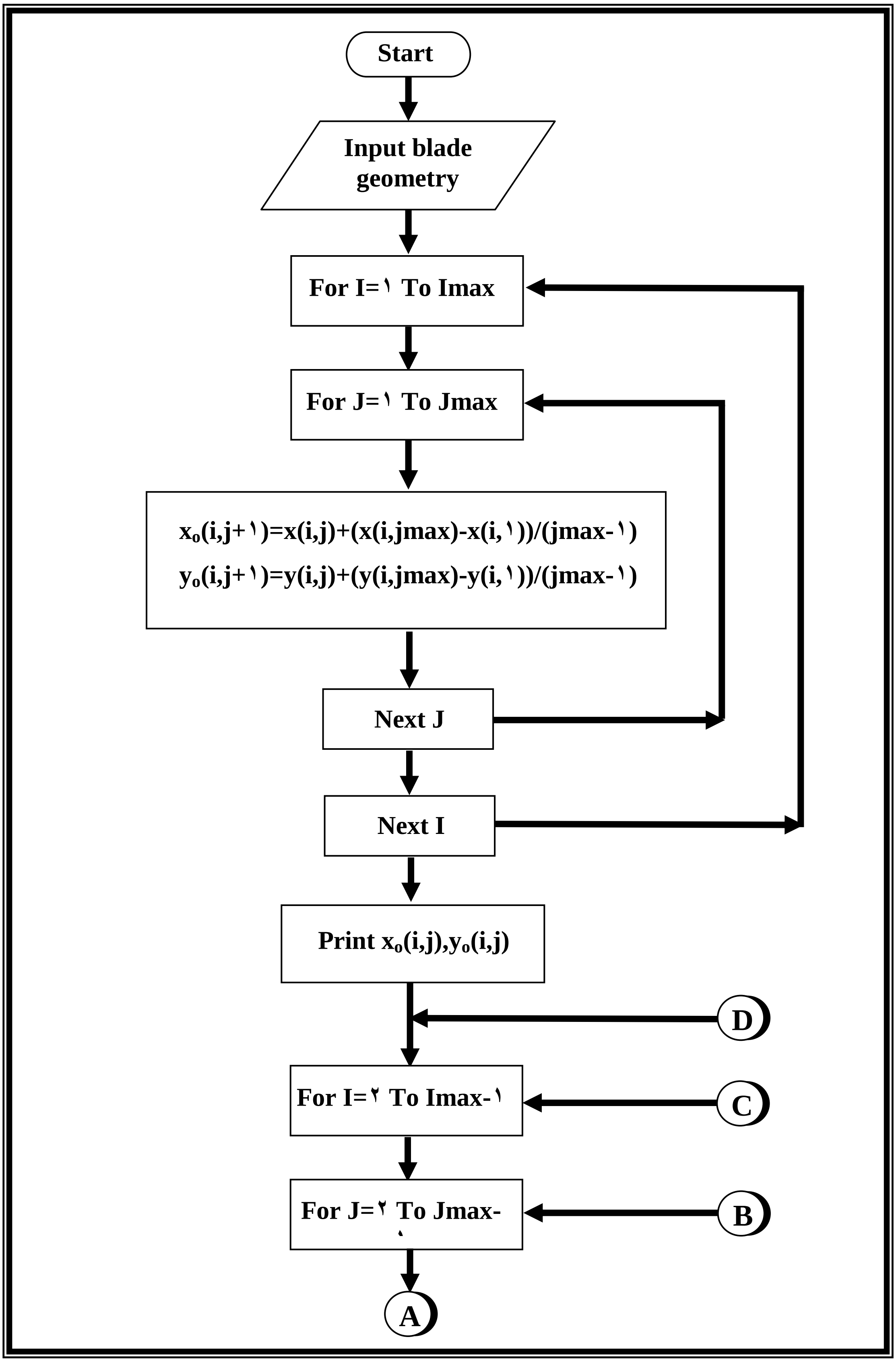

Fig. (٤-٩) Flowchart of Sub Grid Subroutine

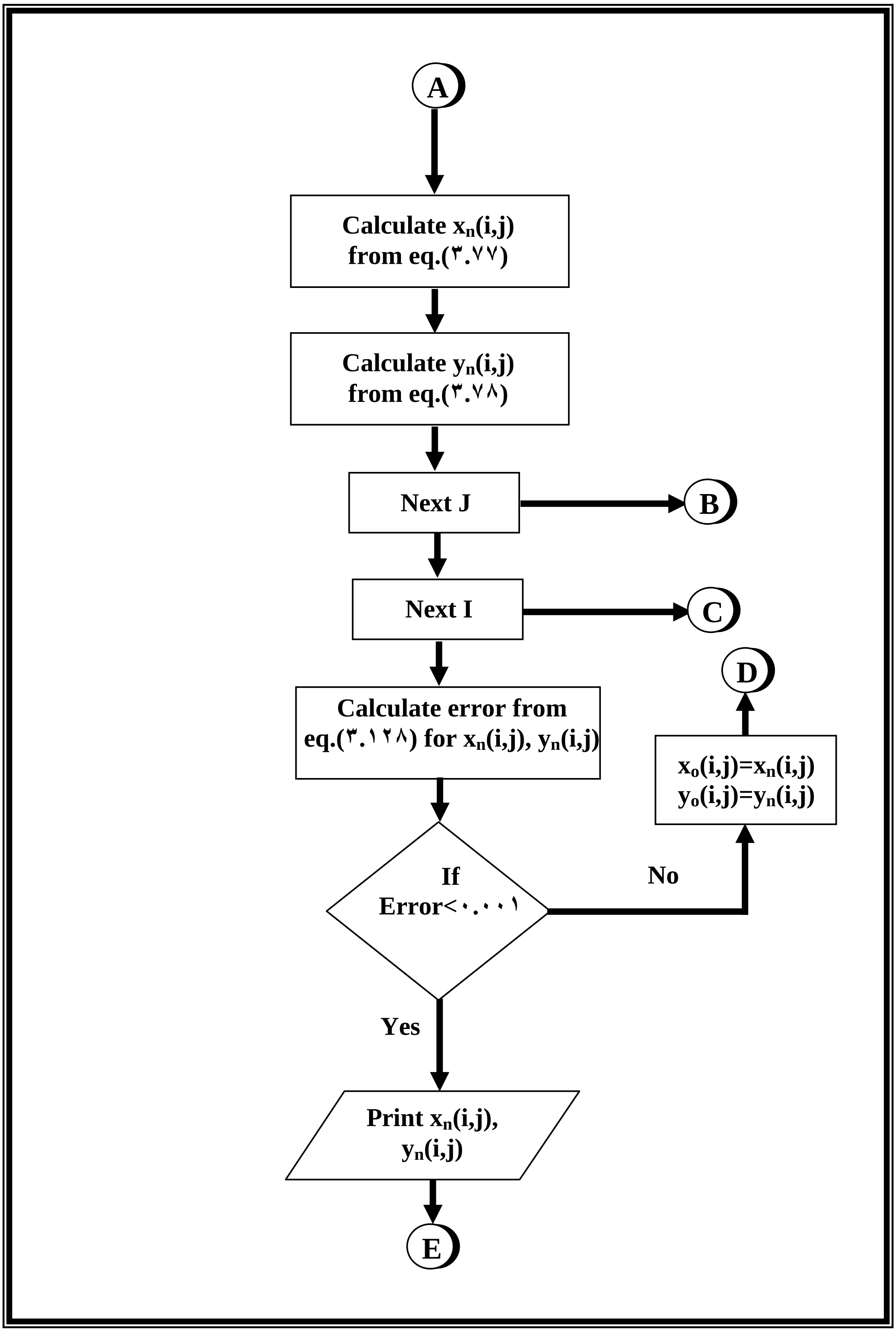

Fig. (٤-٩) Continued

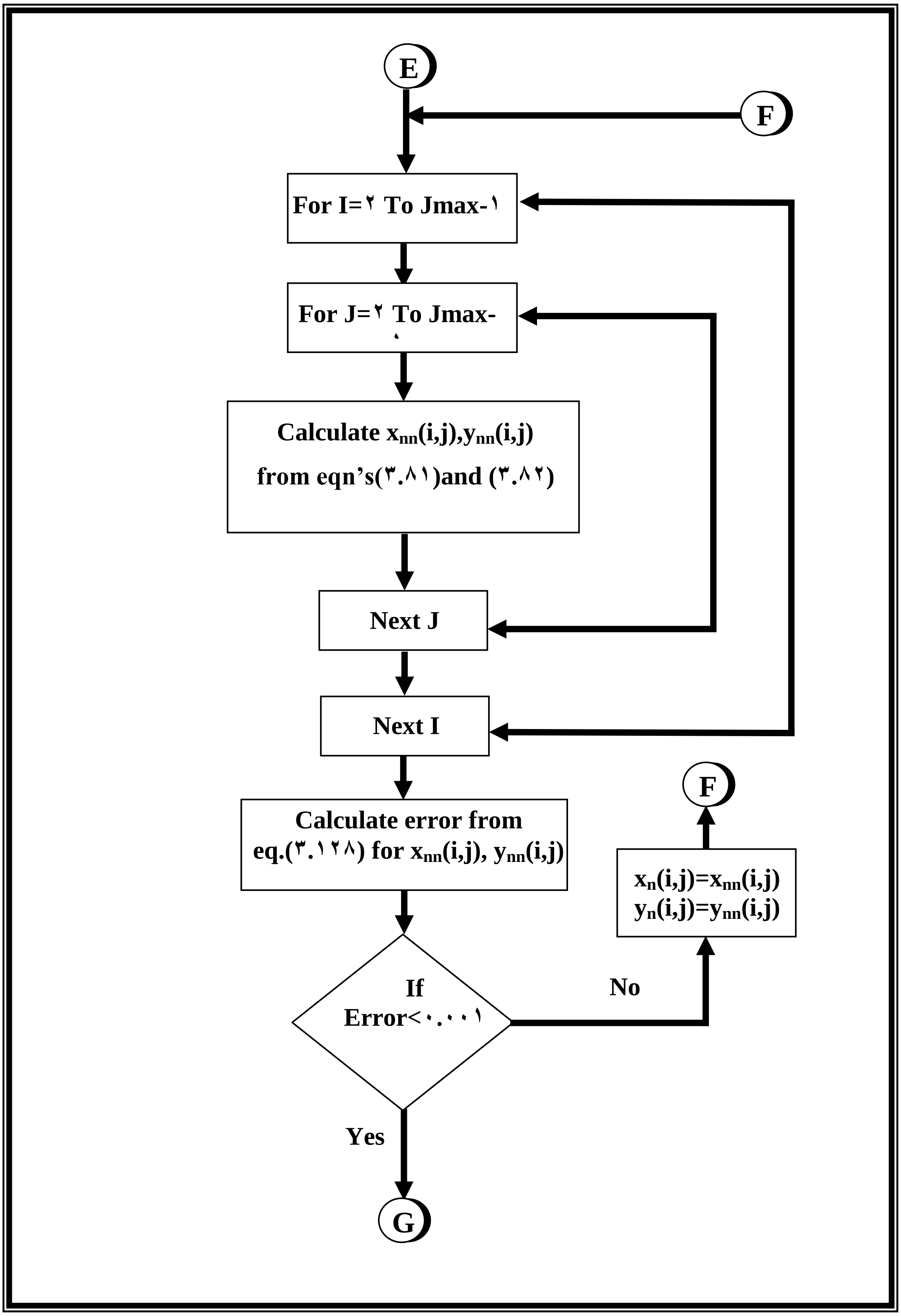

Fig. (٤-٩) Continued

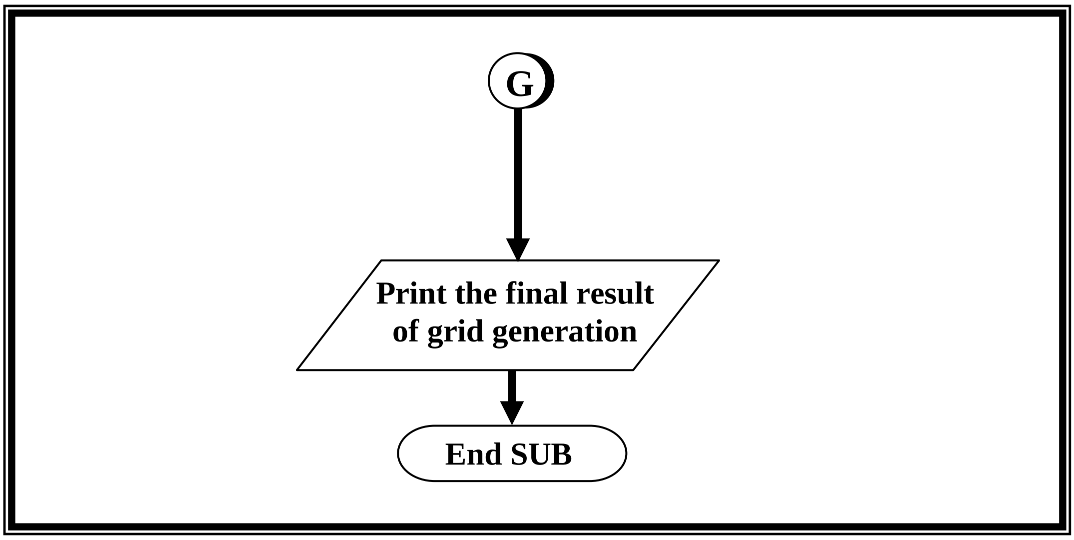

Fig. (٤-٩) Continued

CHAPTER FIVE

5

RESULTS AND DISCUSSION

٥.١ Introduction: -

Prediction of blade temperature distribution was performed by using six cases, hence six different heat transfer correlations.

In each case, the use of finite difference, numerical grid generation and transformation technique of blade geometry was necessary. The grid generation technique was used to divide the geometry into grids ”cells” using the body-fitted coordinate system approach so that the grids are fitted to the boundaries of the blades and therefore the initial conditions that surround the blade [externally and internally] can be used in a useful way.

In the six cases, the blade cooling was assumed to be by using a blade with impingement cooling and trailing edge ejection. The reason behind this choice is that this type of cooling has a wide range of use in practice.

٥.٢ Numerical Results and Discssion: -

٥.٢.١ Analysis No. (١):

The internal boundary conditions for analysis (١) can be summarized in Fig.(٥-١), showing the values of the heat transfer coefficient and the fluid temperature associated with each region of the blade. While the variation of external heat transfer coefficients along the blade surface are shown in Fig.(٤-٢) with the hot gas temperature is equal to (٩٦٣K) around the blade external profile.

Figure (٥-٢) illustrates the temperature distribution within the blade while figure (٥-٣) presents the variation of the blades' external temperature from the leading edge to the trailing edge.

The temperature contour pattern of figure (٥-٢) shows the maximum temperature of (٦٦٧.٧ K) at the leading edge region with falling temperatures along both the pressure and suction surfaces followed by a rise in temperature towards the trailing edge. This pattern is confirmed by the graph of blade surface temperatures in figure (٥-٣).

Closer inspection of figure (٥-٣) shows that over the pressure surface, from the leading edge, the temperature falls quite rapidly before leveling out and then increasing continuously towards the trailing edge. However along the suction surface the fall in temperature from the leading edge region is not great, but this reduction extends over a greater length of the blade than that on the pressure surface.

However the minimum temperature on the suction surface is approximately (٢٠ K) higher than the minimum temperature on the pressure surface i.e., over the mid-chord regions of the blade, the suction surface is hotter than the pressure surface. At the trailing edge the situation is reversed with the pressure surface hotter than the suction surface.

These differences in temperatures between the two surfaces can be accounted for by a number of factors:

١) The blade structure is hollow which reduces the connectivity between the pressure and suction surfaces and hence reduces the tendency to smooth out temperature differences between the two areas.

٢) As a result of (١) above, the influence of the variation of external heat transfer coefficient is much greater. Figure (٥-٤) shows that the resulting temperature variations can be explained by the variation of h_{ext}.

For example, ٨mm along the suction surface (٨,S.S.), there is a rapid fall in h_{ext} which results the reduction in temperature along the suction surface being halted at (٨,S.S.). After this point as h_{ext} begins to fall again the temperature levels also fall.

Comparing this to the pressure surface where h_{ext} falls very quickly from the stagnation point to (٥,P.S.), before rising slowly. The temperature variation is seen to mimic this by falling continuously to (٥,P.S.). The mid-chord regions also exhibit the effect of h_{ext}, with the decreasing temperature along the suction surface from (١٠,S.S.) to (٣٥,S.S.) reflecting the decreasing h_{ext} while the rise in temperatures along the pressure surface from (١٨,P.S.) to (٢٨,P.S.) mimicing the rising h_{ext}.

٣) The cooler pressure surface can also be accounted for by the higher values of the impingement heat transfer coefficients in this region. The variation of the array heat transfer coefficients does affect the variation of the resulting temperature distribution but because these array variations are much smaller than the variation of h_{ext} their influence on the temperature variations is consequentially less.

٤) The trailing edge temperature distribution is more complex than the other blade regions and reflects both the variations of h_{ext} as well as the varying blade wall thickness around the trailing edge slot. The general increase in temperature towards the trailing edge can also be accounted for by the lower value of h_{slot} when compared to the impingement values, h_a.

٥.٢.٢ Analysis No. (٢):

Analysis (٢) results are presented in Figures (٥-٥) and (٥-٦). Figure (٥-٥) observed that the temperature contours are very similar to those from analysis (١) with small differences noticeable around the trailing edge slot.

Figure (٥-٦) shows that the maximum temperature of (٦٦٢ K) at the leading edge region with falling temperatures along both the pressure and suction surfaces followed by a rise in temperature towards the trailing edge.

Figure (٥-٧) shows insignificant difference in blade temperatures away from the trailing edge region and hence the reason why the boundary conditions at the leading edge and impingement array were calculated to be the same as in analysis (١) and analysis (٢).

An inspection of the temperature at each node along the trailing edge in analysis (٢) revealed that at the initial entry section of the trailing edge at the pressure surface the temperature were (٢٠ K) higher when the parallel plate correlation was used as compared to the pipe flow correlation.

However this temperature difference reduced further along the trailing edge until at the exit, the temperature differences were about (٧ K) higher than analysis (١).

At the suction side of the trailing edge, it is obvious the temperature difference at the entry section of the trailing edge was (٥ K) higher when the parallel plate correlation was used and this temperature difference reduced until at the trailing edge exit to become higher than analysis (١) about (٣ k).

This difference in temperatures mimics the difference in h_{slot} between the two analyses. At the first analysis the pipe flow correlation provides a constant h_{slot} of (١٣٥٣ W/m^{٢} K) while from the parallel plate correlation provides a higher h_{slot} of (١٦٥١ W/m^{٢} K) at the trailing edge entrance which decreases rapidly to become (١٢٥٠ W/m^{٢} K) at the trailing edge exit.

٥.٢.٣ Analysis No. (٣):

The internal boundary conditions for this analysis are presented in Fig. (٥-٨),While the external boundary conditions are the same as in analysis (٢)

The results of the thermal analysis are presented in Figures (٥-٩) and (٥-١٠). Figure (٥-٩) shows a pattern very similar to the analysis (٢), (٥,٨) array with again the maximum temperature of (٦٨٨ K) at the leading edge. The temperature levels fall over the mid-chord regions before rising towards the trailing edge.

The graph of the blade surface temperature distribution Figure (٥-١٠) also appears very similar to the analysis (٢) reflecting again the major influence of the external hot gas heat transfer coefficient on the temperature distribution.

For the purpose of comparing the (٥,٨) and (٥,٥) arrays, Figure (٥-١١) plots the blade surface temperature distribution from analysis (٢) and analysis (٣). It is clear that while the pattern remains very similar, the (٥,٨) case, with less jet orifices produces lower blade temperatures than the (٥,٥) case which has more jet orifices.

This apparent contradiction occurs due to the reduction in Re_j as the number of orifice increase leading to a reduction in the levels of the heat transfer coefficient. For the trailing edge region of the blade, the difference between the blade surface temperatures is very small reflecting the diminishing influence of changes to the cooling arrangement of the insert and also reflecting the similarity of the boundary conditions along the trailing edge slot.

٥.٢.٤ Analysis No. (٤):

Figure (٥-١٢) shows the internal boundary conditions of this analysis, when the impingement heat transfer based on Tabakoff correlation.

The resulting blade temperature distribution as shown in figure (٥-١٣), shows a familiar pattern of temperature contours to the analysis (٣) with the maximum temperature at the leading edge region with falling temperatures along both the pressure and suction surfaces followed by a rise in temperature towards the trailing edge.

The minimum temperature on the suction surface is approximately (١٥ K) higher than the minimum temperature on the pressure surface i.e., over the mid-chord regions of the blade, the suction surface is hotter than the pressure surface due to the values of the impingement heat transfer coefficients in the pressure surface region are higher than the values of the impingement heat transfer coefficients in the suction surface.

The plot of blade surface temperature around the outer profile shown in figure (٥-١٤) appears the maximum temperature of (٦٨٩.٣ K) at the leading edge. Over the pressure surface the temperature falls quite rapidly from the leading edge and then increases continuously towards the trailing edge.

However, along the suction surface the fall in temperature from the leading edge region is not great, but this reduction extends over a greater length of the blade than that on the pressure surface. At the trailing edge the pressure surface is hotter than the suction surface.

٥.٢.٥ Analysis No. (٥):

The internal boundary conditions are illustrated in Figure (٥-١٥). This figure shows the specification of the boundary conditions for analysis (٥) utilizing the Chance correlation, [٤٦]

The thermal analysis results shown in figures (٥-١٦) and (٥-١٧), produce the expected result of little variation from the two previous analyses with both the blade temperature distribution and the blade surface temperatures appearing very similar since the impingement jet array boundary conditions did not vary greatly.

It is useful to compare the values of blade surface temperature obtained from the three different heat transfer coefficients used in (٣,٤ and ٥) analyses. Figure (٥-١٨) shows this comparison between the three analyses where the correlations used in these analyses were limited to square arrays.

It is clear that the analysis (٣) for a (٥,٥) array based on Florschuetz et al, [٤٢] correlation produces lower blade temperatures than both of analyses (٤) and (٥). While analysis (٤) is based on Tabakoff, [٤٥] correlation produces higher blade temperatures than both of analyses (٣) and (٥) on the suction surface and produces higher blade temperatures than analysis (٣) and lower blade temperatures than analysis (٥) on the pressure surface.

For analysis (٥) is based on Chance, [٤٦] correlation noticed that it has highest values of blade temperatures on the pressure surface but, on the suction surface produces blade surface temperatures higher than analysis (٣) and lower than analysis (٤).

These differences in temperatures between these three analyses can be explained as shown in figures (٥-١٩) and (٥-٢٠) which illustrated the variation of heat transfer coefficients (h_a) along the array for the suction and pressure surfaces respectively.

Analysis (٥) provides the lowest values of (h_a) over the first two jet rows for both the suction and pressure surfaces whilst the subsequent values of (h_a) over the remaining downstream rows lie between those of the analysis (٣) and analysis (٤).

Analysis (٣), provides higher values of (h_a) than the other two analyses, at all rows except the first row on the suction and pressure surfaces, where analysis (٤) results in the highest values of (h_a). The variation of (h_a) along the array is the same for the three analyses with an initial decrease before (h_a) rises at the downstream rows.

The differences in the values of (h_a) among the analyses are relatively small in all analyses. The maximum divergence between any of the analyses occurs at (٢٥-٣٠) mm on the suction surface where the difference in (h_a) is (١١٤W/m^{٢} K) and occurs between the analysis (٣), (h_a=١٣٨٤ W/m^{٢} K) and the analysis (٤), (h_a=١٢٧٠ W/m^{٢} K). At all other regions the differences in (h_a) are less than (١١٤W/m^{٢} K).

It has been found that the three different heat transfer correlations for the jet impingement areas produced similar values of heat transfer coefficients with the results that the blade temperature distribution also appeared very similar and therefore the use of any of the three correlations is acceptable for this particular type of blade geometry.

٥.٢.٦ Analysis No. (٦):

Figure (٥-٢١) shows the internal boundary conditions of analysis (٦) when the blade is cooled with film cooling.

Figure (٥-٢٢) illustrates the temperature contour pattern within the blade and shows the significant effect that film cooling has on the blade temperatures. Again the highest temperatures occur at the leading edge corresponding to the area of highest (h_{ext}) and no film cooling. Across the pressure and suction surfaces the temperatures fall considerably due to the effect of the multiple rows of film cooling and low temperature reach to (٤٣٠ K).

The variation of the blade surface temperature is shown in figure (٥-٢٣). This shows that the maximum temperature of (٦٤٨ K) at the leading edge with falling temperatures along both the pressure and suction surfaces followed by a rise in temperature toward the trailing edge.

Figure (٥-٢٤) shows the comparison of blade surface temperature between analysis (٢) without film cooling analysis (٦) with film cooling.

Due to the lack of the film cooling around the leading edge, the blade temperatures in this region remain nearly high for this analysis, with the film cooling as for analysis (٢), without the film cooling. However it is clear that the blade temperature decreases rapidly after this area and results in the film cooled blade as much as (١٧٠ K) cooler than the blade without film cooling.

The rise in temperature at the trailing edge can be accounted for by a number of factors such as the reducing trailing edge slot heat transfer coefficient together with the reducing value of (E_f) over this region as the last row of film cooling holes is located well upstream of this area.

Figure (٥-٢٥) shows comparison between blade surface temperature for the six methods of analyses used in this work. It is clear seen that in all analyses the maximum temperature occurs at the leading edge. In the pressure and suction surfaces the temperature decreases followed by a rise in temperature toward the trailing edge.

It is obvious from figure (٥-٢٥) that analysis (٦) with the film cooling gives lower temperature distribution than the other analyses. For the remaining analyses without the film cooling, it can be seen that analysis (٢) for (٥,٨) array and trailing edge heat transfer based on plate flow gives temperature distribution lower than analysis (١) which has the same blade geometry but the trailing edge heat transfer based on pipe flow and lower than both of analyses (٣,٤ and ٥) which has more jet array for the insert geometry i.e.,(٥,٥) array and trailing edge heat transfer based on plate flow.

The temperature distribution obtained by using the finite difference method will be compared here with that obtained in using the finite element method, Ref [١٠].

Figure (٥-٢٦) shows a great similarity between the finite difference and the finite element results, which seems to coincide in most regions along blade surface.

The differences between the results of the two methods are due to the differences in the technique of each method as well as the use of transformation theory, which depends on the transformation of curved boundaries of blade profiles into straight lines.

An inspection to the graphs, we can see that the difference of the finite difference results from the finite element method is very small. This difference was calculated to be (٣.٥٠٣ %) as maximum value and it falls to (٠٪) in most regions.

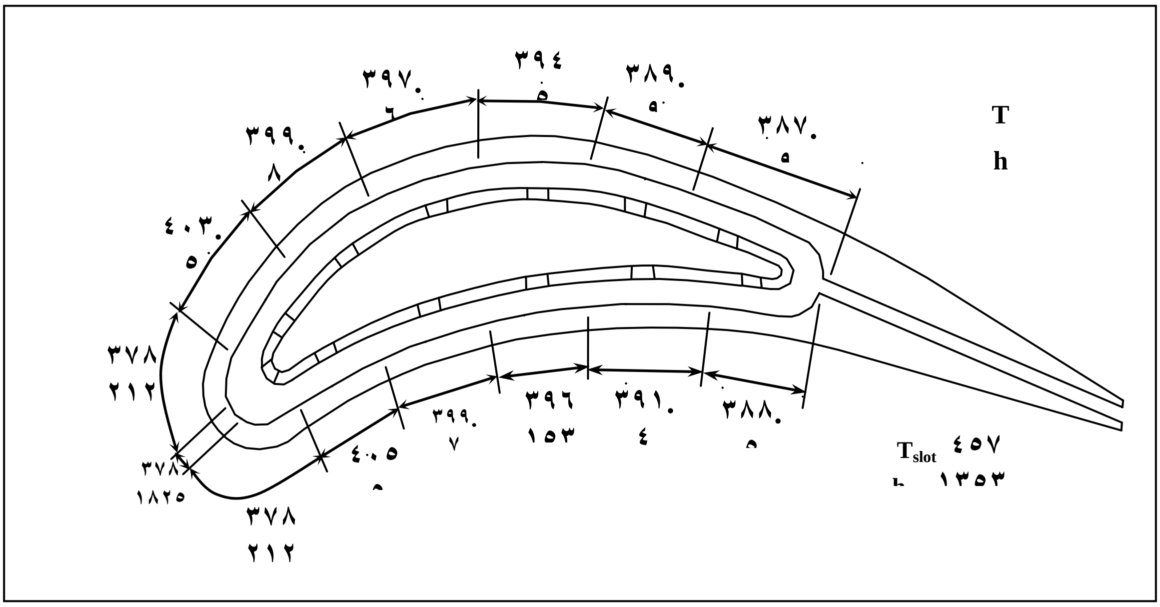

Figure (٥-١) Internal Boundary Condition-**Analysis (١)**

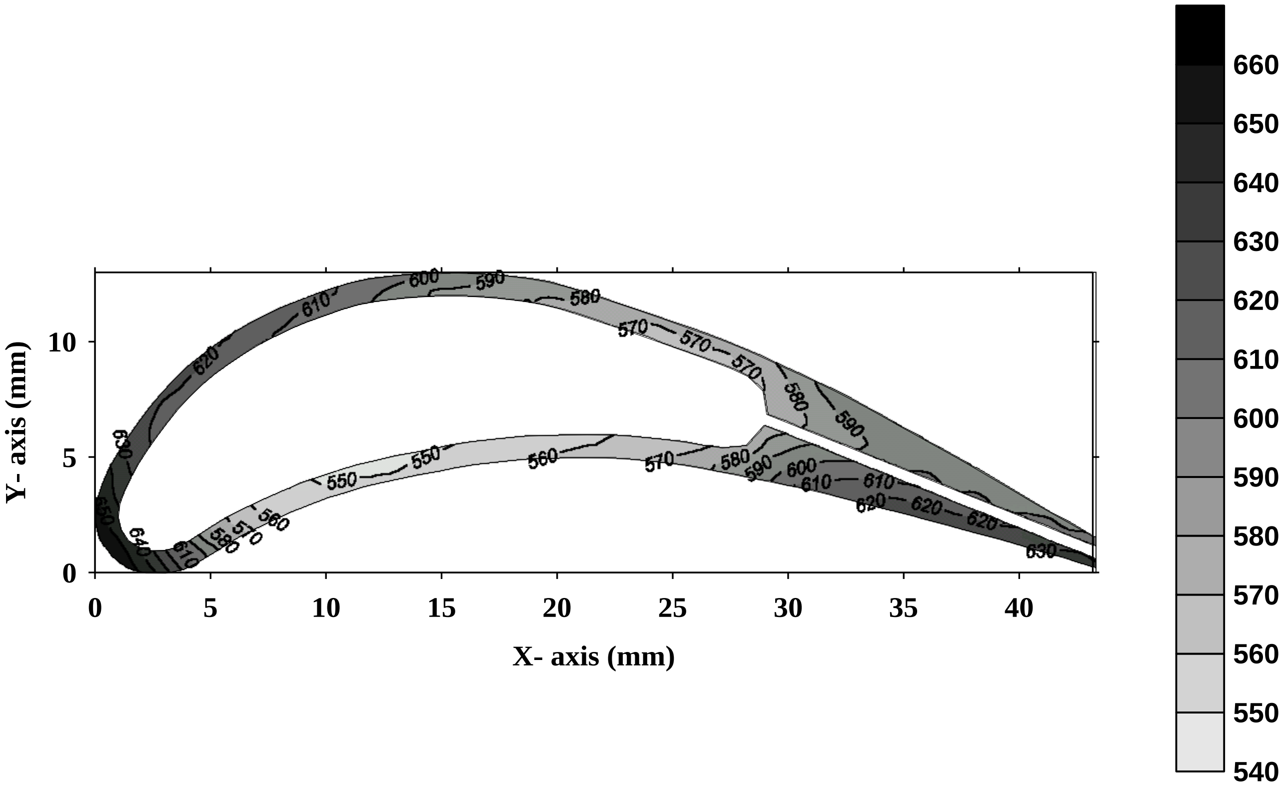

Figure (٥-٢) Isothermal Contour of Blade Temperature Distribution, **Analysis (١).**

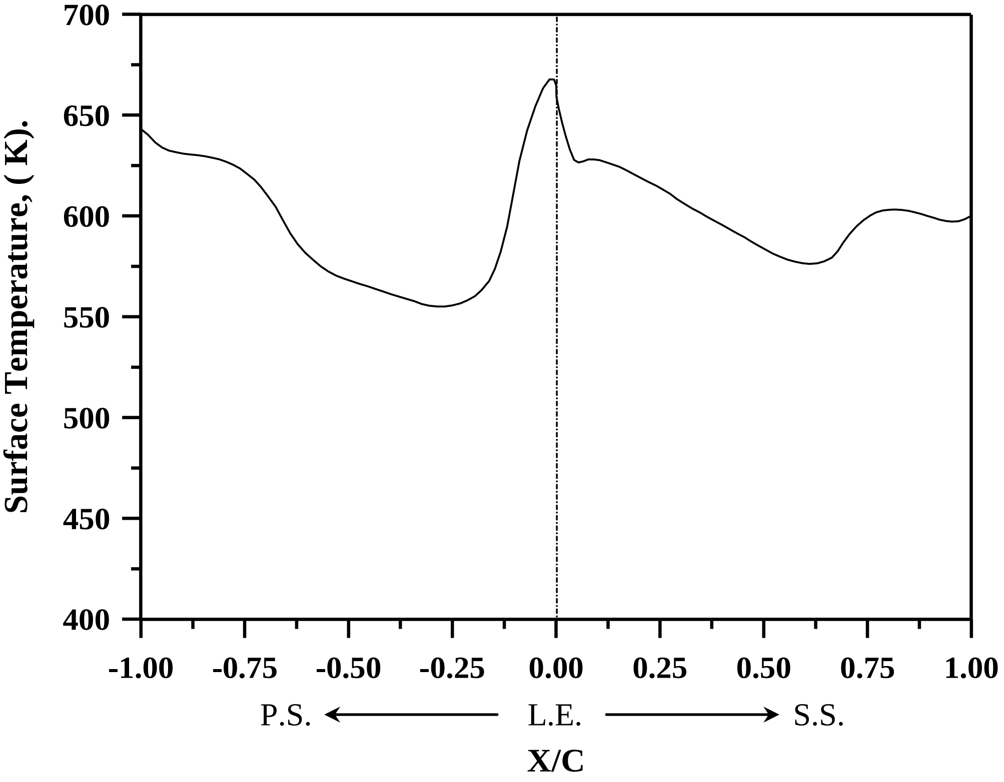

Figure (٥-٣) Blade Surface Temperature Distribution, **Analysis (١)** [Trailing Edge Heat Transfer Based on Pipe Flow].

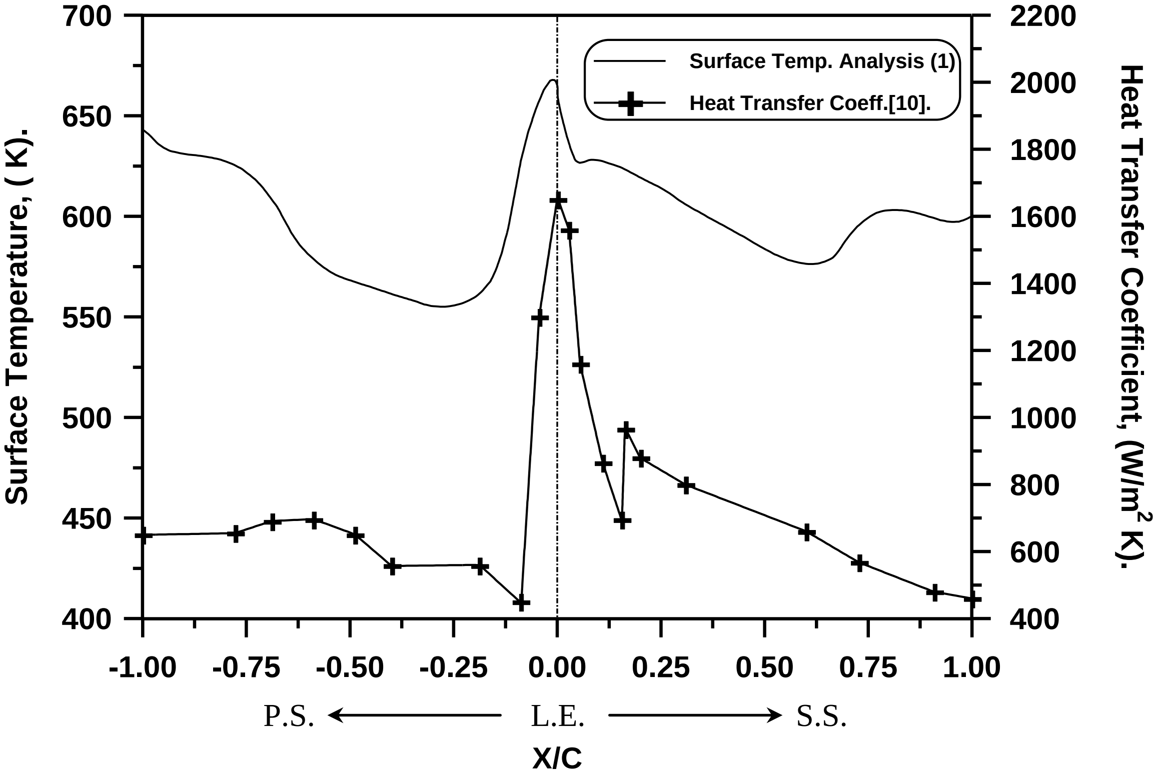

Figure (٥-٤) The Influence of the External Heat Transfer Coefficient on the Blade Surface Temperature Distribution, **Analysis (١).**

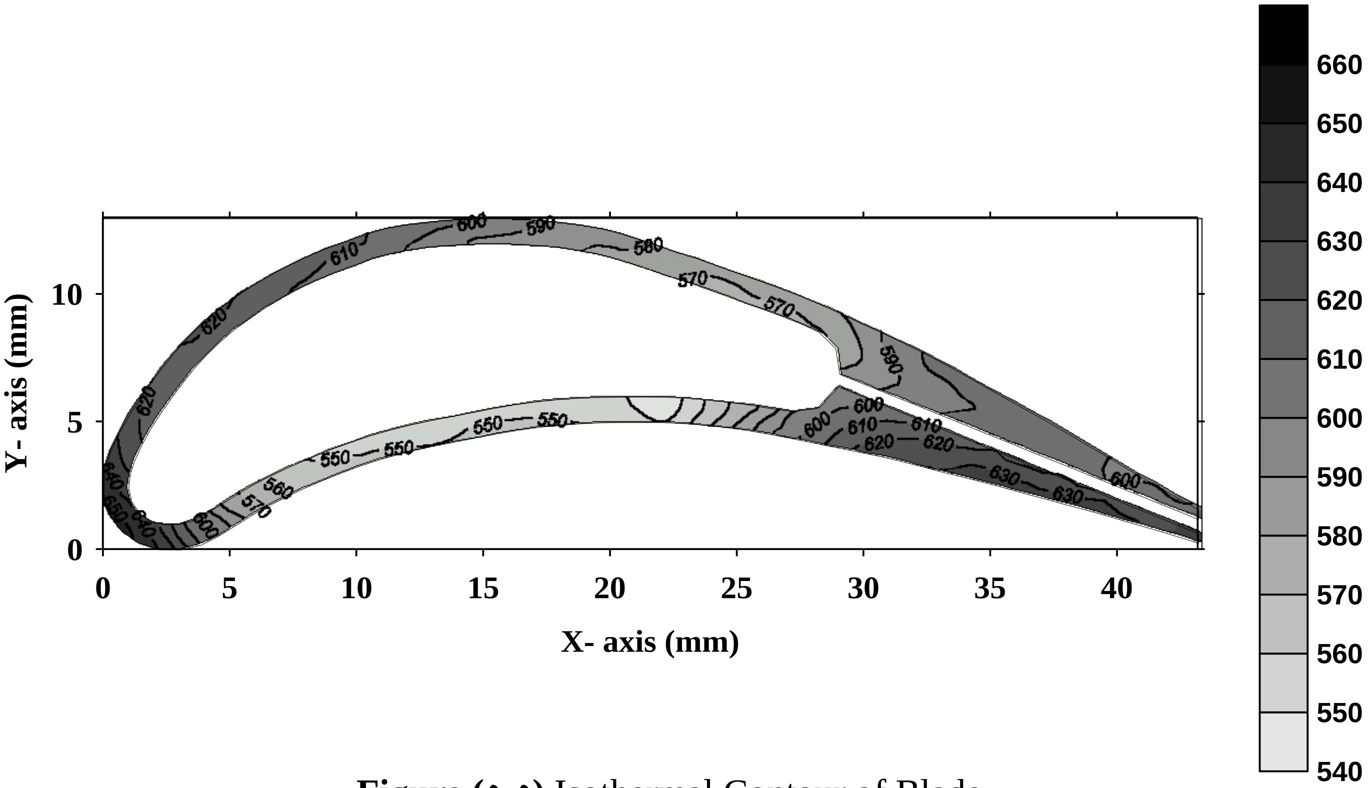

Figure (٥-٥) Isothermal Contour of Blade Temperature Distribution, **Analysis (٢).**

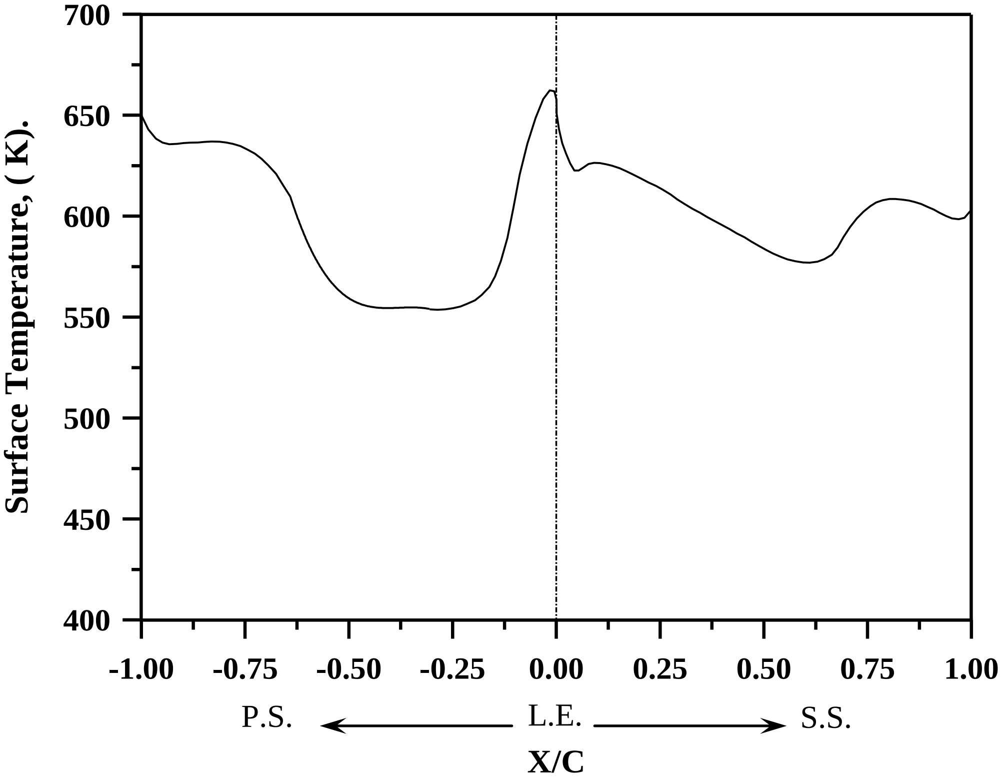

Figure (٥-٦) Blade Surface Temperature Distribution, **Analysis (٢)** [Trailing Edge Heat Transfer Based on Plate Flow].

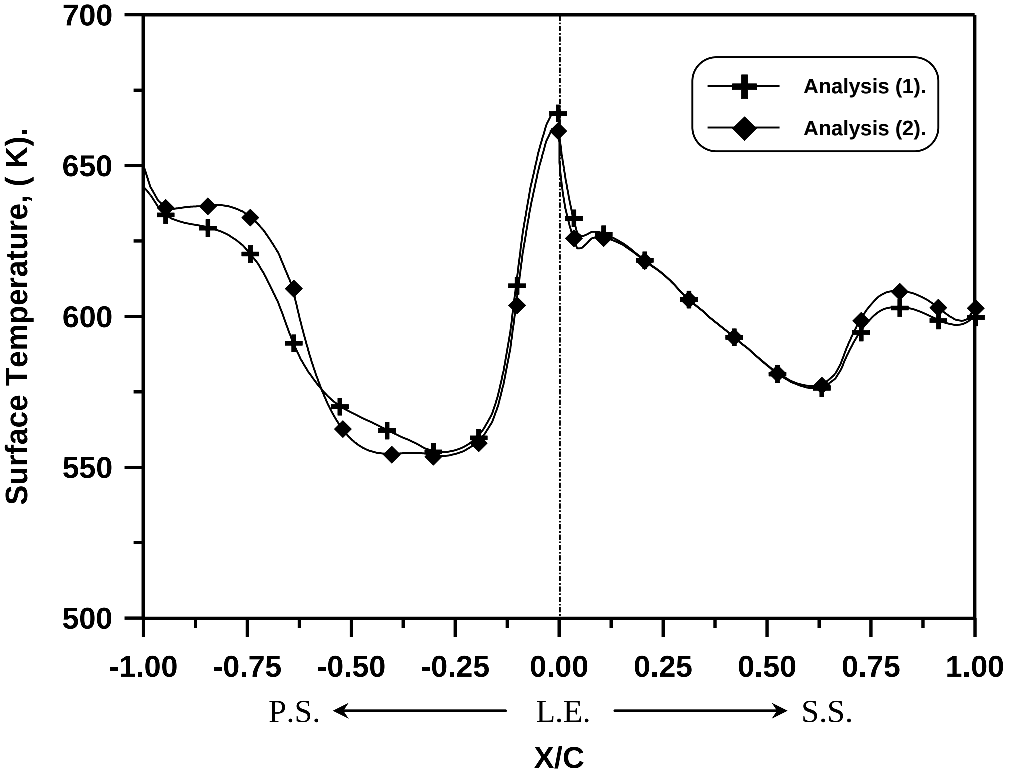

Figure (٥-٧) Comparison of Blade Surface Temperature between **Analysis (١)** and **Analysis (٢)**.

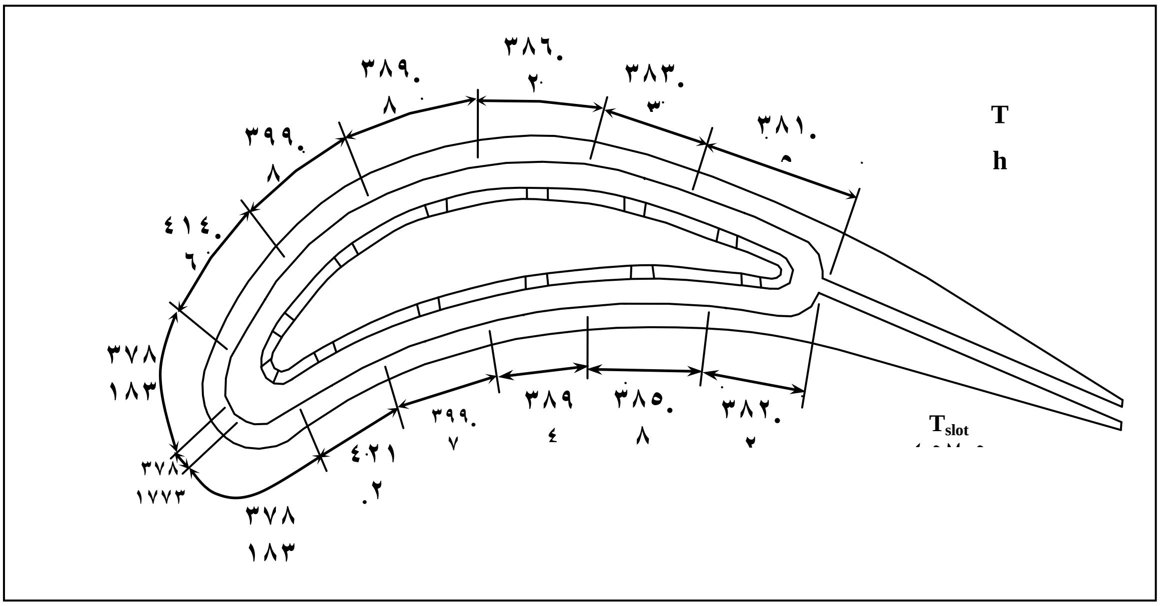

Figure (٥-٨) Internal Boundary Condition-**Analysis (٣)**

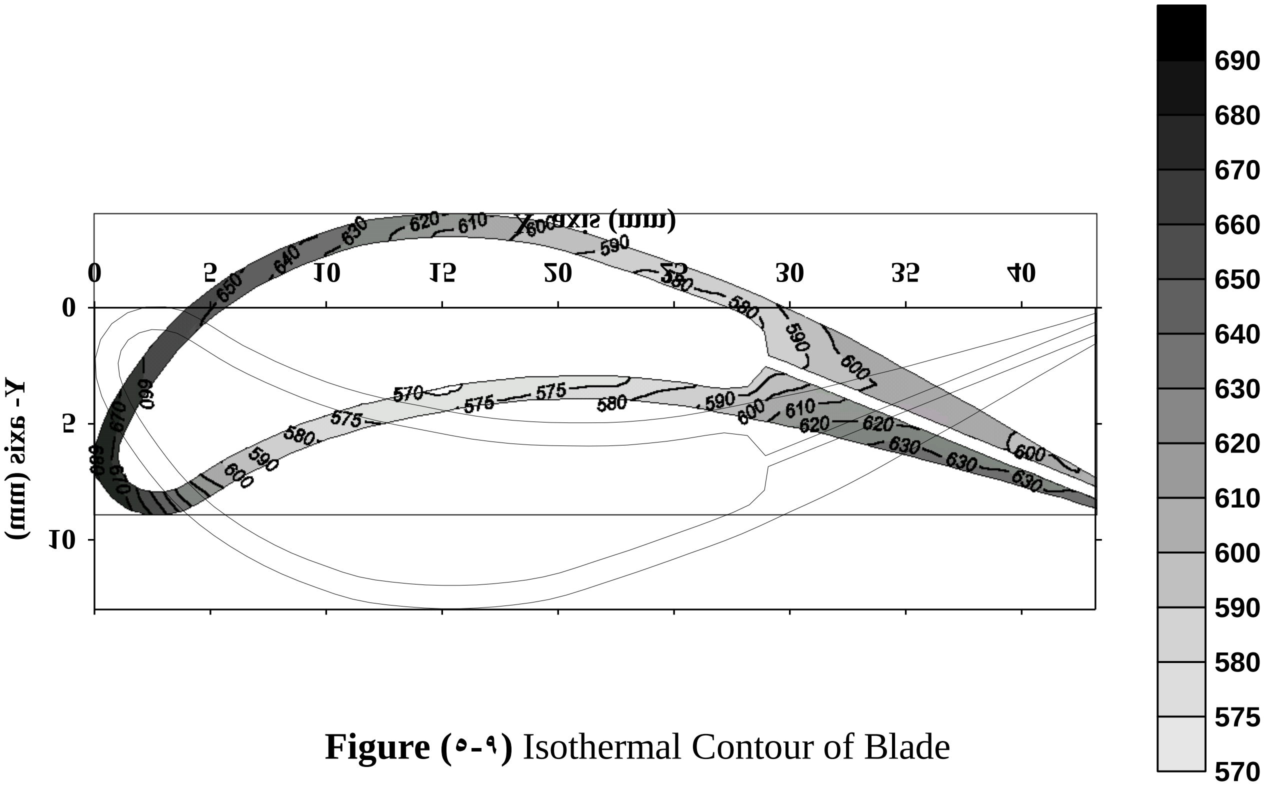

Figure (٥-٩) Isothermal Contour of Blade Temperature Distribution, **Analysis (٣).**

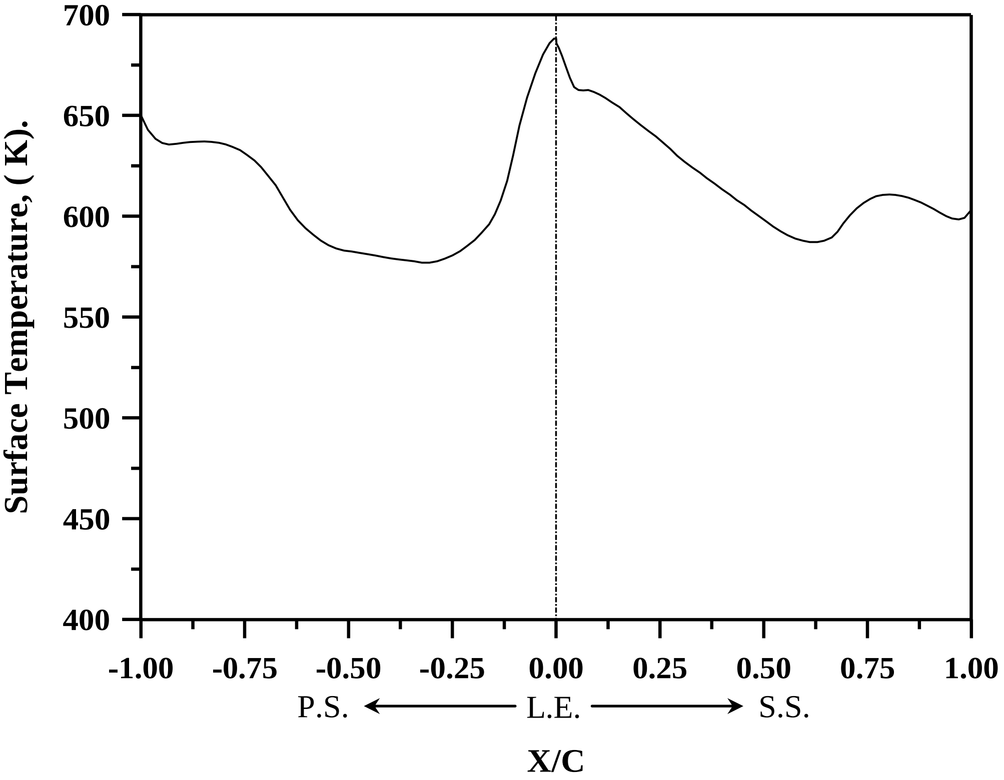

Figure (٥-١٠) Blade Surface Temperature Distribution, **Analysis (٣)** [(٥,٥) Array Based on Florschuetz Correlation].

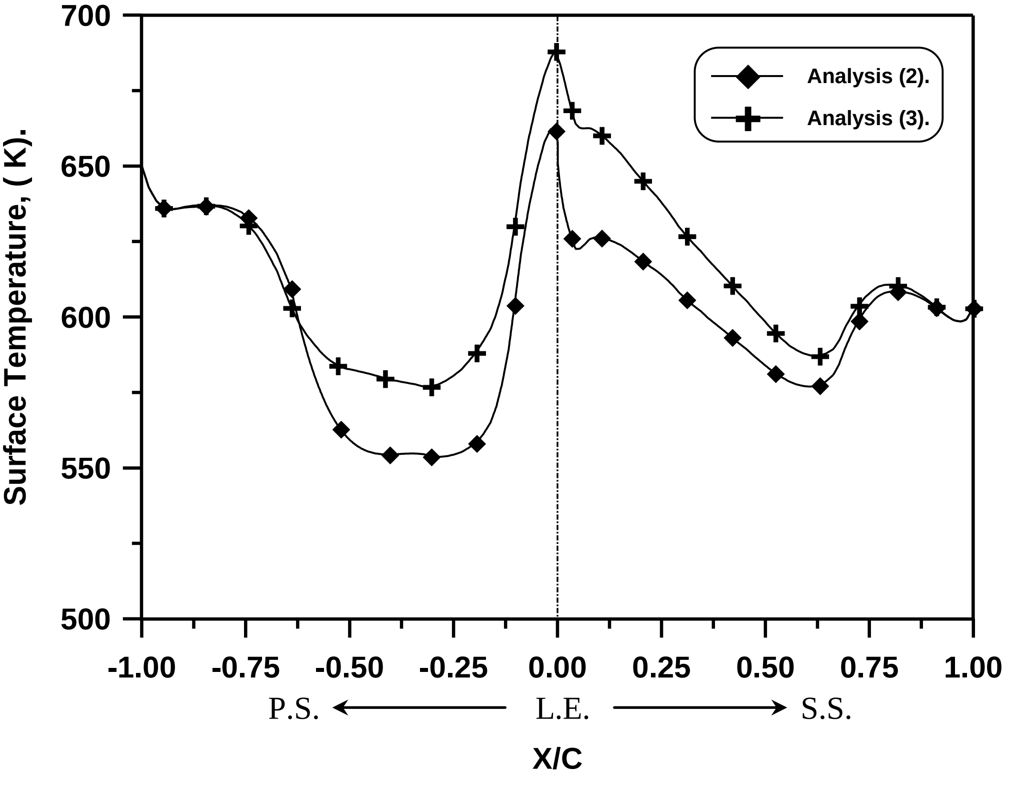

Figure (٥-١١) Comparison of Blade Surface Temperature between **Analysis (٢)**[Array (٥,٨)] and **Analysis (٣)** [Array (٥,٥)] where The Trailing Edge Heat Transfer Based on Plate Flow.

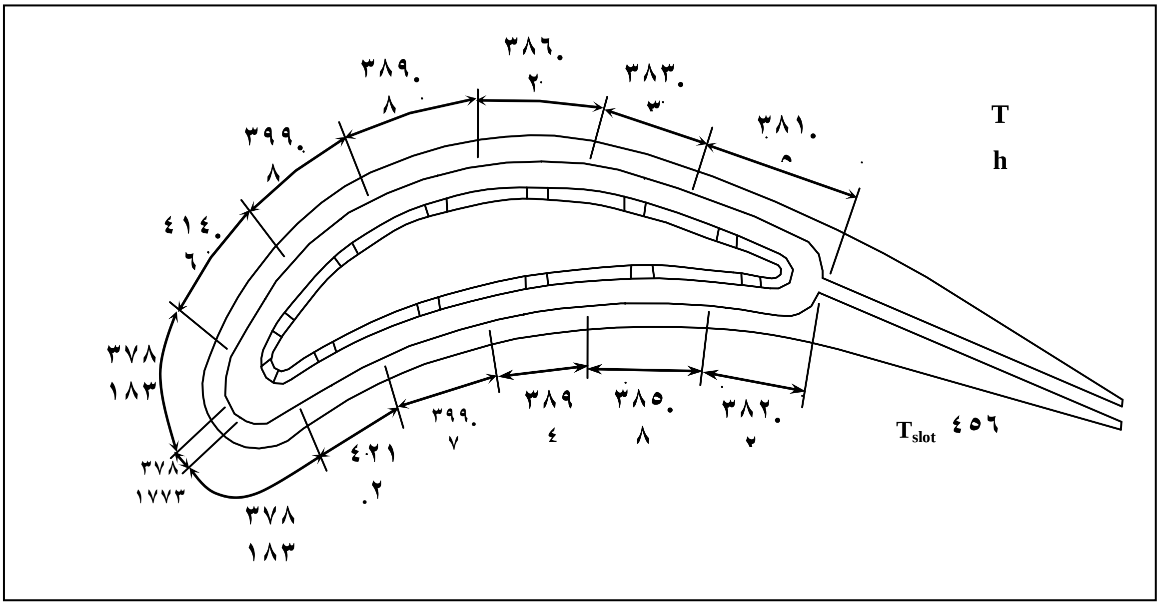

Figure (٥-١٢) Internal Boundary Condition-**Analysis (٤)**

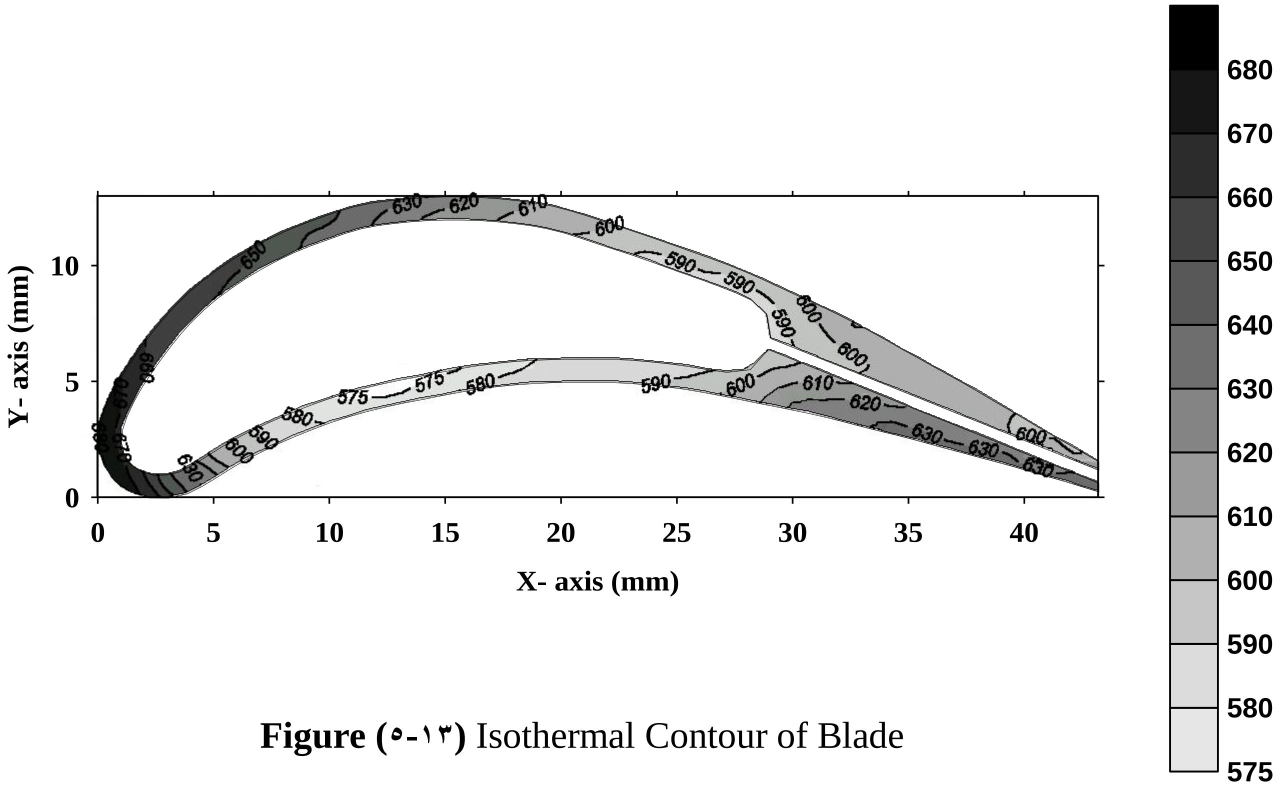

Figure (٥-١٣) Isothermal Contour of Blade Temperature Distribution, **Analysis (٤).**

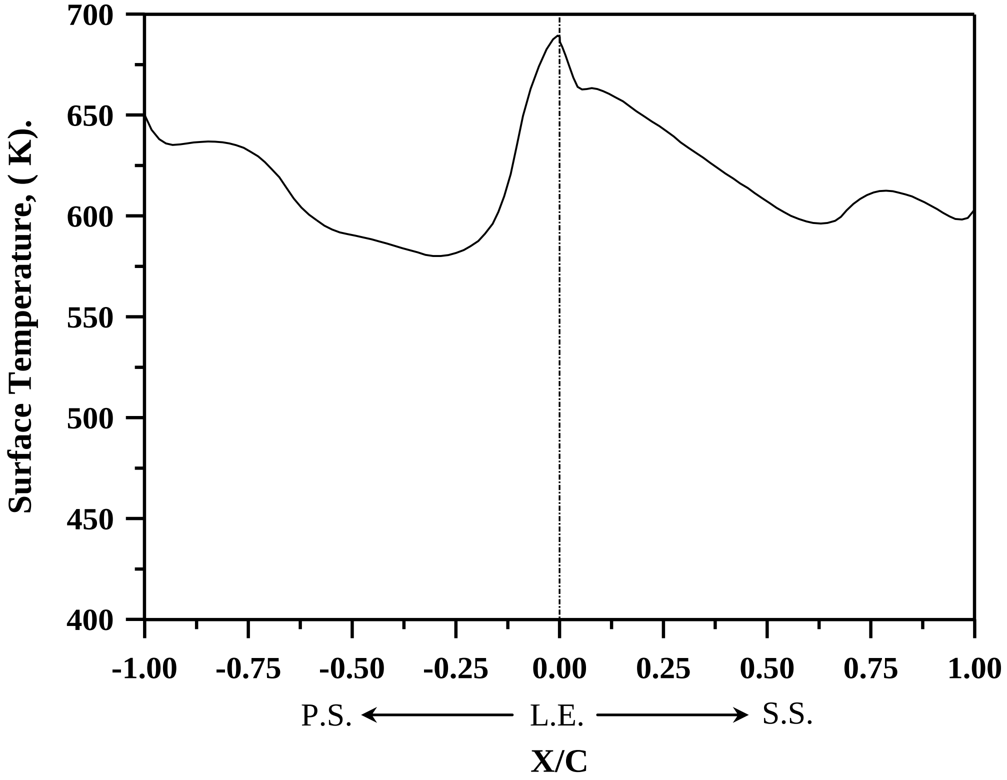

Figure (٥-١٤) Blade Surface Temperature Distribution, **Analysis (٤)** [(٥,٥) Array based on Tabakoff Correlation.

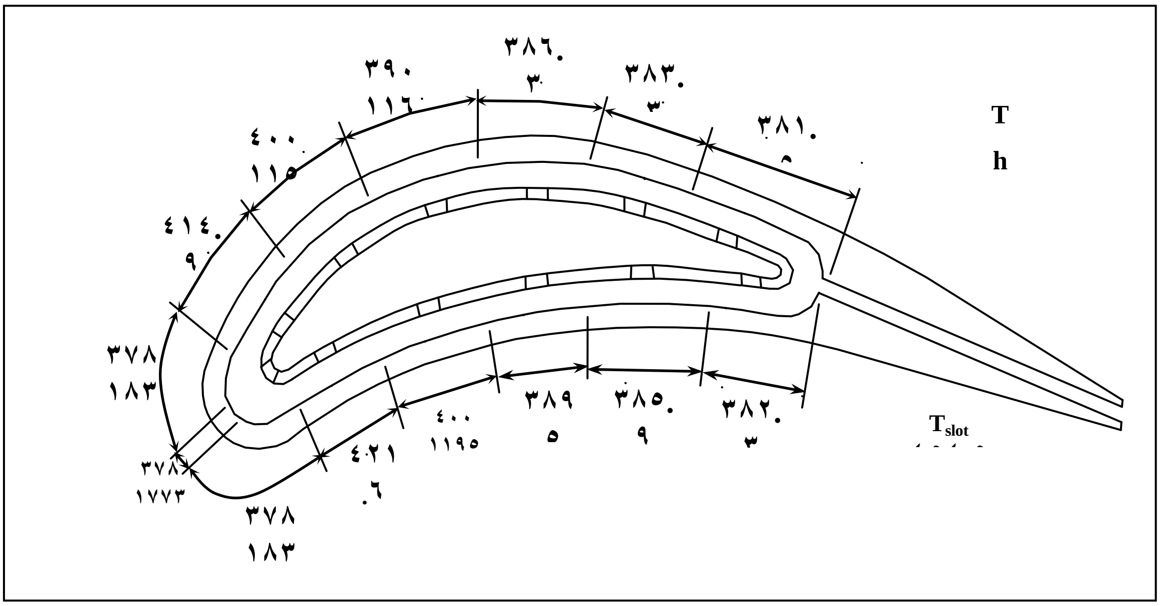

Figure (٥-١٥) Internal Boundary Condition-**Analysis (٥)**

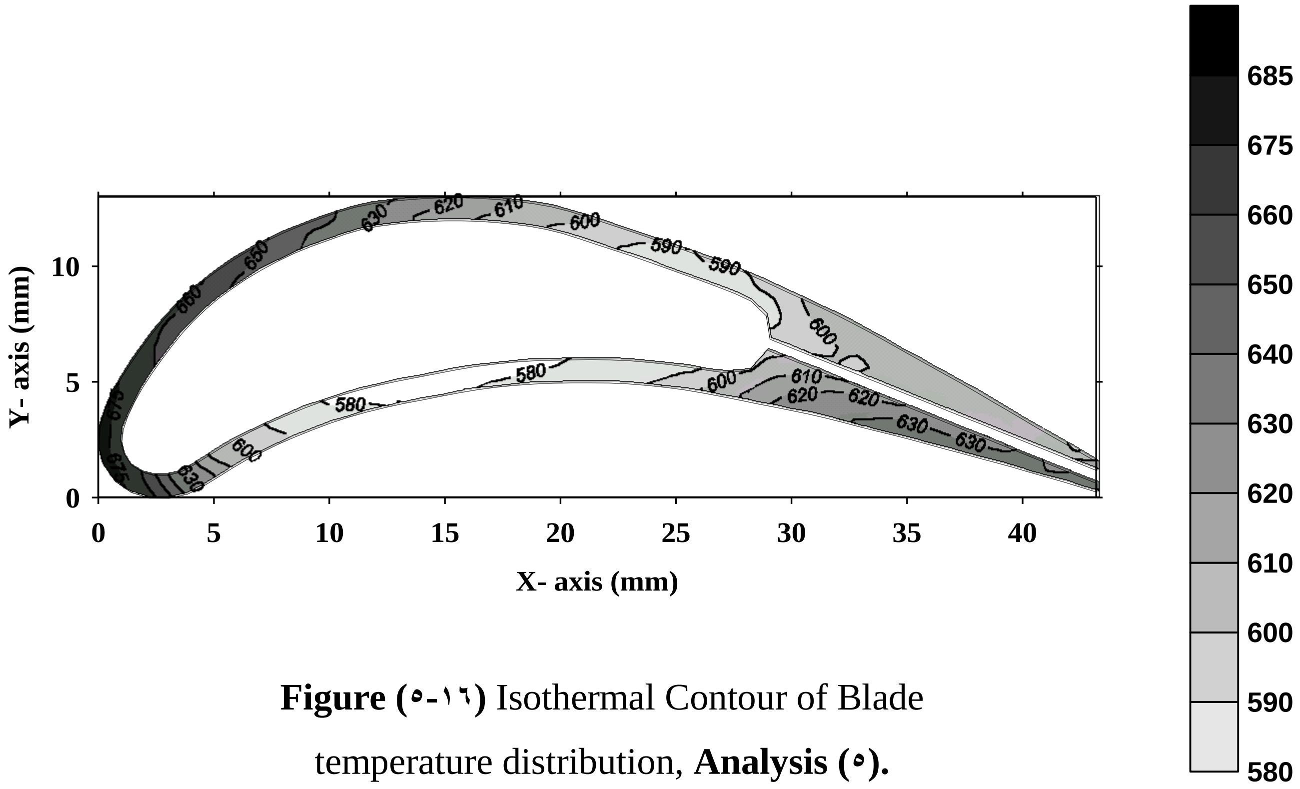

Figure (٥-١٦) Isothermal Contour of Blade temperature distribution, **Analysis (٥).**

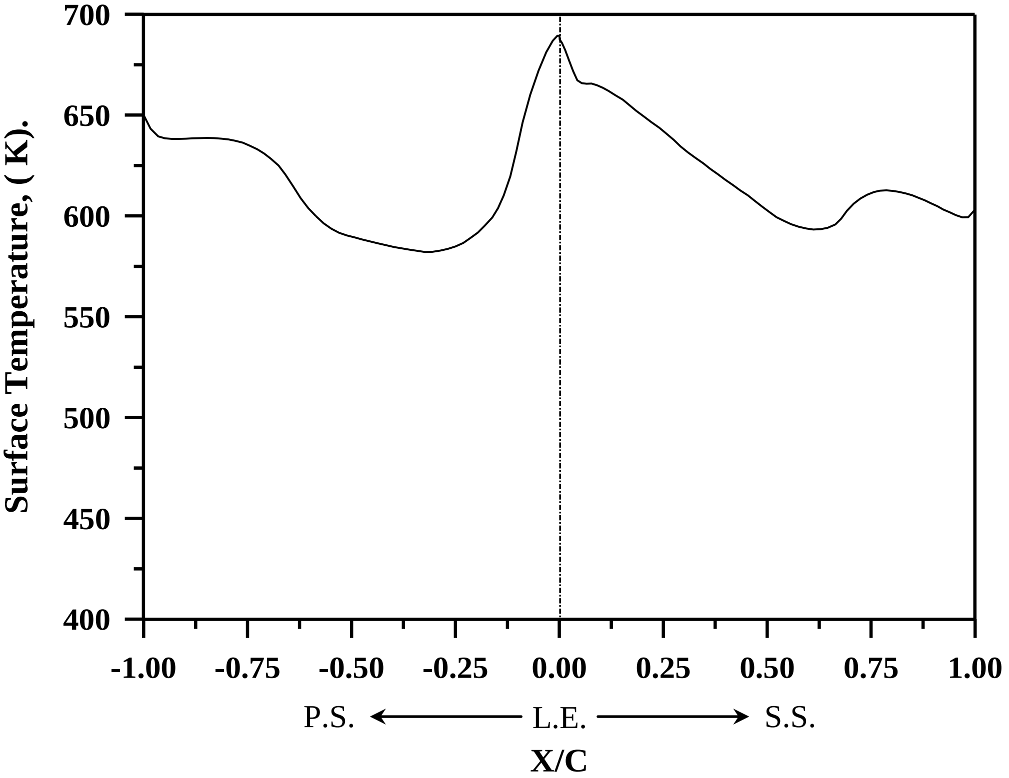

Figure (٥-١٧) Blade Surface temperature distribution, **Analysis (٥)** [(٥,٥) Array Based on Chance Correlation].

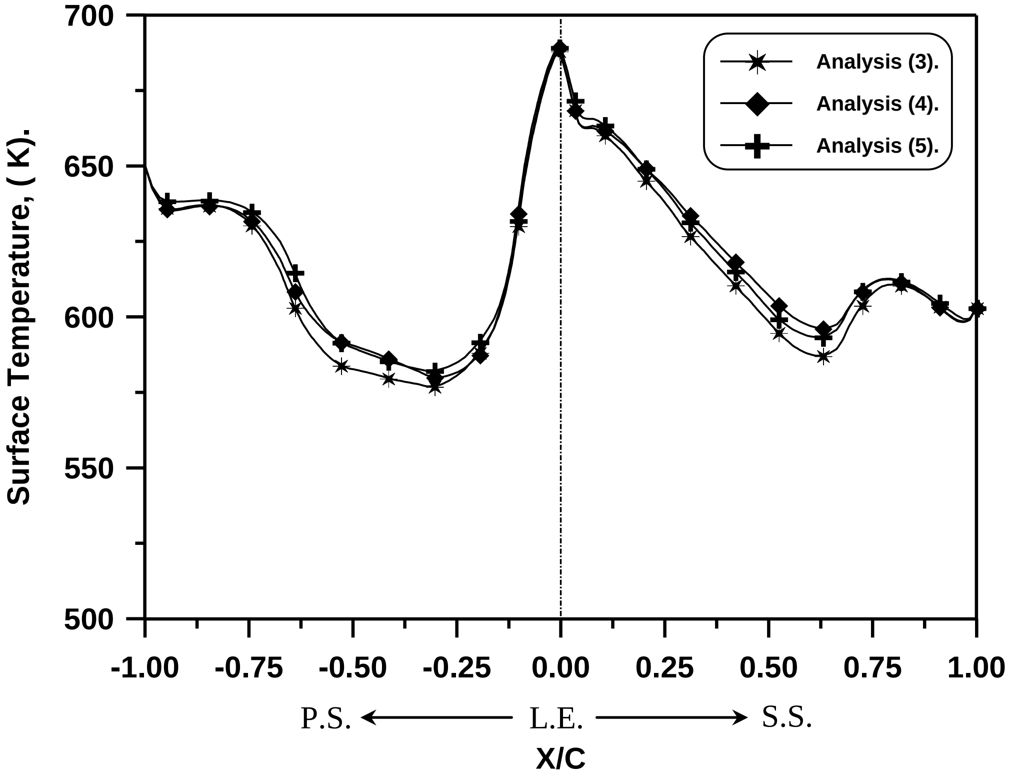

Figure (٥-١٨) Comparison of Blade Surface Temperature Between Analyses (٣,٤ and ٥) [The Same Insert Geometry ,with (٥,٥) Array].

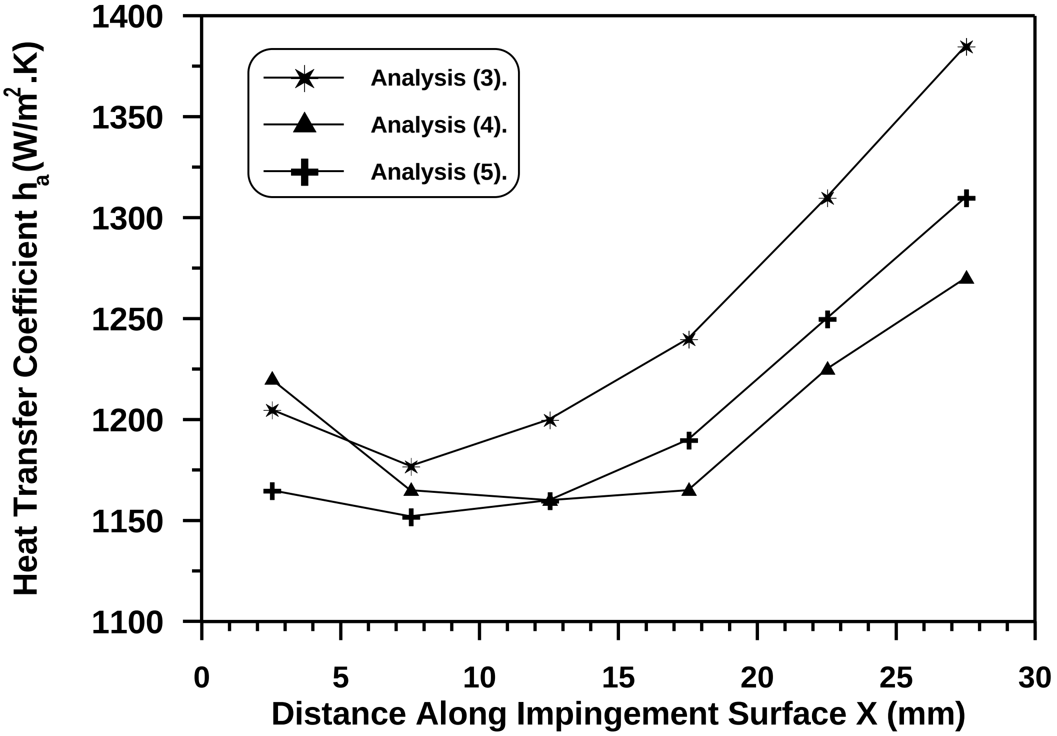

Figure (٥-١٩) Suction Surface Impingement Array Heat Transfer Coefficient.

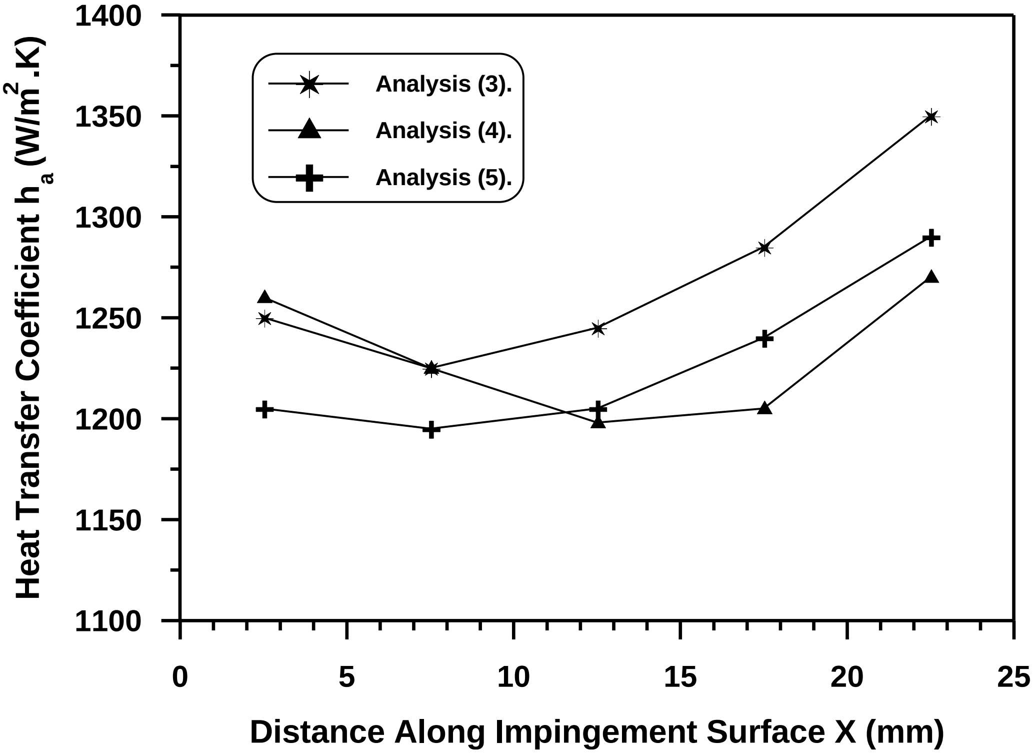

Figure (٥-٢٠) Pressure Surface Impingement Array Heat Transfer Coefficient.

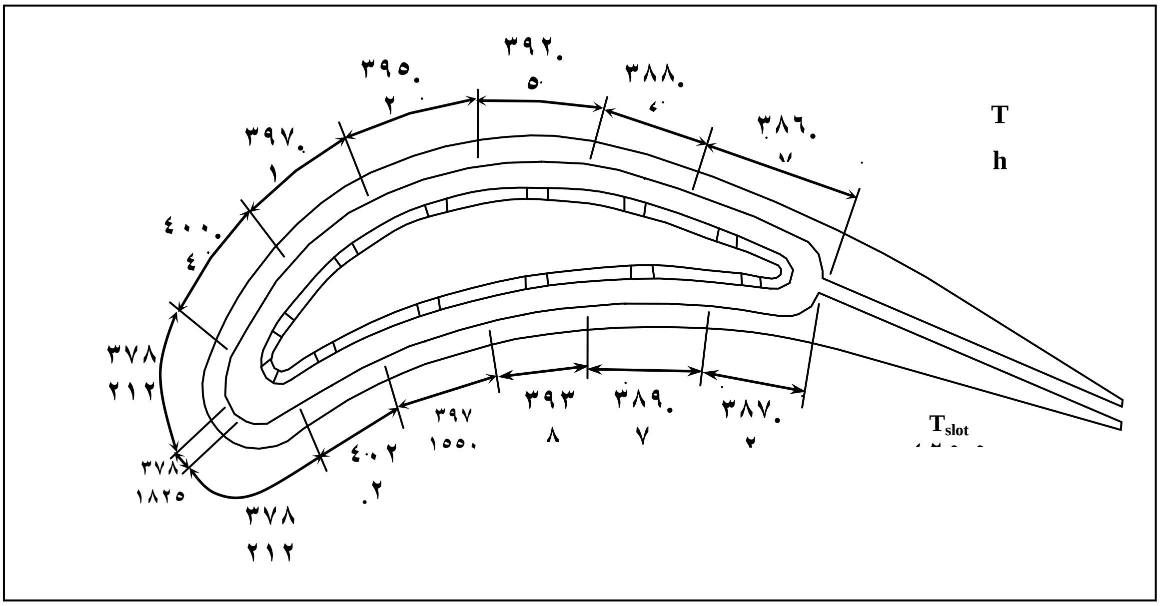

Figure (٥-٢١) Internal Boundary Condition-**Analysis (٦)**

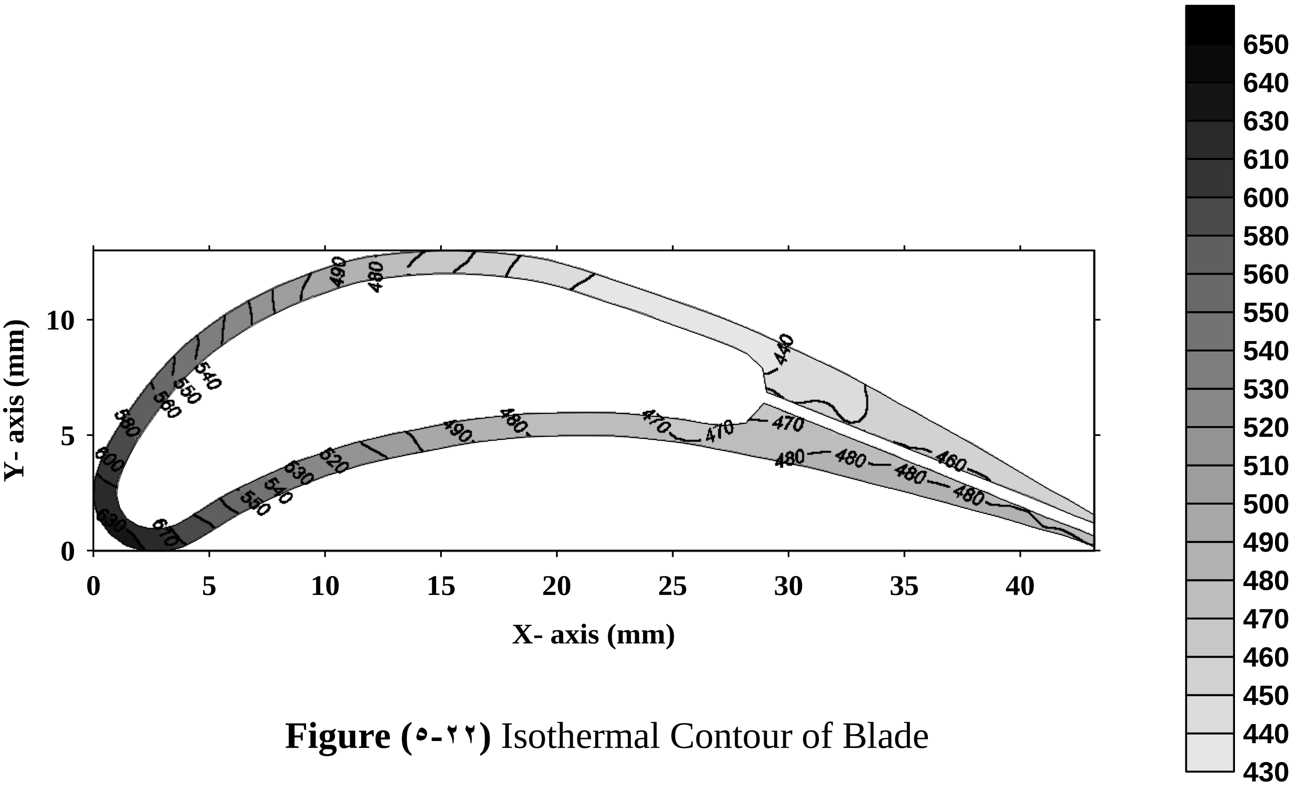

Figure (٥-٢٢) Isothermal Contour of Blade temperature distribution, **Analysis (٦)**

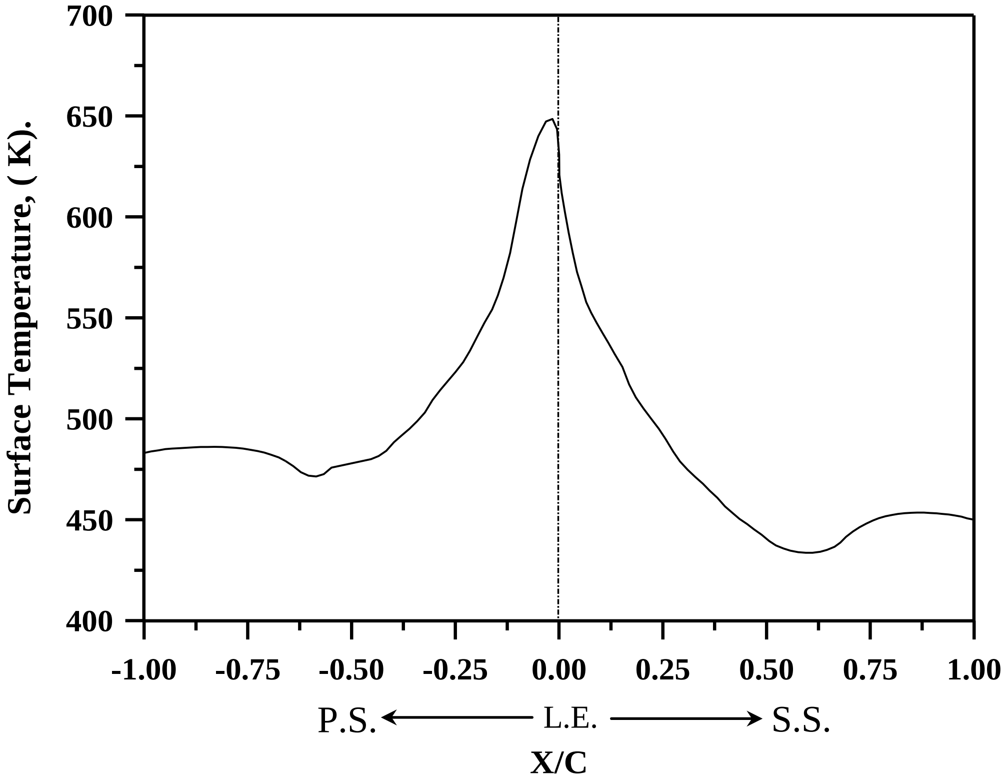

Figure (٥-٢٣) Blade Surface temperature distribution, Analysis (٦) [(٥,٨) Array with Film Cooling].

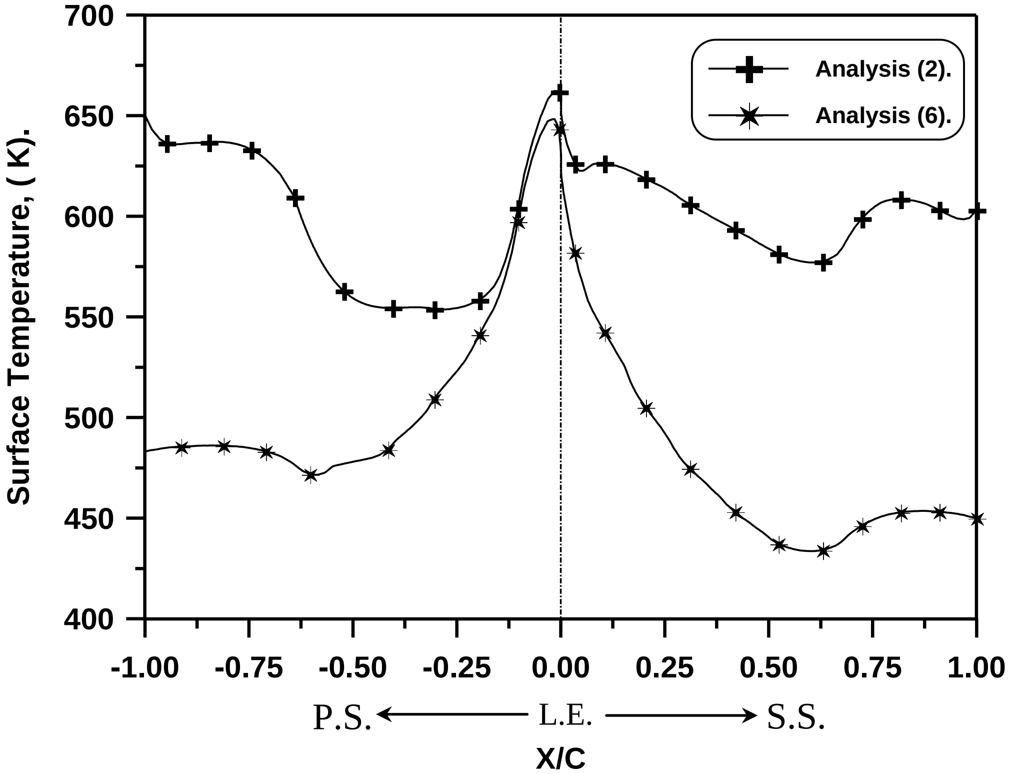

Figure (٥-٢٤) Comparison of Blade Surface Temperature Between **Analysis (٢)** Without Film Cooling and **Analysis (٦)** With Film Cooling

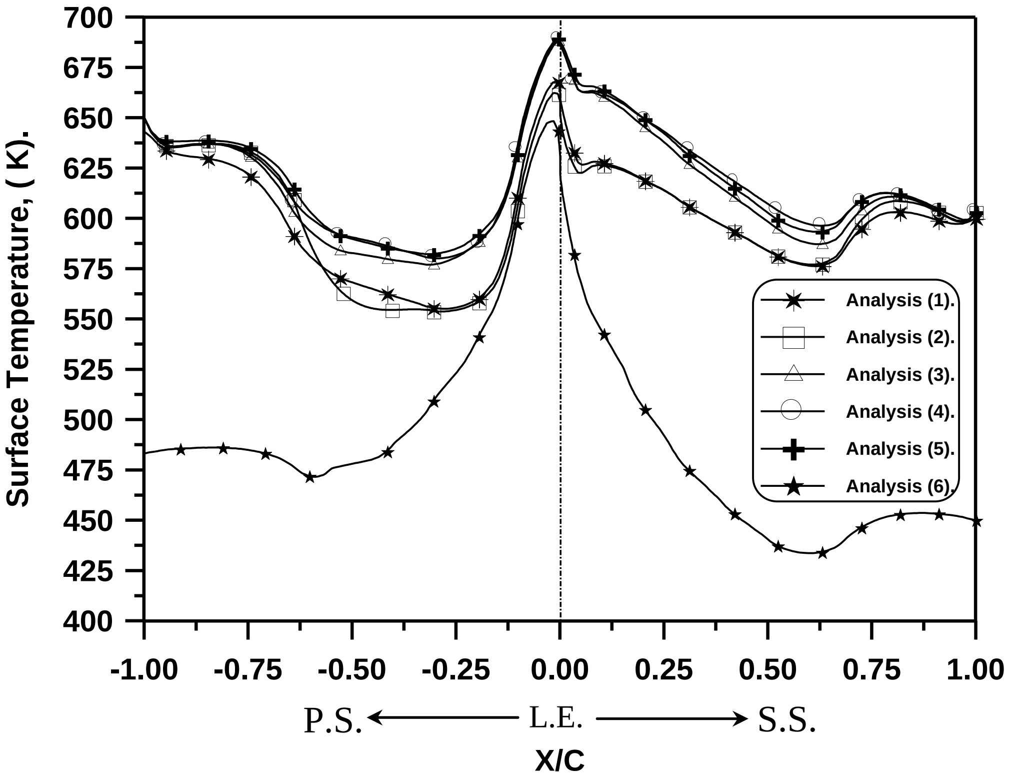

Figure (٥-٢٥) Comparison between Blade Surface Temperature For the Six Analyses.

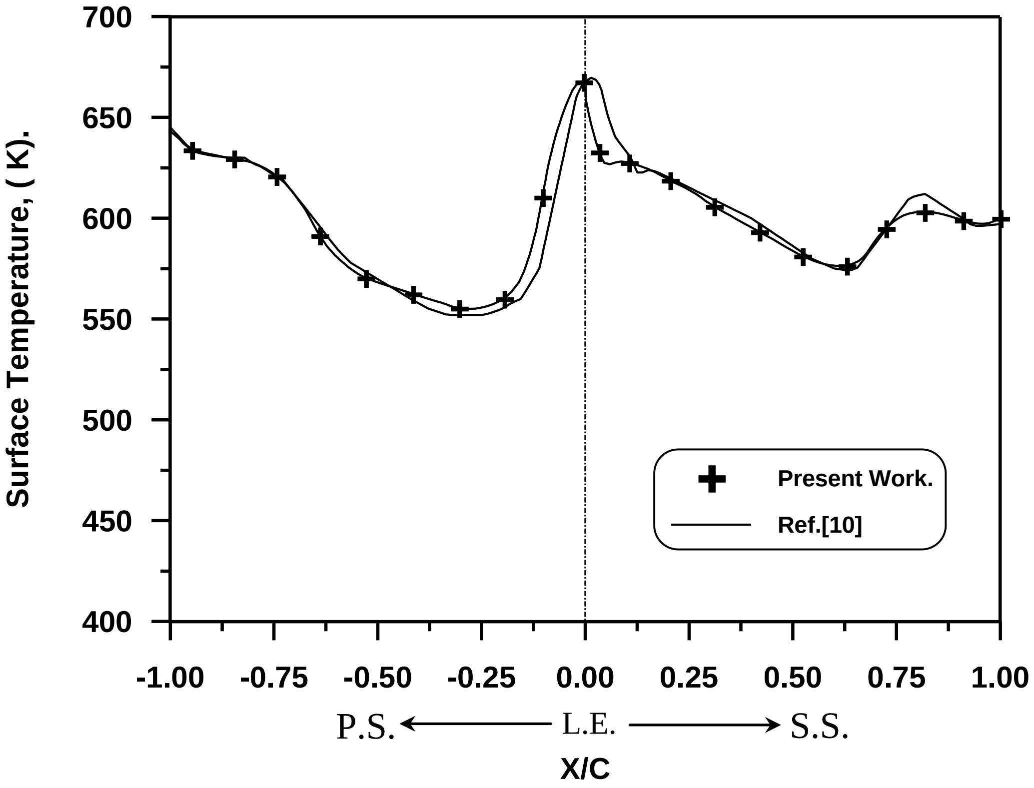

Figure (٥-٢٦) Comparison between blade Surface Temperature of Present Work and Reference [١٠].

CHAPTER SIX

6

CONCLUSIONS AND SUGGESTIONS

٦.١ Conclusions: -

The main conclusions that can be drawn from this work are summarized in the following points:

١) Six case studies are used for thermal analyses of the blade, which requires the specification of external and internal boundary conditions. It is also found from the results obtained that the best cooling method to the turbine blade have been obtained for the sixth case when the blade cooled by impingement and film cooling method.

٢) The analysis procedure used gave a good results in terms of their accuracy when compared with the results of other researchers.

٣) Numerical finite difference was used successfully in obtaining temperature distribution for complicated geometries as compared to the finite element results.

٤) The body fitted coordinates method represents an efficient flexible tool for treating difficult geometries.

٥) An impingement-cooled blade can be dealt with a two-dimensional thermal analysis through the use of heat transfer correlations, which provide spanwise averaged values of the heat transfer coefficients.

٦) The heat transfer coefficient for the trailing edge slot can be based on two heat transfer correlations, one based on pipe flow and the other on the flow between parallel plates. Both correlations result in similar blade temperature distribution.

٧) The effect of increasing the number of cooling air jets, which impinge on the hot blade surfaces, results in an increase in the blade temperature. This is because the increase in number of jets of high intensity cooling regions is accompanied by a reduction in the jet Reynolds number.

٨) Several different heat transfer correlations can be used to describe the impingement jet array areas as they all produce similar values of heat transfer coefficients and hence similar blade temperatures.

٩) Film cooling can be analyzed by varying the external boundary conditions of the blade and results in an appreciable reduction in blade temperatures about (١٧٠ K) cooler than the blade without film cooling.

٦.٢ Suggestions for Further Work: -

The following suggestions are suggested for further work:

١- A three-dimensional analysis of an impingement cooled blade or an array of impinging jets with the aim of investigating the effect of the local variation of the heat transfer coefficient around the jets.

٢- Replacement of the trailing edge slot with a number of discrete trailing edge passages and considering the effect of the ejected cooling air on the external boundary conditions in the trailing edge region.

٣- Determination of the temperature distribution could be demonstrated in case of transient heat transfer to specify the distribution during turbine operation.

REFERENCES

[١] Jack D. Mattingly, “Elements of Gas Turbine Propulsion” McGraw-Hill, Inc., ١٩٩٦.

[٢] Budugur Lakshminarayana, “Fluid Dynamics and Heat Transfer of Turbomachinery”, John Wiley and Sons, Inc., ١٩٩٦.

[٣] On the Web, http:\ www.google.com, (Key Words “Turbine Blade Cooling”), ٢٠٠٤. [Paper]

[٤] El-Wakil, M.M., “Power-Plant Technology”, McGraw-Hill, Inc., ١٩٨٥.

[٥] Turner A.B., Long C.A., Childs P.R.N., Hills N.J., and Millward J.A., “A Review of Some Current Problems in Gas Turbine Systems”, http:\ www.google.com, (Key Words “Gas Turbine”), ١٩٩٨.[Paper]

[٦] Cohen, H., Rogers G.F.C., and Saravanamut too H.I.H.,“Gas Turbine Theory” Longman Group UK Limited ١٩٨٧.

[٧] Thompson J.F., “Grid Generation techniques in Computational Fluid Dynamics”, AIAA Journal, Vol.٢٢, No.١١, November, pp. ١٥٠٥-١٥٢٢, ١٩٨٤.

[٨] Anderson D.A., John C. Tennehill and Richard H. Pletcher, “Computational Fluid Mechanics and heat Transfer”, McGraw-Hill Company, ١٩٨٤.

[٩] Gilding B.H., “A Numerical Grid Generation Technique” Computers and Fluids Journal Vol.١٦, No.١, pp. ٤٧-٥٨,١٩٨٨.

[١٠] Walker M.J.B., “Turbine Blade Internal Heat Transfer”, M.Sc. Thesis, Cranfield Institute of Technology, ١٩٨٩.

[١١] Dawes W.N., “ The Solution-Adaptive numerical Simulation of the Three-Dimensional Viscous Flow in the Serpentine Coolant Passage of a Radial Inflow Turbine Blade”, Journal of Turbomachinery, Vol.١١٦, January, pp.١٤١-١٤٨, ١٩٩٤.

[١٢] Tekriwal P., “Heat Transfer Predictions with Extended K.E turbulence Model in Radial Cooling Ducts Rotating in Orthogonal Mode”, Journal of Heat Transfer, Vol.١١٦, May, pp. ٣٦٩-٣٨٠, ١٩٩٤.

[١٣] Dilzer M., Gutmann C., Schulz A. and Witting S., “Testing of a Low Cooled Ceramic Nozzle Vane Under Transient Conditions”, Journal of Engineering for Gas Turbines and Power, Vol.١٢١, April, pp.٢٥٤- ٢٥٨, ١٩٩٩.

[١٤] Natalini G. and Sciubba E., “ Minimization of the Local Rates of Entropy Production in the Design of Air-Cooled Gas Turbine Blades” Journal of Engineering for Gas Turbines and Power, Vol.١٢١, July, pp. ٤٦٦-٤٧٥, ١٩٩٩.

[١٥] Jaleel J. M., “The Effectiveness of Finite Difference method on Curved Boundary Air Cooled Turbine Blades”, Journal of Military College of Engineering, No.٢٥, pp. ١٩-٣٢, ٢٠٠١.

[١٦] Kudor D.S., “Effect of Cooling Air Passage Shape on Gas Turbine Blade Temperature Distribution”, M.Sc. Thesis Al-Mustansiria University, Iraq, ٢٠٠٣.

[١٧] Marie L.H.,Eriksson L.E. and Suden B., “Convective Heat Transfer on an Inlet Guide Vane”, http:\ www.google.com, (Key Words “Turbine Blade Cooling”), ٢٠٠٣.[Paper]

[١٨] Debruge L.L. and Han L.S., “Heat Transfer in a Channel with a Porous Wall for Turbine Cooling Application”, Journal of Heat Transfer, November, pp. ٣٨٥- ٣٩٠, ١٩٧٢.

[١٩] Peter L.M., “Analysis of Metal Temperature and Coolant Flow with a Thermal-Barrier Coating on a Full-Coverage-Film-Cooled Turbine Vane”, NASA Technical Paper ١٣١٠,pp. ١-١٢, ١٩٧٨.

[٢٠] Eckert E.R.G., “Analysis of Film Cooling and Full-Coverage Film Cooling of Gas Turbine Blades” Journal of Engineering for Gas Turbine and Power, Vol.١٠٦, January, pp. ٢٠٦-٢١٣, ١٩٨٤.

[٢١] Nicholson J.H., Forest A.E., Oldfield M.L.G. and Schultz D.L., “Heat Transfer Optimized Turbine Rotor Blades-An Experimental Study Using Transient Techniques”, Journal of Engineering for Gas Turbines and Power Vol.١٠٦, January, pp. ١٧٣-١٨١, ١٩٨٤.

[٢٢] Frederick C.Y., Gladden H.J., Gauntner J.W. and Gauntner D.J., “Comparison of Cooling Effectiveness of Turbine Vanes With and Without Film Cooling”, NASA TM x-٣٠٢٢, June, pp.١-٢, ١٩٧٤.

[٢٣] Hay N., lamparad D. and Benmansour S., “Effect of Crossflow on the Discharge Coefficient of Film Cooling Holes”, Journal of Engineering for Power, Vol.١٠٥, April, pp. ٢٤٣-٢٤٨, ١٩٨٣.

[٢٤] Nealy D.A., Mihelc M.S., Hylton L.D. and Gladden H.J., “Measurements of Heat Transfer Distribution over the Surfaces of Highly Loaded Turbine Nozzle Guide Vanes”, Journal of Engineering for Gas Turbine and Power, Vol.١٠٦, January, pp. ١٤٩-١٥٨, ١٩٨٤.

[٢٥] York R.E., Hylton L.D, Mihelc M.S., “ An Experimental Investigation of Endwall Heat Transfer and Aerodynamics in a Linear Vane Cascade”, Journal of Engineering for Gas Turbine and Power, Vol.١٠٦, January, pp.١٥٩-١٦٧, ١٩٨٤.

[٢٦] Hussian A.K., “Experimental Study of Radiation from Coated Turbine Blades” Ph.D. Thesis Submitted to Cranfield Institute of Technology, England, ١٩٩٠.

[٢٧] Salcudean M., Gartshore I., Zhang K. and Mclean I., “An Experimental Study of Film Cooling Effectiveness Near the Leading Edge of a Turbine Blade”, Journal of Turbomachinery, Vol. ١١٦, January, pp. ٧١-٧٩, ١٩٩٤.

[٢٨] McMillin R.D. and Lau S.C., “Effect of Trailing-Edge Ejection on Local Heat (Mass) Transfer in Pin Fin Cooling Channels in Turbine Blades”, Journal of Turbomachinery, Vol. ١١٦, January, pp. ١٥٩-١٦٨, ١٩٩٤.

[٢٩] Ou S. and Han J.C., “Unsteady Wake Effect on Film Effectiveness and Heat Transfer Coefficient From a Turbine Blade With One Row of Air and Co$_٢$ Film Injection” Journal of Heat Transfer, Vol.١١٦, November, pp. ٩٢١-٩٢٨ ١٩٩٤.

[٣٠] Zhang L. and Han J.C., “Influence of Mainstream Turbulence on Heat Transfer Coefficients From A Gas Turbine Blade”, Journal of Heat Transfer, vol.١١٦, November, pp. ٨٩٦-٩٠٣, ١٩٩٤.

[٣١] Abuaf N. and Kercher D.M., “Heat Transfer and Turbulence in a Turbulated Blade Cooling Circuit”, Journal of Turbomachinery, Vol. ١١٦, January, pp. ١٦٩-١٧٧, ١٩٩٤.

[٣٢] Moss R.W., Ainsworth R.W. and Garside T., “Effects of Rotation on Blade Surface Heat Transfer, An Experimental Investigation”, Journal of Turbomachinery, Vol. ١٢٠, July, pp. ٥٣٠-٥٤٠, ١٩٩٨.

[٣٣] Drost V. and Bolcs A., “Performance of a Turbine Airfoil with Multiple Film Cooling Stations, Part II: Aerodynamic Losses”,http:\ www.google.com, (Key Words “Turbine Blade Cooling”), ١٩٩٩.[Paper]

[٣٤] Ken I.T.and Takasago S.A., “Contribution of Heat Transfer to Turbine Blades and Vanes for High Temperature Industrial Gas Turbines”, http:\ www.google.com, (Key Words “Turbine Blade Cooling”), ٢٠٠٠.[Paper]

[٣٥] Stefan L.F., “Surface Temperature Mapping of Gas Turbine Blading by Means of High Resolution Pyrometry”, http:\ www.google.com, (Key Words “Turbine Blade Cooling”), ٢٠٠١.[Paper]

[٣٦] Incropera F.P. and Dewitt D.P., “Introduction to Heat Transfer” John Wiley and Sons, ١٩٨٥.

[٣٧] Incropera F.P. and Dewitt D.P., “Fundamentals of Heat and Mass Transfer” John Wiley and Sons, NewYork, ١٩٩٦.

[٣٨] Anderson J.D., “Computational Fluid Dynamics”, McGraw-Hill, Inc., ١٩٩٥.

[٣٩] Hoffmann K.A., “Computational Fluid Dynamics for Engineers”, ١٩٨٩.

[٤٠] Chupp R.E., Helms H.E., McFadden P.W. and Brown T., “Evaluation of Internal Heat Transfer Coefficients for Impingement- Cooled Turbine Airfoils”, Journal of Aircraft, Vol.٦, PP ٢٠٣-٢٠٨, ١٩٦٩.

[٤١] Holman J.P., “Heat Transfer”, McGraw-Hill Book Co., NewYork, ١٩٨٩.

[٤٢] Florshuetz L.W. Metzger D.E., Su C.C.,Isoda Y. and Tseng H.H., “Jet Array Impingement Flow Distribution and Heat Transfer Characterstics-Effect of Initial Crossflow and Nonuniform Array Geometry”, NASA CR ٣٦٣٠, ١٩٨٢.

[٤٣] Florshuetz L.W. Metzger D.E. and Truman C.R., “Jet Impingement with Crossflow-Correlation of Streamwise Resolved Flow and Heat Transfer Distributions”, NASA CR ٣٣٧٣, ١٩٨١.

[٤٤] Rohsenow W.M., Hartnet J.P. and Ganic E.N., “Handbook of Heat Transfer Fundamentals”, ٢nd ed. McGraw-Hill Book Co., ١٩٨٧.

[٤٥] Tabakoff W. and Kercher D.M., “Heat Transfer by a Square Array of Round Air Jets Impinging Perpendicular to a Flat Surface Icnluding the Effect of Spent Air”, Journal of Engineering for Power, January, pp. ٧٣-٨٢, ١٩٧٠.

[٤٦] Chance J.L., “Experimental Investigation of Air Impingement Heat Transfer Under an Array of Round Jets”, Journal of Heat Transfer, Vol.٥٧, PP ١٠٨-١١٢, ١٩٧٤.